Instituto Alberto Luiz Coimbra de
Pós-Graduação e Pesquisa de Engenharia

AN EARLY-STAGE APPROACH TO OPTIMISE THE SYNTHESIS, DESIGN AND OPERATION OF A MARINE ENERGY SYSTEM FOR LIQUEFIED NATURAL GAS CARRIERS

Crístofer Hood Marques

Tese de Doutorado apresentada ao Programa de Pós-graduação em Engenharia Oceânica, COPPE, da Universidade Federal do Rio de Janeiro, como parte dos requisitos necessários à obtenção do título de Doutor em Engenharia Oceânica.

Orientadores: Carlos Rodrigues Pereira Belchior
Jean David Job Emmanuel Marie Caprace

Rio de Janeiro
Fevereiro de 2018

AN EARLY-STAGE APPROACH TO OPTIMISE THE SYNTHESIS. DESIGN AND OPERATION OF A MARINE ENERGY SYSTEM FOR LIQUEFIED NATURAL GAS CARRIERS

Crístofer Hood Marques

TESE SUBMETIDA AO CORPO DOCENTE DO INSTITUTO ALBERTO LUIZ COIMBRA DE PÓS-GRADUAÇÃO E PESQUISA DE ENGENHARIA (COPPE) DA UNIVERSIDADE FEDERAL DO RIO DE JANEIRO COMO PARTE DOS REQUISITOS NECESSÁRIOS PARA A OBTENÇÃO DO GRAU DE DOUTOR EM CIÊNCIAS EM ENGENHARIA OCEÂNICA.

Examinada por:

Prof. Carlos Rodrigues Pereira Belchior, D.Sc.

Prof. Jean David Job Emmanuel Marie Caprace, D.Sc.

Prof. Luiz Alberto Oliveira Rocha, Ph.D.

Prof. Kazuo Nishimoto, Ph.D.

Prof. Antonio Carlos Fernandes, Ph.D.

RIO DE JANEIRO, RJ – BRASIL
FEVEREIRO DE 2018

Marques, Crístofer Hood

An early-stage approach to optimise the synthesis, design and operation of a marine energy system for liquefied natural gas carriers/Crístofer Hood Marques. – Rio de Janeiro: UFRJ/COPPE, 2018.

XXIV, 96 p.: il.; $29,7$cm.

Orientadores: Carlos Rodrigues Pereira Belchior
Jean David Job Emmanuel Marie Caprace

Tese (doutorado) – UFRJ/COPPE/Programa de Engenharia Oceânica, 2018.

Referências Bibliográficas: p. 82 – 89.

1. Fixed pitch propeller. 2. Dual-fuel Diesel engine. 3. Operational profile. 4. Net present value. 5. Optimisation. I. Belchior, Carlos Rodrigues Pereira *et al.* II. Universidade Federal do Rio de Janeiro, COPPE, Programa de Engenharia Oceânica. III. Título.

Dedico este trabalho
primeiramente à minha esposa,
por ela ter aguentado meus
períodos de mal humor durante a
realização do mesmo.
Entretanto, não devo, nem
posso, esquecer de todos que me
apoiaram, incentivaram e
auxiliaram durante minha vida
acadêmica. Começando pela
minha mãe e meu pai, passando
pelos demais familiares e amigos,
e terminando nos colegas de
classe, professores e colegas de
profissão. De outro modo, eu
provavelmente não teria chegado
a esse ponto.

Agradecimentos

Eu gostaria de começar agradecendo à minha esposa que, embora tenha dito que o único lugar que ela não iria por temer a violência era o Rio de Janeiro, me acompanhou nessa jornada e viu que não há motivo para tanto receio.

Agradeço à Universidade Federal de Rio Grande (FURG) por ter concedido o afastamento para que eu pudesse realizar o curso de doutoramento fora da cidade.

Ao meu orientador Prof. Belchior que foi meu amigo desde o primeiro momento e a quem muito devo minha permanência na cidade do Rio de Janeiro.

Ao meu orientador Prof. Caprace por ter aceitado começar a orientação após mais de dois anos decorridos do início do curso, em um momento de indecisão e incerteza de minha parte quanto a proposta de tese.

À equipe do laboratório LEME/LEDAV da COPPE/UFRJ por ter me acolhido, especialmente à Dona Carmem pelo carinho.

Ao gerente de vendas da Wartsila, Sr. Mário Barbosa, por todos os esclarecimentos a repeito de motores Diesel marítimos de dois combustíveis e de soluções para navios transportadores de gás natural liquefeito.

Ao colega Prof. Jeferson Avila Souza da FURG que deu a assistência necessária para eu realizar as simulações remotamente no LabSiN.

Ao amigo, também riograndino, Cléo Henrique que chegou ao Rio pouco depois de mim para ganhar a vida como músico profissional, pela amizade e momentos descontraídos.

Por fim, eu não poderia deixar de agradecer ao casal de amigos Caio e Jéssica por terem adotado a mim e minha esposa como familiares logo que nos conhecemos. Não fosse por eles, nossa estadia na “cidade maravilhosa” não teria sido tão divertida.

Resumo da Tese apresentada à COPPE/UFRJ como parte dos requisitos necessários para a obtenção do grau de Doutor em Ciências (D.Sc.)

UMA ABORDAGEM INICIAL PARA OTIMIZAR A SÍNTESE, PROJETO E OPERAÇÃO DE UM SISTEMA DE ENERGIA MARÍTIMO PARA NAVIOS TRANSPORTADORES DE GÁS NATURAL LIQUEFEITO

Crístofer Hood Marques

Fevereiro/2018

Orientadores: Carlos Rodrigues Pereira Belchior
Jean David Job Emmanuel Marie Caprace

Programa: Engenharia Oceânica

Uma vez que as decisões de maior impacto são feitas nos primeiros estágios do projeto do navio, o desenvolvimento de ferramentas de projeto para disponibilizar mais informações mais cedo é desejável. Além disso, ainda há margem para melhorias na otimização da seleção do sistema de energia, considerando uma abordagem integrada. Portanto, o presente trabalho visa proporcionar uma abordagem preliminar e abrangente para a otimização de projeto, síntese e operação, considerando aspectos econômicos e técnicos, bem como o estado do mar ao longo da rota. Para evitar hélices que possam apresentar problemas de resistência, cavitação e vibração, são usadas restrições. Vários hélices, dezesseis motores e quatro perfis operacionais são avaliados. Um algoritmo de otimização do tipo evolução diferencial, cuja função objetivo a ser maximizada é o valor presente líquido, é aplicado. O estudo de caso foi projetado usando um transportador de gás natural liquefeito de 175,000 m^3 que navega entre Lake Charles (EUA) e Tokyo Bay (Japão), através do Canal do Panamá. Todas as combinações adequadas para 15,023 hélices são encontradas. A abordagem mostra um ganho de 22% entre o pior indivíduo da população inicial e o pior indivíduo da população final. A potência no freio necessária é aproximadamente 22% maior para mar agitado do que para água parada. Uma diferença de mais de 120 % foi encontrada comparando combinações variadas de cenas econômicas e perfis de combustível. A abordagem mostra um ganho significativo e destaca o valor de explorar uma ampla gama de configurações de sistemas de energia de forma integrada, considerando a condição climática.

Abstract of Thesis presented to COPPE/UFRJ as a partial fulfillment of the requirements for the degree of Doctor of Science (D.Sc.)

AN EARLY-STAGE APPROACH TO OPTIMISE THE SYNTHESIS, DESIGN AND OPERATION OF A MARINE ENERGY SYSTEM FOR LIQUEFIED NATURAL GAS CARRIERS

Crístofer Hood Marques

February/2018

Advisors: Carlos Rodrigues Pereira Belchior
Jean David Job Emmanuel Marie Caprace

Department: Ocean Engineering

Since decisions of the greatest impact are made in early stages of ship design, developing design tools to make more information available sooner is desirable. Moreover, there is still room for improvements on the optimisation of energy system selection considering an integrated approach. Therefore, the present work aims to provide a comprehensive early-stage approach to perform the optimisation of design, synthesis and operation, considering economic and technical aspects as well as route weather. Constraints are used to avoid propellers that could present issues concerning strength, cavitation and vibration. Various propellers, sixteen engines and four operational profiles are assessed. A differential evolution optimisation algorithm whose objective function to be maximised is the net present value is applied. The case study is designed using a liquefied natural gas carrier of 175,000 m^3 sailing between Lake Charles (USA) and Tokyo Bay (Japan), via Panama Canal. All suitable matchings for 15,023 propellers are found. The approach shows a gain of 22% between the worst individual of the initial population and the worst individual of the final population. The required brake power is approximately 22% higher for rough weather than for still water. A difference of over 120% was found by comparing varied matchings of economic scenes and fuel profiles. The approach shows a significant gain and highlights the value of exploring a broad range of energy system configurations in an integrated manner, considering the weather condition.

Contents

List of Figures xi

List of Tables xiii

List of Abbreviations xiv

List of Symbols xvii

1 Introduction 1

1.1 Background 1

1.2 State of the art 4

1.2.1 Gap to be filled 8

1.3 Dissertation proposal 9

2 Literature review 10

2.1 Propulsion alternatives 10

2.2 Diesel engines 10

2.3 Dual-fuel Diesel engines 11

2.4 Standard selection of slow speed Diesel engines 14

2.5 Re-liquefaction plant 15

2.6 Exhaust gas emissions 16

2.7 Emissions reduction 17

2.8 Waste heat recovery systems 19

3 Developed engine model 22

3.1 Methodology 22

3.1.1 Engine layout diagrams 23

3.1.2 Specific fuel consumption at SMCR 23

3.1.3 Specific fuel consumption at part load 25

3.2 Statement of the model 29

3.3 Validation of the model 30

3.4 Strengths of the model 33

3.5 Limitations of the model 34

4 **Developed approach** **35**

4.1 Methodology 35

4.2 Computation of resistance for specified weather conditions 39

4.3 Computation of total resistance in service 42

4.4 Computation of propulsion factors 42

4.5 Computation of propeller performance 43

4.6 Constraints 44

4.6.1 Propeller blade strength 44

4.6.2 Cavitation 44

4.6.3 Propeller peripheral velocity 45

4.6.4 Resonance 45

4.7 Computation of brake power in service 46

4.8 Computation of SMCR 46

4.9 Determination of suitable engines 47

4.10 Computation of CAPEX 48

4.11 Computation of OPEX 49

4.12 Computation of NPV 51

4.13 Differential evolution optimisation algorithm 52

5 **Case study** **53**

5.1 Ship 53

5.2 Route 56

5.3 Operational profile 57

5.4 Economic and optimisation parameters 58

6 **Results and discussion** **60**

6.1 Optimization algorithm parameters 60

6.2 Optimisation summary 61

6.3 Engine and fuel profile effect 63

6.4 Weather effect 65

6.5 Economic scene effect 72

6.6 Strengths of the approach 73

6.7 Limitations of the approach 75

7 **Conclusion** **77**

8 **Written articles and future work** **79**

8.1 Written articles 79

8.2 Future work 80

References **82**

A Linked articles **90**

A.1 First article 91
A.2 Second article 92
A.3 Third article 93
A.4 Fourth article 94
A.5 Fifth article 95
A.6 Sixth article 96

List of Figures

1.1 LNGCs with different cargo tank geometries. 2

2.1 Propulsion plant scheme with slow speed two-stroke diesel engine and re-liquefaction plant. 11
2.2 DFDE propulsion plant scheme without re-liquefaction plant. 12
2.3 DFDD propulsion plant scheme. 13
2.4 Gas injection pressure concepts for slow speed two-stroke dual-fuel Diesel engines. 13
2.5 Layout diagrams of slow speed dual-fuel Diesel engines programme from MAN Diesel & Turbo. 14
2.6 Engine layout diagram of the engine 10S90ME- C9.5-GI. 15
2.7 Re-liquefaction plant scheme. 16
2.8 Engine room arrangement with EGR. 18
2.9 Engine room arrangement with SCR. 19
2.10 Engine room arrangement with a hybrid system of SO_x scrubber. . . 20
2.11 Main WHRS principles. 21

3.1 Polynomial surfaces of the specific fuel consumptions normalised with respect to NMCR and respective percentage errors of regression. . . . 26
3.2 Polynomial surfaces of the exhaust gas parameters normalised with respect to NMCR and respective percentage errors of regression. . . . 26
3.3 Polynomial curves of the specific fuel consumptions normalised with respect to SMCR and respective percentage errors of regression. . . . 28
3.4 Polynomial curves of the exhaust gas parameters normalised with respect to SMCR and respective percentage errors of regression. . . . 29
3.5 Fuel consumption and exhaust gas parameters from the model compared with catalogue data for the engine 8G70ME-C9.5-GI. . . . 31
3.6 Fuel consumption and exhaust gas parameters from the model compared with catalogue data for the engine 8S70ME-C8.5-GI. 31
3.7 Modelling errors for the engine 8G70ME-C9.5-GI. 32
3.8 Modelling errors for the engine 8S70ME-C8.5-GI. 33

4.1 Optimisation approach towards synthesis, design and operation of an LNGC energy system. 37
4.2 Brake power and shaft speed estimation in service for each route-track. 38
4.3 Net present value estimation for each matching of engine and fuel profile. 39
4.4 Iterative procedure of the differential evolution optimisation algorithm. 40
4.5 Encounter Angle. 41
4.6 Engine layout diagrams considered and a SMCR of 50 MW and 75 rpm. 47

5.1 LNGC for the case study. 53
5.2 Energy system scheme. 54
5.3 Route between Lake Charles and Tokyo Bay via Panama Canal and the topology of absolute wind speed [m/s] for December 2015. 56

6.1 Optimisation algorithm convergence for different values of n_P and n_G. 61
6.2 Evolution of the optimisation variables throughout the generations. . 62
6.3 Engine configuration and fuel profile effects for the SDO_2. 67
6.4 Total resistance throughout the voyage. 68
6.5 Propeller's open water efficiency throughout the voyage for the SDO_1. 68
6.6 Required shaft speed throughout the voyage for the SDO_1. 69
6.7 Required brake power throughout the voyage for the SDO_1. 69
6.8 SMCR points for weather conditions from different months. 71
6.9 Fluctuation in fuel and LNG prices. 72
6.10 Evolution of the optimisation variables for the selected economic scenes. 74

List of Tables

1.1 Features of the references to be considered or improved. 7

2.1 NO$_x$ emission limits in g/kWh. 16
2.2 Fuel oil sulphur limits expressed in percentage by weight 17

3.1 Available ME-GI slow speed dual-fuel engines and their particulars to chart layout diagrams. 23
3.2 Coefficients of the polynomial surfaces. 25
3.3 Coefficients of the polynomial curves. 27
3.4 Specific features at NMCR for gas and diesel mode. 30

4.1 Coefficient C_n of the hull girder vertical natural frequency. 45
4.2 Suitable engines and number of cylinders. 48

5.1 Ship parameters. 54
5.2 Energy system parameters. 55
5.3 Route parameters. 57
5.4 Operational profile. 58
5.5 Economic parameters. 59
5.6 Optimisation variables. 59

6.1 Optimisation summary. 62
6.2 Improved synthesis, design and operation (SDO) from the final population. 64
6.3 Influence of the matchings of engine configuration and fuel profile for the SDO$_2$. 66
6.4 Varying weather conditions for 2015. 70
6.5 Optimal synthesis, design and operation for varying adverse weather conditions. 71
6.6 Selected economic scenes. 73
6.7 Optimal synthesis, design and operation for the selected economic scenes. 75

List of Abbreviations

0-DEM	Zero-dimensional engine model, p. 8
BN	Beaufort number [-], p. 41
BOG	Boil-off gas, p. 1
BOR	Boil-off rate [%], p. 1
CAPEX	Capital expenditure [US$], p. 9
CEAS-ERD	Computerised Engine Application System - Engine Room Dimensioning, p. 15
CFD	Computational fluid dynamics, p. 8
COGES	Combined gas turbine electric and steam system, p. 5
CTU	Collecting tank unit, p. 17
DFDD	Dual-fuel direct drive, p. 12
DFDE	Dual-fuel Diesel electric, p. 12
DOP	Dynamic optimisation problem, p. 81
ECA	Emission control area, p. 16
EGR	Exhaust gas recirculation, p. 2
EM	Engine margin [-], p. 46
FP	Fuel profile, p. 57
FW	Freshwater, p. 17
GCU	Gas combustion unit, p. 11
HC	Hydrocarbons, p. 16
HFO	Heavy fuel oil, p. 11

HP	High pressure, p. 12
IMO	International Maritime Organisation, p. 16
ISO	International Organisation for Standardisation, p. 22
LCB	Longitudinal centre of buoyancy [%], p. 54
LNGC	Liquefied natural gas carrier, p. 1
LNG	Liquefied natural gas, p. 1
LP	Low pressure, p. 12
MCR	Maximum continuous rating, p. 46
MDO	Marine diesel oil, p. 11
MEP	Mean effective pressure [Pa], p. 14
MF	Exhaust gas mass flow [kg/s], p. 24
MGO	Marine gas oil, p. 11
MVEM	Mean value engine model, p. 5
NMCR	Nominal maximum continuous rating, p. 15
NPV	Net present value [US$], p. 5
OPEX	Operational expenditure [US$], p. 2
PM	Particulate materials, p. 2
PPI	Producer price index [-], p. 48
PT	Power turbine, p. 21
RT	Route-track, p. 56
SCR	Selective catalytic reduction, p. 2
SDO	Synthesis, design and operation, p. 62
SFC	Specific fuel consumption, p. 50
SFOC	Specific fuel oil consumption [g/kWh], p. 24
SGC	Specific gas consumption [g/kWh], p. 24

SMCR	Specified maximum continuous rating, p. 14
SMF	Specific exhaust gas mass flow [kg/kWh], p. 24
SM	Service margin [-], p. 42
SPOC	Specific pilot oil consumption [g/kWh], p. 24
ST	Specific temperature [K/MW], p. 24
ST	Steam turbine, p. 21
SW	Seawater, p. 18
TFEM	Transfer function engine model, p. 8
WCU	Water cleaning unit, p. 18
WHRS	Waste heat recovery system, p. 3
WTU	Water treatment unit, p. 17

List of Symbols

$1 + k_1$	Form factor of the hull [-], p. 41
A_E/A_O	Blade-area ratio [-], p. 43
A_p	Projected area of the propeller [m^2], p. 44
A_{BT}	Transverse bulb area [m^2], p. 54
B	Moulded breadth [m], p. 45
$CAPEX_m$	Capital expenditure on machinery [US$], p. 48
$CAPEX_{rp}$	Capital expenditure on the re-liquefaction plant [US$], p. 48
CIF_{LNG}	Cost-insurance-freight price of liquefied natural gas [US$/kg], p. 51
CR	Crossover factor [-], p. 52
C_M	Midship section coefficient [-], p. 54
C_U	Speed reduction coefficient [-], p. 41
C_β	Direction reduction coefficient [-], p. 39
C_m	Maintenance cost [US$], p. 49
C_n	Coefficient dependent on vibration order and ship type [-], p. 45
C_{LNG}	Purchase cost of the LNG cargo [US$], p. 49
C_{WP}	Water-plane area coefficient [-], p. 54
$C_{f,G}$	Total gaseous fuel cost [US$], p. 50
$C_{f,O}$	Total fuel oil cost [US$], p. 50
$C_{f,PO}$	Total pilot oil cost [US$], p. 50

$C_{f,oth}$	Fuel cost related to other consumers on-board, p. 49
$C_{f,pL}$	Total liquid fuel cost [US$], p. 50
$C_{f,pro}$	Fuel cost related to propulsion [US$], p. 49
$C_{f,rel}$	Fuel cost related to boil-off gas re-liquefaction [US$], p. 49
C_{form}	Ship form coefficient [-], p. 41
C_{jou}	Journey cost [US$], p. 49
$C_{m,E}$	Engine maintenance cost [US$], p. 51
C_{stern}	Stern shape parameter [-], p. 54
D	Propeller diameter [m], p. 43, 44
D_m	Moulded depth [m], p. 45
E_{ID}	Engine identification [-], p. 59
F	Mutation factor [-], p. 52
FOB_{LNG}	Free-on-board price of liquefied natural gas [US$], p. 49
FP_{ID}	Fuel profile identification [-], p. 59
Fy	Annual net cash flow [US$/year], p. 51
J	Advance ratio [-], p. 43
K_Q	Torque coefficient [-], p. 43
K_T	Thrust coefficient [-], p. 43
L	Length on waterline [m], p. 54
LHV_g	Standard lower heating value for gaseous fuel [J/kg], p. 54
LHV_l	Standard lower heating value for liquid fuel [J/kg], p. 54
LHV_{BOG}	Lower heating value of boil-off gas [J/kg], p. 54
LHV_{HFO}	Lower heating value of heavy fuel oil [J/kg], p. 55
LHV_{MGO}	Lower heating value of marine gas oil [J/kg], p. 55
L_s	Shaft length [m], p. 49

L_{pp}	Length between perpendiculars [m], p. 45
Lx	Points defining an engine envelop, where x may be 1, 2, 3 or 4, p. 14
P/D	Pitch ratio [-], p. 43
P_B	Brake power [W], p. 24
P_O	Open water power [W], p. 43
P_S	Power delivered by each blade [W], p. 44
$P_{B,rw}$	Brake power in rough weather [W], p. 68
$P_{B,sw}$	Brake power in still water [W], p. 69
$P_{Bc,x}$	Brake power per cylinder, where x may be L1, L2, L3 or L4 [W/cyl], p. 23
P_{MCR}	Brake power at the maximum continuous rating point [W], p. 46
P_{NMCR}	Brake power at the nominal maximum continuous rating point [W], p. 49
P_{SMCR}	Brake power at the specified maximum continuous rating point [W], p. 46
P_{com}	Electric power required by the BOG compression system [W], p. 50
$P_{i,j+1}$	One offspring member, p. 52
$P_{i,j}$	i^{th} individual of the j^{th} generation of the population Π, p. 52
P_{oth}	Electric power required by other consumers [W], p. 50
Q	Torque [Nm], p. 43
R	Random number between 0 and 1 [-], p. 52
R_A	Model-ship correlation resistance [N], p. 41
R_B	Additional pressure resistance of bulbous bow near the water surface [N], p. 41
R_F	Frictional resistance [N], p. 41

R_W	Wave resistance [N], p. 41
R_n	Reynolds number, p. 43
R_{APP}	Appendage resistance [N], p. 41
$R_{T,rw}$	Total propulsion resistance in rough weather [N], p. 65
$R_{T,ser}$	Total resistance in service [N], p. 42
$R_{T,sw}$	Total propulsion resistance in still water [N], p. 39
$R_{T,tri}$	Trial total resistance [N], p. 42
R_{TR}	Additional pressure resistance due to transom immersion [N], p. 41
S	Route-track length [m], p. 56
SFC_{GE}	Specific fuel consumption of the generation engine [g/kWh], p. 50
$SFOC_{GE}$	Specific fuel oil consumption of generation engines [g/kWh], p. 54
$SFOC_{HFO}$	Specific heavy fuel oil consumption [g/kWh], p. 56
SGC_{BOG}	Specific boil-off gas consumption [g/kWh], p. 56
SGC_{GE}	Specific gas consumption of generation engines [g/kWh], p. 54
$SPOC_{GE}$	Specific pilot oil consumption of generation engines [g/kWh], p. 54
$SPOC_{HFO}$	Specific pilot heavy fuel oil consumption [g/kWh], p. 56
SP_{BOG}	Power required to re-liquefy a mass flow unit of boil-off gas [Ws/kg], p. 50
S_C	Maximum allowable stress of the propeller material [Pa], p. 44
T	Temperature [K], p. 24
T_m	Draught moulded [m], p. 54
Th	Thrust [N], p. 42
V_S	Cylinder swept volume [m^3], p. 24

V_h	Heel volume [m^3], p. 49
V_{BOG}	Total volume of liquefied natural gas becoming boil-off gas, including naturally and forced generated amounts [m^3], p. 49
V_{LNG}	Volume of liquefied natural gas in the tanks [m^3], p. 50
V_{rel}	Volume of liquefied natural gas coming from the re-liquefaction plant [m^3], p. 49
Vd_{LNG}	Volume of liquefied natural gas delivered at unloading terminal [m^3], p. 51
Vp_{LNG}	Cargo volume of liquefied natural gas purchased at loading terminal [m^3], p. 49
Vt_{LNG}	Ship's total cargo capacity in volume [m^3], p. 49
WRC_m	Machinery weight-related cost [US$/kg], p. 48
WRC_{rp}	Weight-related cost of the re-liquefaction plant [US$/kg], p. 48
W_m	Machinery weight [kg], p. 48
W_p	Propeller weight [kg], p. 49
W_s	Shaft weight [kg], p. 49
W_{rp}	Re-liquefaction plant weight [kg], p. 48
Z	Number of blades, p. 43
Z_c	Number of cylinders of an engine, p. 23
Z_p	Number of propellers, p. 42
Δt_{rnd}	Period to accomplish a round trip [s], p. 63
Δ_V	Displacement including the virtual added mass of water [kg], p. 45
Π	Population, p. 52
α, β, γ	Randomly chosen members of the population Π, p. 52
δt	Duration of a certain condition [s], p. 50
δ_1, δ_2	Functions related to crossover, p. 52

$\dot{m}_{BOGc}$	Total mass flow of boil-off gas consumed, p. 50
$\dot{m}_{BOGg}$	Mass flow of boil-off gas naturally generated [kg/s], p. 50
$\dot{m}_{BOGr}$	Mass flow of boil-off gas to be re-liquefied [kg/s], p. 50
η_G	Generator efficiency [%], p. 50
η_O	Open water efficiency [%], p. 43
η_R	Relative rotative efficiency [%], p. 42
η_S	Shaft efficiency [%], p. 46
$\eta_{E,avg}$	Average engine efficiency [%], p. 63
η_{GB}	Gearbox efficiency [%], p. 46
$\eta_{O,avg}$	Average open water efficiency [%], p. 63
μ	Mean, p. 27
∇	Moulded displacement volume [m^3], p. 54
ρ	Density of the water [kg/m^3], p. 43
ρ_{LNG}	Density of the liquefied natural gas [kg/m^3], p. 49
σ	Standard deviation, p. 27
$\sigma_{0.7R}$	Mean cavitation number [-], p. 44
$\tau_{c0.7R}$	Thrust loading coefficient [-], p. 44
θ_l	Encounter angle for laden trip [°], p. 56
c_m	Maintenance unit cost [US$/Ws], p. 59
c_{HFO}	Unit cost of heavy fuel oil [US$/kg], p. 59
c_{MGO}	Unit cost of marine gas oil [US$/kg], p. 59
c_{lf}	Liquid fuel unit cost [US$/kg], p. 50
f	Excitation frequency due to the propeller [Hz], p. 46
f_{ins}	Installation cost factor [-], p. 49
h_B	Centre of bulb area above keel line [m], p. 54

h_s	Centre of propeller shaft above keel line [m], p. 55
m_{LNG}	Mass of liquefied natural gas delivered per round trip [kg], p. 63
n	Engine shaft speed [rev/s], p. 23
n_G	Number of generations [-], p. 60
n_P	Number of individuals in the population Π [-], p. 60
n_h	Integer related to the harmonics [-], p. 46
n_r	Engine rated speed [rev/s], p. 16
n_y	Period of economic analysis [year], p. 51
n_{MCR}	Engine shaft speed at the maximum continuous rating point [rev/s], p. 46
n_{NMCR}	Engine shaft speed at the nominal maximum continuous rating point [rev/s], p. 49
n_{RTb}	Number of route-tracks in ballast, p. 49
n_{RTl}	Number of route-tracks in laden, p. 51
n_{SMCR}	Engine shaft speed at the specified maximum continuous rating point [rev/s], p. 46
n_{rnd}	Number of round trips a year, p. 51
n_{rw}	Shaft speed in rough weather [rev/s], p. 68
n_{sw}	Shaft speed in still water [rev/s], p. 68
p_v	Water vapour pressure [Pa], p. 44
p_0	Static pressure at the shaft centre line [Pa], p. 44
r	Revolutions of crankshaft per complete working cycle [rev/cycle], p. 24
r_d	Discount rate [%], p. 51
sm_d	Service margin component due to displacement [-], p. 42
sm_f	Service margin component due to fouling [-], p. 42

sm_h	Service margin component due to the hull form [-], p. 42
sm_w	Service margin component due to weather [-], p. 42
sm_{wd}	Service margin component due to water depth [-], p. 42
t	Thrust deduction factor [-], p. 42
$t_{0.75R}$	Blade thickness at 75% of the propeller radius [m], p. 44
v_A	Advance velocity of the propeller [m/s], p. 42
v_{10}	Wind speed at a height of 10 m above sea level [m/s], p. 41
$v_{rw,hb}$	Higher level of service speed in ballast [m/s], p. 59
$v_{rw,hl}$	Higher level of service speed in laden [m/s], p. 59
$v_{rw,ib}$	Intermediary level of service speed in ballast [m/s], p. 59
$v_{rw,il}$	Intermediary level of service speed in laden [m/s], p. 59
$v_{rw,lb}$	Lower level of service speed in ballast [m/s], p. 59
$v_{rw,ll}$	Lower level of service speed in laden [m/s], p. 59
v_{rw}	Service speed in rough weather [m/s], p. 39
v_{sw}	Service speed in still water [m/s], p. 39
v_{tip}	Blade tip peripheral velocity [m/s], p. 45
w	Wake factor [-], p. 42

Chapter 1

Introduction

Next, it is presented a background about liquefied natural gas carriers, their energy system and propulsion design. The state of the art about simulation and optimisation of the ship energy system is presented subsequently. At the end of this chapter, the doctoral dissertation proposal is addressed.

1.1 Background

Liquefied natural gas carriers (LNGCs) are specialised ships designed to transport liquefied natural gas (LNG). They are fitted with insulated double-hulled tanks with basically two types of geometry, such as shown in Fig. 1.1. The tanks are designed to contain the cargo slightly above atmospheric pressure at a cryogenic temperature without any means of external refrigeration. Typically, the storage tanks operate at 0.3 bar_g[1] with a design pressure of 0.7 bar_g and a negative temperature around -169 °C, such that the LNG density lies between 430 and 470 kg/m^3, depending on its composition and state. The composition is predominantly methane (CH_4) and smaller fractions of ethane (C_2H_6), propane (C_3H_8), butane (C_4H_{10}) and nitrogen (N_2).

Despite the high level of insulation of the cargo tanks, some vaporisation occurs because it is impossible to avoid the heat transfer from the surroundings to the cargo. This evaporated LNG is called boil-off gas (BOG) and its evaporation rate, which is called boil-off rate (BOR), is generally about 0.10 to 0.15% in volume per day, depending on the thermal insulation system [1]. In this sense, a detailed dynamic BOG model, which accounts for the variation of mass flow, composition and thermodynamic properties, was developed in [2]. Since vaporisation induces a pressure increase in the tank, a certain amount of the vapour phase should be taken out of the tank to avoid dangerous overpressure. Usually, this outlet gas flow is used as fuel by the marine energy system of the ship to reduce its main fuel consumption [3].

---

[1] Gauge pressure

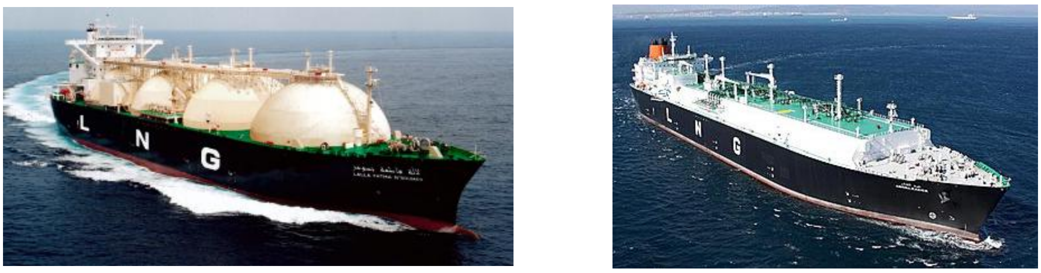
(a) Spherical tank or MOSS technology (b) Prismatic tank or membrane technology

Figure 1.1: LNGCs with different cargo tank geometries.

For many years steam propulsion plants were practically an exclusive option for LNGCs due to its capability to burn the unavoidable BOG directly in the power boiler. However, as environmental, economic and technical expectations have increased, the drawbacks of the steam turbine power plant have made it a less attractive option. Among these drawbacks is the comparatively low efficiency of the plant, its high fuel consumption, high exhaust emissions and large engine room space requirement. On the other hand, advances in the design of dual-fuel Diesel engines, shipboard BOG re-liquefaction plants, and marine gas turbines, provide meaningful alternatives to the traditional steam power plant. Moreover, propulsion systems based on slow speed two-stroke Diesel engines driving fixed pitch propellers with the inboard re-liquefaction system have been successfully used in large LNGCs.

However, when conventional fuel prices are higher than LNG price, the operational expenditure (OPEX) of propulsion systems that are unable to use BOG as fuel is increased [1]. Moreover, conventional fuels are not as clean as the BOG, once natural gas is considered environmentally friendly for various reasons [4]. Thus, an option to overcome these drawbacks is to apply dual-fuel Diesel engines, which are compression ignition ones capable to work in two operational modes: Diesel mode and gas mode [5].

Owing to environmental concerns, controls on exhaust gas emissions continue to tighten regionally and internationally dictating further responses from engine designers. Carbon dioxide (CO_2), nitrogen oxides (NO_x), sulphur oxides (SO_x) and particulate materials (PM) are the gaseous emissions of most concern. Thereby, in-engine measures to decrease these emissions, including common rail fuel systems, emulsified fuel, direct water injection and charge air humidification, have been studied. In addition, exhaust gas after-treatment, such as selective catalytic reduction (SCR) and exhaust gas recirculation (EGR) systems, as well as gas scrubbers, also have been developed for this purpose.

Regarding the reduction of CO_2 emission, the solutions are mainly burning alternative fuels, as BOG for instance, and decreasing the fuel consumption. The latter is achieved by means of the increase of the ship energy efficiency. Measures that positively affect it include the improved hull and ship structure designs, which result in decreased ship resistance, as well as more efficient thrusters designs that can increase the ship propulsive efficiency. Further, more efficient propulsion types and the exploitation of the rejected energy as much as possible have been pursued. In this sense, waste heat recovery systems (WHRSs) have emerged [5].

Since the prime mover is usually operated until the end of the ship's lifetime, its selection is one of the major steps in merchant shipbuilding projects. Although a complete criteria list for choosing main machinery is given in [6] and many considerations are presented in [7], BULUT *et al.* [8] defined six major selection criteria. Based on interviews with a group of technical experts and managers of selected shipping companies, the author highlighted: power, acquisition cost, fuel consumption, maintenance, the majority in existing merchant fleet and damage history of the model.

Power is on the top of the list because the engine needs to be capable to provide enough power to satisfy the ship's operational profile. Acquisition cost is considered one of the major indicators of the financial feasibility of a project because it represents about 10% of the total cost of a new building project. Another significant indicator of financial feasibility is fuel consumption. Maintenance attributes can though divide into two considerations: firstly, how easy it can be performed and secondly, how much it costs.

Differently, majority in existing merchant fleet, or common practice, is an important aspect for other reasons. If a specific model and brand of Diesel engine are frequently preferred, this may denote its superiority in overall circumstances. A similar indicator is the damage history of the model, or reliability, which illustrates its structural and mechanical hardness in the practical life. These two latter criteria illustrate why the design of a new machinery system is typically done by considering a traditional concept as a base [9].

For ships navigating across large oceans, considerations about the weather conditions are essential for safe and efficient operations. The environment exposes the ship to loads from wind, waves, and currents changing the operating point of the ship's energy system [10]. To ensure safe passage, arrival on time, minimized operational costs and minimal environmental impact it is important that the weather expected to be found throughout the route is taken into account since the early-stage project. Thus, the integrated nature of a ship energy system makes the collaboration among multiple engineering disciplines to be required in the design process.

Furthermore, one of the challenges of ship design is that the decisions of the greatest impact are made in early stages of design when the least information and greatest uncertainty are present [11]. Hence, developing ship design tools to make more information available sooner and pushing decision points for later is quite advisable. In this sense, simulations of the overall ship energy system and optimisation studies are of great interest.

1.2 State of the art

Studies about ship energy system simulation and optimisation were briefly discussed below in order to present the state of the art overview.

BENVENUTO *et al.* [12] presented a computer simulation model able to predict the dynamic behaviour of a whole marine propulsion system and to evaluate the influence of its three main elements: ship, propeller and prime mover. The developed procedure was able to represent the system operating both in steady-state and in transient conditions (manoeuvring). The adoption of a fixed pitch versus a controllable pitch propeller and various choices relative to the plant control system were assessed.

KYRTATOS *et al.* [13] carried out a propulsion plant simulation of a container ship to assess the engine performance in different operating conditions. This paper considered the application of a detailed mathematical model for the prediction of the transient response of a large two-stroke marine Diesel engine. Load fluctuations caused by either change in the requested engine speed set point or by load changes were assumed to simulate severe weather conditions. The simulation module consisted of a Diesel engine model for performance prediction plus appended models for the shaft, propeller, and ship hull dynamics, as well as for the engine speed governor.

MICHALSKI [14] conceived an algorithmic method for preliminary selection of parameters of a ship propulsion system fitted with fixed pitch propeller and Diesel engine. The case study was about inland navigation, where hull resistance and service speed varies significantly, and the objective function was minimising the total fuel expenditure for a given voyage distance and time. Wageningen propellers of Ka series operating with 19A nozzles were considered, but the engine was taken simply as a constant figure of specific fuel consumption.

CHEN and SHIH [15] addressed a two-objective parametric optimisation problem regarding Wageningen B-screw series propeller design. The objective function was set by users who could freely weight the relative importance of the propeller's open water efficiency and vibration. Cavitation and strength constraints were considered and the vibration forces and moments were computed by a modified version of a program developed at the University of Michigan.

DIMOPOULOS *et al.* [16] performed a study focused on the optimisation of synthesis, design, and operation of a marine energy system for a cruise liner fitted with a combined gas turbine electric and steam system (COGES). Various configuration options, types of technologies and existence of components were incorporated. In addition, time-varying operational requirements were considered, resulting in a time-dependent operation optimisation problem. The complete optimisation problem was solved using a novel algorithm, inspired by evolutionary and social behaviour metaphors. A parametric analysis with respect to the fuel price demonstrated changes in the optimal synthesis of the system. The objective function of this optimisation was maximising the net present value (NPV). Similar works about LNGCs fitted with COGES, which also did not model either the propeller or the ship movement, are [17] and[18].

THEOTOKATOS [19] investigated the transient response of the overall ship propulsion plant for a merchant ship under various operating conditions. The two-stroke marine Diesel engine was approached by means of a mean value engine model (MVEM) and the propeller was modelled by the Wageningen B-screw series polynomials. In addition, the ship movement along its longitudinal axis was calculated using the differential equation of surge dynamics and the ship resistance was considered as a second order function of the velocity.

ALDOUS and SMITH [20] described a speed optimisation model for LNGCs considering ship geometric parameters, propeller characteristics, and engine specifications. The effect of various economic input parameters on the optimal speed for profit maximisation and cost minimisation were explored. A medium speed four-stroke dual-fuel Diesel engine with electric transmission and a conventional two-stroke engine with direct drive transmission were compared. The ship resistance was calculated using the Holtrop method and the Wageningen B-screw series polynomials were used to model propellers. Both engines were modelled by catalogue values.

THEOTOKATOS and TZELEPIS [21] carried out the mapping of performance and emission parameters for a merchant vessel propulsion system over the ship operating envelop. Thus, the system was simulated at various ship resistance conditions in the range from still water up to 55% added resistance. The two-stroke marine Diesel engine was approached by a MVEM and the Wageningen B-screw series polynomials were used to model the propeller. The ship resistance for still water was estimated by using the Holtrop method.

DIMOPOULOS *et al.* [22] presented the DNV COSSMOS modelling framework for integrated marine machinery systems. This is a tool based on mathematical descriptions of the physical and chemical process phenomena within machinery components and energy systems. It is capable to model, simulate and optimise ship energy systems in the steady state and transient conditions. Two case studies were performed to illustrate the advantages of this: the thermo-economic design and operation optimisation of a combined cycle system for large bulk carriers, and the transient operation simulation of an electric marine propulsion system.

MAN [23] presented an overview about LNGCs fitted with slow speed dual-fuel Diesel engines of HP concept and the high-pressure gas supply system. Furthermore, ordinary and dual-fuel Diesel engines within various configurations were compared in order to show the most suitable propulsion solution for modern ships. Configurations with one and two engines driving directly fixed and controllable pitch propellers, with and without re-liquefaction system, were addressed. Three different sizes of LNGCs were studied and the measure of merit used for the comparison was NPV.

CICHOWICZ *et al.* [24] introduced a methodology of assessing the dynamic energy performance of a ship at a global level for any given period of time. All the major energy systems inboard were modelled and integrated into an overall energy model, which was subjected to a set of environmental conditions and operational requirements. In this manner, the energy flows inboard were presented as a function of time for four case studies. A MVEM was used for modelling the engine, the Wageningen B-screw series polynomials were used for modelling the propeller and the still water resistance was estimated by the Holtrop method.

LU *et al.* [25] developed an accurate and practical ship operational performance prediction model that can be used to select the optimal routes for minimum fuel consumption, taking into consideration average ship speed, encountering sea states and voyage time. This model was developed by modifying the Kwon added resistance modelling method for taking into account the ship's specific characteristics achieved from its operational data (ship's noon reports) and sea trial data. The Holtrop method was used to estimate the still water resistance of the ship. Besides, a time-dependent fuel consumption increase rate after ship dry-docking was identified.

YANG and YEH [26] investigated the thermodynamic and economic performance optimisation for an organic Rankine cycle system recovering the waste heat of exhaust gas from a large marine Diesel engine for a merchant ship. A number of working fluids was employed in the ORC system with and without pre-heater equipped to evaluate the system's maximal performances. Besides the optimal operating pressures, the optimal pre-heater effectiveness for each working fluid was obtained. The measures of merit used in this work were thermal efficiency and net power output index.

Table 1.1 summarises particularities found in the literature references to be considered or improved by the approach to be proposed. It is worth noticing that not all of these features are aimed to be dealt with herein. They serve as a guide to identify the current research gap in that field and elaborate the dissertation proposal.

Table 1.1: Features of the references to be considered or improved.

Reference	To be considered	To be improved
[12]	+ dynamic simulation	- engine as 2D table
	+ simplicity	- service speed as output
[13]	+ dynamic simulation	- service speed disregarded
	+ various operating conditions	- ship not modelled
	+ two-stroke Diesel engine	
[14]	+ propeller optimisation	- Keller's cavitation criterion
	+ service speed optimisation	- fuel cost minimisation
	+ changeable operating conditions and hull resistance	- constant specific fuel consumption
[15]	+ genetic algorithm	- Keller's cavitation criterion
	+ strength constraint	- efficiency maximisation
	+ vibration consideration	- only propeller study
[16]	+ synthesis, design and operation optimisation	- propeller and hull disregarded
	+ particle swarm algorithm	- costs minimisation
[17, 18]	+ synthesis, design and operation optimisation	- propeller and hull disregarded
	+ NPV maximisation	- weather disregarded
	+ particle swarm algorithm	- COGES system
[19]	+ dynamic overall propulsion simulation	- optimisation disregarded
	+ two-stroke Diesel engine	- propulsion selection disregarded
[20]	+ pitch ratio optimisation	- efficiency maximisation
	+ speed optimisation	- profit maximisation
	+ dual-fuel Diesel engine	- one operating condition
[21]	+ overall propulsion simulation	- optimisation disregarded
	+ several operating conditions	- arbitrary service margins
	+ emissions estimation	
[22]	+ simulation and optimisation	- DNV COSSMOS software
	+ components model library	
[23]	+ dual-fuel two-stroke Diesel engine	- optimisation disregarded
	+ system with and without re-liquefaction	- arbitrary service margin
	+ emission fees	
[24]	+ systematic and scientific approach	- optimisation disregarded
	+ integrated overall energy model	- selection disregarded
[25]	+ weather consideration	- minimising fuel consumption
	+ route optimisation	- system selection disregarded
[26]	+ thermodynamics and economics	- propulsion disregarded
	+ equipment cost evaluation	

1.2.1 Gap to be filled

None reference studying optimisation of energy system selection, considering engine, propeller and weather conditions within an integrated approach, has been found. The lack of studies about optimisation of Diesel engine selection might arise from the lack of engine models suitable for optimisation problems. According to SCHULTEN [27], five main sorts of engine models could be recognised: computational fluid dynamics (CFD) models, phenomenological multi-dimensional models, crank angle models, mean value models and transfer function models.

Within CFD engine models, which are the most complexes, the volume studied is divided into thousands of volumes or elements, and the basic conservation equations are solved for each volume. Being usually used only for processes occurring inside the cylinder and the ducts of admission and discharge, this modelling provides detailed information and requires powerful computers, besides high computational time. On the other hand, if the cylinder is divided into a smaller number of volumes (tens) and, additionally to the basic conservation equations, phenomenological equations are solved, a phenomenological multi-dimensional model is obtained. These both approaches are definitely not suitable for optimisation problems considering the overall energy system of a ship.

Crank angle models are also called zero-dimensional engine models (0-DEMs) because these models do not have a strict mathematical dependence on any of the dimensions. It consists in treating each one of the various engine elements as a control volume and solving the differential equations with a time step equivalent to one degree of the crankshaft rotation. Nevertheless, whether an engine model is inserted into a larger system, such as a propulsion system, the variations that occur for each crankshaft angle of rotation are generally not of primary interest. In this case, overall engine operating parameters are the focus and they can be obtained by using a MVEM. This model basically has the same origin of the 0-DEM, but as its time step is in the order of one crankshaft rotation, the variation of each parameter within the cylinder is replaced by a mean value. Some references about 0-DEMs are [13, 28–30], whereas MVEMs were addressed in [19, 21, 24, 31–33]. Besides those, a combination of MVEM and 0-DEM for a large marine four-stroke Diesel engine was presented in [34].

When there is no interest in the engine's internal processes, the engine can be merely represented by functions that relate, for instance, load and speed to specific fuel consumption. This is the so-called transfer function engine model (TFEM), which is the simplest and fastest method. Precisely for these reasons, this sort of modelling is the most suitable for the design optimisation of the ship's overall energy system. Some references in this field are [12, 35–38]. However, none reference performed the engine selection optimisation since all models found must be calibrated for each single engine, which is inappropriate for iterative procedures.

1.3 Dissertation proposal

The present doctoral dissertation proposes a comprehensive early-stage approach to optimise the design, synthesis, and operation of LNGC energy systems considering economic and technical aspects, besides weather conditions. This approach must assess various configurations of propellers and prime movers to find the best matching and also consider a different number of propulsion chains. The need for a re-liquefaction plant must also be assessed. Constraints must be incorporated in order to avoid propellers that can present issues regarding strength, cavitation, and vibration. This approach must assess different operational profiles, regarding service speeds and fuel, in order to maximise the NPV. This measure of merit considers OPEX, income and capital expenditures (CAPEX).

By using the proposed approach, one is expected to be able to automatically search a broad range of possible alternatives, then make small refinements to achieve the optimal arrangement. Although this can be seen as an extension of what one could theoretically accomplish manually, the labour involved would be prohibitive. Thus, the main contributions of the present work is an engine model suitable to optimise the selection of dual-fuel two-stroke Diesel engines, as well as a comprehensive and integrated approach to optimise the energy system of LNGCs. Furthermore, with some adjustments, the methodology developed herein can apply to any ships.

In the next chapters are presented a brief literature review about LNGC energy systems (Chap. 2), then the development of an engine model suitable for optimisation problems, that is, one that does not need to be calibrated for each engine separately (Chap. 3). Afterwards, it is presented the developed approach (Chap. 4), the case study (Chap. 5), results and discussion (Chap. 6), and lastly the study's conclusions (Chap. 7). Besides, an additional chapter addressing the articles written during the doctoral period and future work proposals is included at the end of this document (Chap. 8).

Chapter 2

Literature review

This chapter addresses the main concepts of the most promising propulsion alternatives for LNGCs. Basic knowledge about re-liquefaction plant, environmental regulations and manners of reducing gaseous emissions are included as well. Lastly, alternatives to enhance the performance of the energy system by using the exhaust gas waste heat is presented.

2.1 Propulsion alternatives

As an alternative to the steam power plant, there are primarily the gas turbine and the diesel engine power plants, whereas secondarily fuel cells and Stirling engines, as well as renewable energy systems have been studied. Furthermore, combined and co-generation systems have also been used successfully on-board ships [39]. Gas turbine power plants present high power density, the capability to burn BOG and efficiency higher than steam turbine power plants. On the other hand, low redundancy, low efficiency in sea level and its high fuel consumption, as well as the fact of being a relatively untried technology for merchant ships make it a still unsure option. Nowadays, the Diesel engine is the most common prime mover for merchant ships and, with the development of on-board BOG re-liquefaction systems, it became also the most interesting alternative for LNGCs.

2.2 Diesel engines

Slow speed two-stroke diesel engines and on-board BOG re-liquefaction system have been used successfully in large LNGCs. A propulsion plant scheme as this one is illustrated in Fig. 2.1 (adapted from [40]), where is shown that all the generators and propulsion engines are fed with liquid fuel whereas the BOG is re-liquefied. The generators supply electric power for the re-liquefaction plant and for the other consumers on-board. Conceptually, the propulsion is separated from the BOG treatment in this case. There is also a gas combustion unit (GCU) in case the BOG amount is greater than the re-liquefaction capacity.

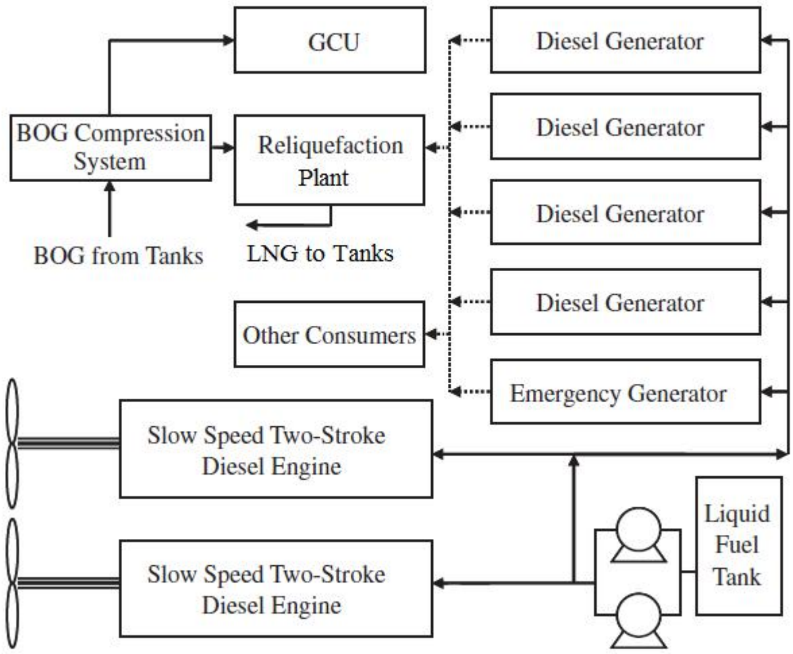
GCU
Diesel Generator
BOG Compression System
Reliquefaction Plant
Diesel Generator
Diesel Generator
BOG from Tanks
LNG to Tanks
Diesel Generator
Other Consumers
Emergency Generator
Slow Speed Two-Stroke Diesel Engine
Liquid Fuel Tank
Slow Speed Two-Stroke Diesel Engine

Figure 2.1: Propulsion plant scheme with slow speed two-stroke diesel engine and re-liquefaction plant.

Slow speed Diesel engines driving directly propellers, such as shown in Fig. 2.1, are the arrangement of most of the commercial ships, with proven performance and reliability. However, when conventional liquid fuel prices are higher than LNG price, the OPEX of this propulsion system is increased, as it is unable to use the BOG as fuel. Moreover, regarding environmental controls, conventional fuels are not as clean as the BOG. Thus, an option to overcome these drawbacks is to apply dual-fuel Diesel engines.

2.3 Dual-fuel Diesel engines

They are compression ignition engines capable of working with either conventional liquid fuels or gaseous fuels, namely that, in diesel or gas operating mode, respectively. During the diesel mode, these engines work as conventional Diesel engines, burning liquid fuels as heavy fuel oil (HFO), marine diesel oil (MDO) and marine gas oil (MGO), for instance. In the gas mode, a liquid pilot fuel injection is required to start the combustion process.

The specification of medium speed four-stroke dual-fuel Diesel machinery for LNG carrier new buildings in 2002 marked the ousting of steam turbine propulsion in commercial ships [5]. These engines require relatively low pressure (about 6 bar_g)

for the BOG to be used as fuel and are applied ordinarily with electric transmission, the reason why is known as dual-fuel Diesel electric (DFDE). It offers high fuel efficiency and freedom of fuel choice between fuel oil and BOG. On the other hand, DFDE systems include high capacity electric switchgear, frequency converters, and electric motors, which require a crew with special skills to maintain.

Figure 2.2 (adapted from [40]) illustrates an example of a DFDE scheme without re-liquefaction plant. In this case, the dual-fuel generators provide electric power for the electric motors, which drive the propeller through a gearbox, and for other consumers on-board. A GCU should be used when BOG is greater than the generators' consumption.

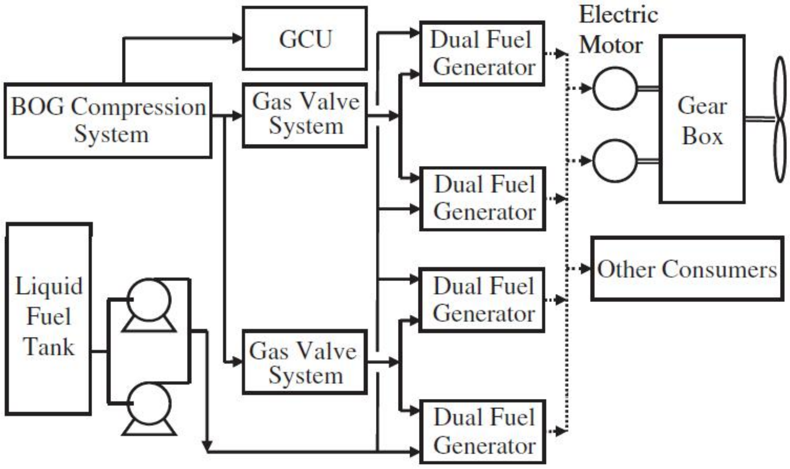

Figure 2.2: DFDE propulsion plant scheme without re-liquefaction plant.

An option to overcome the DFDE drawbacks is to use dual-fuel direct drive (DFDD), in which slow speed two-stroke dual-fuel Diesel engines should be used. They are a recent technology, such that the first LNG carrier fitted with this kind of machinery entered into service in 2016 [41]. Typical values of energy efficiency for DFDD systems can reach about 52% against 41% reached with DFDE. Figure 2.3 (adapted from [40]) illustrates a DFDD propulsion plant scheme where all the engines are dual-fuel ones, such that a re-liquefaction plant could be necessary or not, depending on the operational profile of the ship. LNGC energy systems must always include a GCU for the disposal of excess BOG to avoid pressure build-up in the cargo tanks. The use of GCU is typically required during the ship loading and unloading operations and when the BOG demand is low, as well as during the ship cool-down operation when excess BOG is generated.

When a slow speed two-stroke dual-fuel Diesel engine is working in gas mode there are two basic concepts about the gas injection pressure: low pressure (LP) and high pressure (HP). The LP concept illustrated in Fig. 2.4a is based on the premixed lean-burn principle, that is, gaseous fuel is injected into the cylinder at the mid-stroke position, such that an injection pressure below 16 bar_g is enough. When

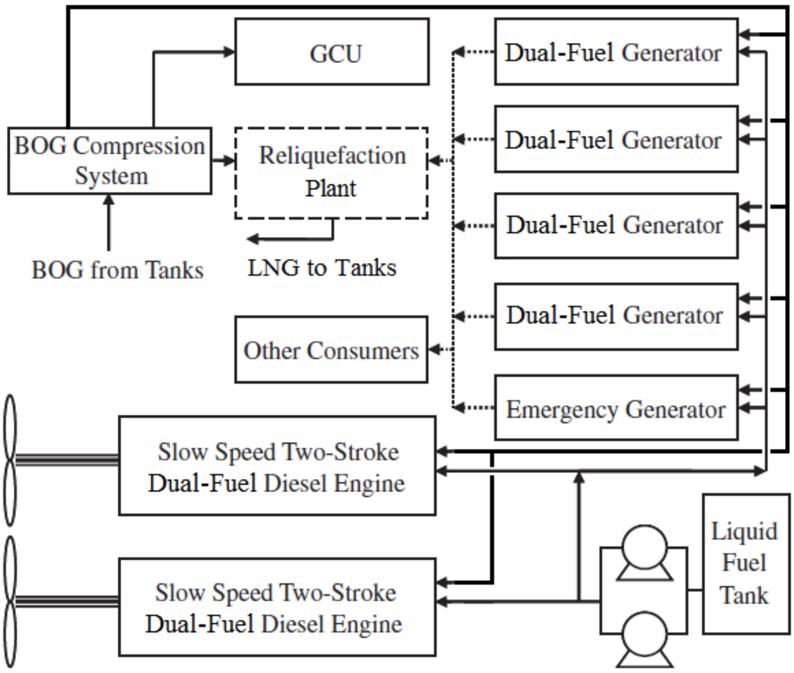
GCU
Dual-Fuel Generator
BOG Compression System
Reliquefaction Plant
Dual-Fuel Generator
Dual-Fuel Generator
BOG from Tanks
LNG to Tanks
Dual-Fuel Generator
Other Consumers
Emergency Generator
Slow Speed Two-Stroke Dual-Fuel Diesel Engine
Liquid Fuel Tank
Slow Speed Two-Stroke Dual-Fuel Diesel Engine

Figure 2.3: DFDD propulsion plant scheme.

the piston is close to the compression stroke end, the air/fuel charge is ignited by a liquid pilot fuel [42]. Differently, the HP concept is based on the diffusion combustion principle, as illustrated in 2.4b. In this case, the gas injection occurs close to the top dead centre, practically at the same time of the pilot fuel injection, such that a pressurised gas injection around 300 bar_g is necessary [43].

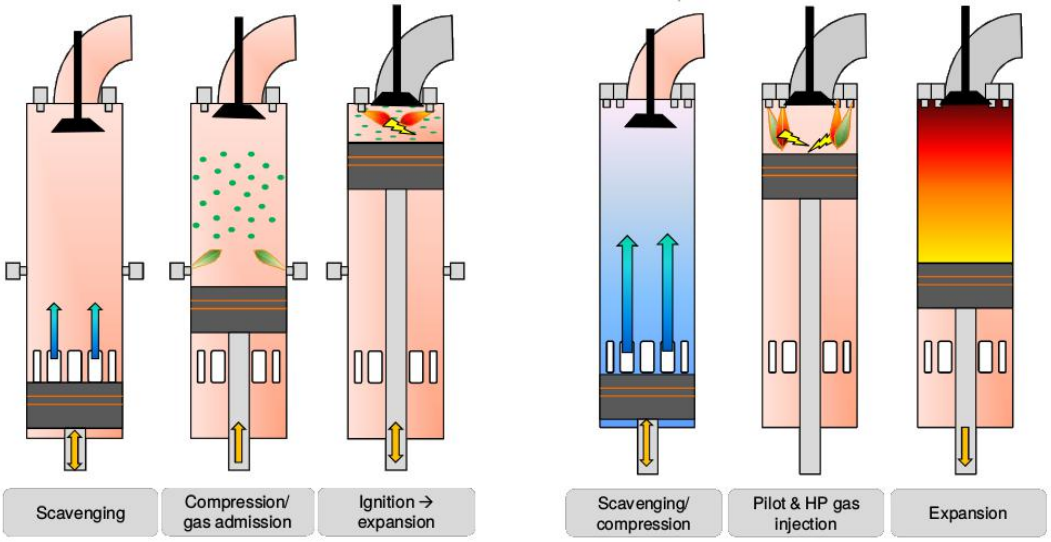
Scavenging
Compression/ gas admission
Ignition → expansion
Scavenging/ compression
Pilot & HP gas injection
Expansion

(a) LP concept (b) HP concept

Figure 2.4: Gas injection pressure concepts for slow speed two-stroke dual-fuel Diesel engines.

2.4 Standard selection of slow speed Diesel engines

In order to install the necessary propulsion power, the marine engineer needs details about the ship's resistance as well as the matching propeller/ship load and the delivered engine power [39]. The ship's power requirements, including margins and propeller speed, should be determined. In other words, there must be obtained the specified maximum continuous rating (SMCR), which is the operational point of maximum power at the maximum speed required in the continuous operation of the engine.

Considering engine's brake power and speed are both known at SMCR point, next step on engine selection is acquiring the layout diagram of the entire engines programme from various manufacturers. Then, by placing the SMCR point on them, one could identify every engine of each manufacturer able to supply the required power and speed. Figure 2.5 (adapted from [44]) shows engine layout diagrams of marine slow speed dual-fuel Diesel engines from MAN Diesel & Turbo Corporation.

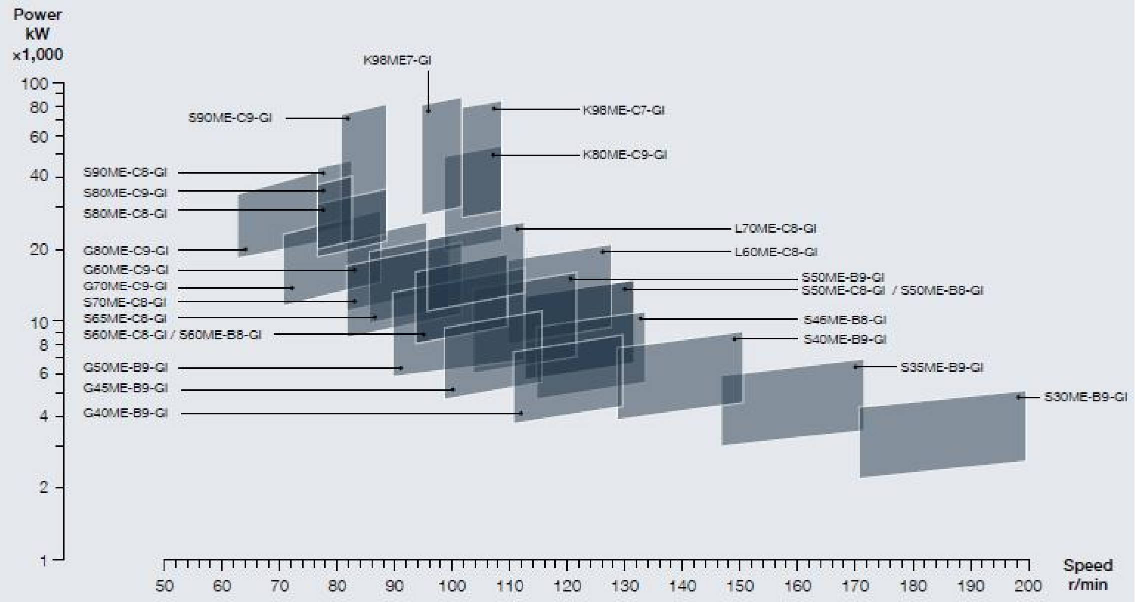

Figure 2.5: Layout diagrams of slow speed dual-fuel Diesel engines programme from MAN Diesel & Turbo.

Next step is determining how many cylinders are necessary through detailed information about each engine. Depending on the number of cylinders, every engine also owns a layout diagram wherein the ratio of power and speed can be selected. It is limited by envelopes defining the area where nominal maximum firing pressure is available for the selection of the SMCR. An engine layout diagram is limited by two lines of constant mean effective pressure (MEP), L1-L3 and L2-L4, and by two constant engine speed lines, L1-L2 and L3-L4, as illustrated in Fig. 2.6 (adapted from [45]). It is also shown SMCR point and nominal maximum continuous rating (NMCR) point, which is the same as L1.

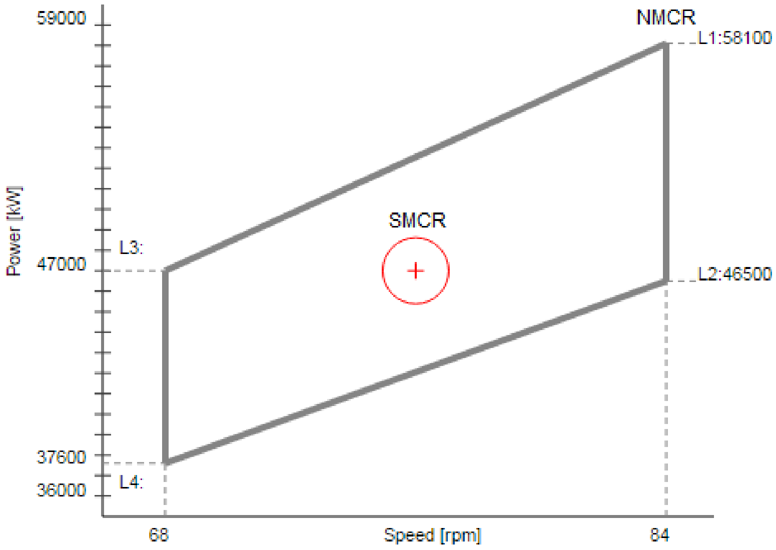

Figure 2.6: Engine layout diagram of the engine 10S90ME- C9.5-GI.

After listing engines and their number of cylinders to fulfil the requirements, the last step is considering some applicable selection criteria. Among these, technical aspects, as for example engine steady state performance data, can be achieved from engine shop trial measurements as well as by using catalogues. Furthermore, some engine manufacturers provide computational applications as the Computerised Engine Application System - Engine Room Dimensioning (CEAS-ERD) [45].

2.5 Re-liquefaction plant

The on-board re-liquefaction system is ideal for long journeys, avoiding BOG losses that are more significant as the journey is longer. Figure 2.7 (adapted from [1]) illustrates an example of turbo-expander refrigeration system for gas liquefaction. This type of system works by compressing and expanding a suitable fluid by the Brayton refrigeration thermodynamic cycle [46]. Typically, N_2 or CH_4 are used as the working fluid. The main advantages of using N_2 is that it is inherently safe and makes the system compact as it does not require any refrigerant storage and make-up. Additionally, starting up and shutting down the plant is quick, venting in an emergency situation is not a safety concern and no flaring is necessary.

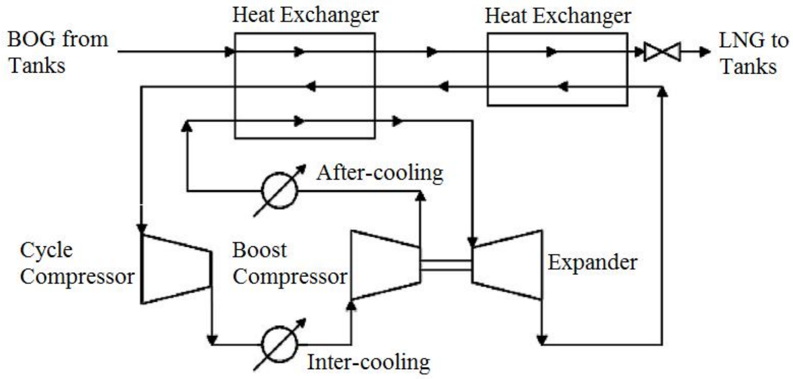

Figure 2.7: Re-liquefaction plant scheme.

2.6 Exhaust gas emissions

The exhaust gas from marine engines consists largely of N_2, oxygen (O_2), carbon dioxide (CO_2) and water vapour (H_2O), with some small quantities of carbon monoxide (CO), sulphur oxides (SO_x), nitrogen oxides (NO_x), non-combusted hydrocarbons (HC) and particulate materials (PM). Out of these, SO_x, NO_x, CO, HC and PM are considered noxious or toxic emissions. For some gases, such as SO_x and CO_2, the emission ratio is determined by fuel composition. On the other hand, for other gases, namely NO_x, CO, HC and PM, the emission ratio is dependent on load and speed of the engine, besides ambient conditions and engine technology.

The International Maritime Organisation (IMO) determines different levels (Tiers) of NO_x control applied based on the ship construction date. Within any particular Tier the actual limit value is determined from the engine rated speed (n_r), as shown in Tab. 2.1 (adapted from [47]). Nonetheless, the Tier III controls apply only to the specified ships while operating in emission control areas (ECAs) established to limit NO_x emissions. Outside such areas, Tier II controls apply. Differently, SO_x and PM emission controls apply to all fuel oil combustion equipment and devices on-board. These controls divide between those applicable inside ECAs and those applicable outside such areas. They are primarily achieved by limiting the maximum sulphur content of the fuel oils. These fuel oil sulphur limits are subject to a series of step changes over the years, as shown in Tab. 2.2 (adapted from [47]).

Table 2.1: NO_x emission limits in g/kWh.

Tier	Ship construction date	$n_r < 130$	$130 \leq n < 2000$	$n_r \geq 2000$
I	on or after 01/01/2000	17.0	$45 \cdot n^{-0.20}$	9.8
II	on or after 01/01/2011	14.4	$44 \cdot n^{-0.23}$	7.7
III	on or after 01/01/2016	3.40	$9 \cdot n^{-0.20}$	2.0

Temperature, time and oxygen concentration are the dominating influences in the formation of NO_x. Hence, the higher the temperature, oxygen concentration and residence time at high temperature in the cylinder, the greater the amount of NO_x created. This explains why low-speed two-stroke engines generate higher NO_x emissions than medium and high-speed four-stroke engines of equivalent power output [5]. That is the reason why as engine speed increases, NO_x limit decreases in Tab. 2.1.

Table 2.2: Fuel oil sulphur limits expressed in percentage by weight

Outside an ECA	Inside an ECA
4.5% prior to 1 January 2012	1.5% prior to 1 July 2010
3.5% on and after 1 January 2012	1.0% on and after 1 July 2010
0.5% on and after 1 January 2020*	0.1% on and after 1 January 2015

*Depending on the outcome of a review to be concluded by 2018 as to the availability of the required fuel oil, this date could be deferred to 1 January 2025.

2.7 Emissions reduction

Apart from the use of alternative fuels, primary and secondary measures can be pursued for reducing NO_x emission levels. The former aims reducing the amount of NO_x formed during combustion by optimising engine parameters, such as valve timing, fuel injection and turbo-charging. In this way, emission levels can be reduced by 30 to 60%. The latter aims removing NO_x from the exhaust gas by downstream cleaning techniques (exhaust gas after-treatment). That way, reductions of over 95% can be achieved [5]. Some examples of exhaust gas after-treatment concepts are exhaust gas recirculation (EGR) and selective catalytic reduction (SCR).

The EGR concept consists in cooling and cleaning an exhaust gas amount (30 to 40%) and recirculate it to scavenge air side [48]. Therefore, part of the O_2 in scavenge air is replaced by exhaust gas, which is rich in CO_2 and H_2O. The effect on NO_x formation is partly due to a reduction of the O_2 concentration in the combustion zone, and partly due to the higher heat capacities of H_2O and CO_2. Scavenge air with increased heat capacity reaches lower peak combustion temperature. This method can achieve reduction of 50 to 60% of NO_x emission, but in return, its reliable operation calls for fuels with low sulphur contents. Figure 2.8 (adapted from [48]) illustrates an engine room arrangement, where there are many types of equipment necessary to make EGR works. This figure shows a tank of caustic soda (NaOH), water treatment unit (WTU), collecting tank unit (CTU) and sludge tank, as well as a scrubber alongside the engine. Freshwater is abbreviated as FW in that figure.

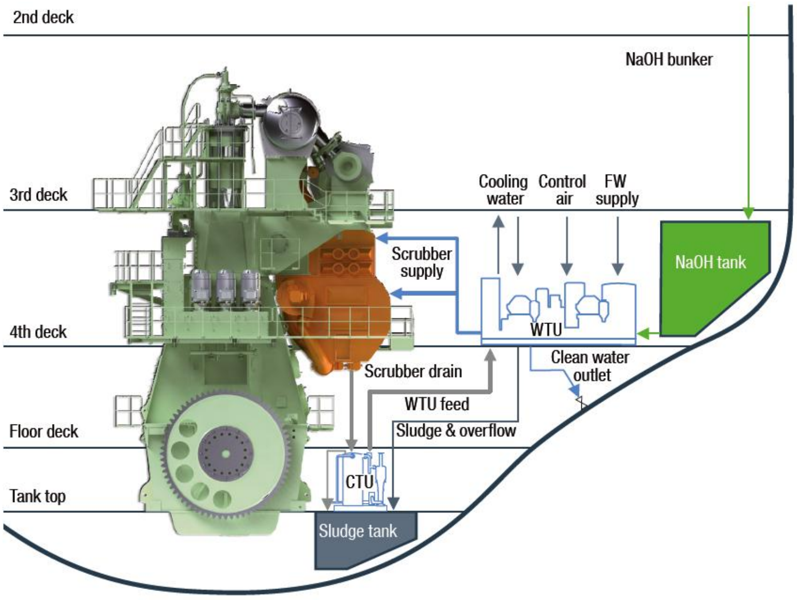

Figure 2.8: Engine room arrangement with EGR.

On the other hand, the SCR process consists in reducing NO_x catalytically in N_2 and H_2O by adding ammonia (NH_3) as a reducing agent in an SCR reactor [48]. Furthermore, parts of the soot and HC in the exhaust gas are also removed by oxidation in the SCR process reactor. This concept can achieve a reduction of over 90% of NO_x emission, but in return, its reliable operation also calls for fuels with low sulphur contents. Figure 2.9 (adapted from [48]) illustrates a SCR engine room arrangement, where some additional subsystems are also required. This figure shows a urea tank, a urea supply system, a control system, a vaporiser/mixer and an SCR reactor, as well as a soot blower and a compressor.

Regarding SO_x and PM emission reduction, the simplest solution is burning fuels with low sulphur content. However, fuel oils with low sulphur are more expensive than those of high sulphur; thus, alternative exhaust gas after-treatments have been developed. Chemical and washing/scrubbing desulphurisation processes can remove SO_x and PM from the exhaust gas by bringing it into intensive contact with an alkaline fluid. In open loop systems, the alkaline fluid is seawater (SW) whereas, in closed loop systems, recirculated freshwater (FW) mixed with caustic soda (NaOH) is used. These two concepts can be combined in a hybrid installation, such as illustrated in Fig. 2.10 (adapted from [48]).

Just as EGR and SCR, scrubber systems require additional equipment, such as a tank of caustic soda (NaOH), a sludge tank, a circulation tank, a water cleaning unit (WCU), a circulation pump and a cooler (Fig. 2.10). Moreover, exhaust gas scrubbers are heavy, need significant installation space and produce large quantities of waste-water and sludge. This water has to be properly treated before discharge into the sea, and the sludge must be disposed of at reception facilities ashore.

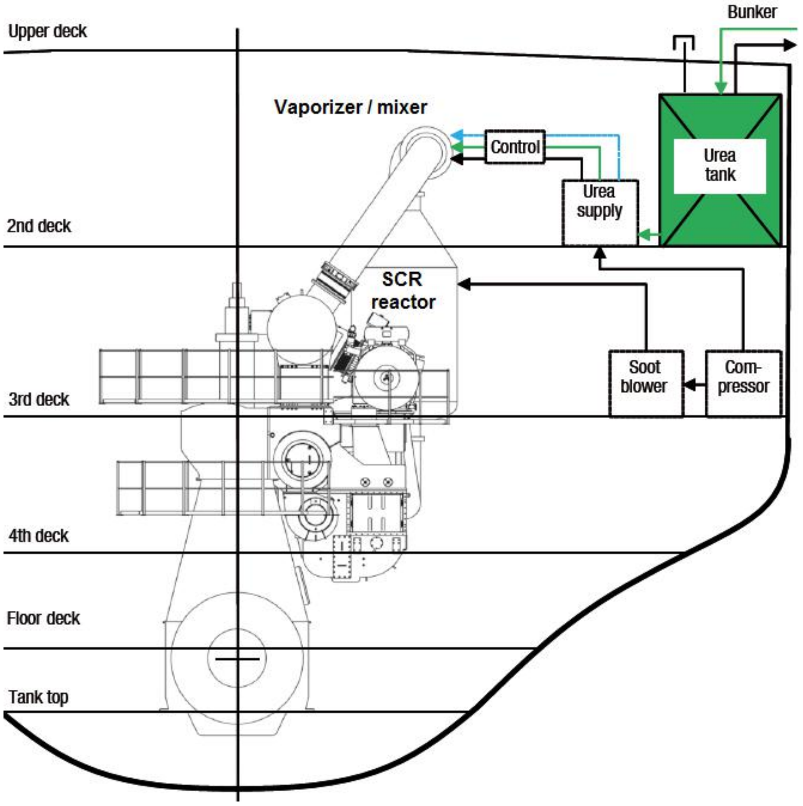

Figure 2.9: Engine room arrangement with SCR.

As can be noticed, there are manners to burn low quality and cheap fuels and fulfil the IMO requirements by applying exhaust gas after-treatment equipment. However, all those alternatives bring drawbacks such as voluminous subsystems to be installed in the engine room, use of environmentally unfriendly chemicals, as well as they slightly deteriorate the engine efficiency and increase the CO_2 emissions. Therefore, using natural gas as the fuel is the most recommended solution in order to reduce emissions. Its main constituent (CH_4) contains the highest amount of hydrogen per unit of energy of all fossil fuels. The specific CO_2 emissions are typically reduced by 20% compared with HFO or MDO. The corresponding reduction in NO_x emissions lies between 85 and 90%, whereas SO_x and PM are almost eliminated. Moreover, benzene emissions are reduced by around 97%, there is no visible smoke, no sludge deposits and no lead emissions [5].

2.8 Waste heat recovery systems

In order to enhance the overall energy efficiency of a power plant, an option ever more considered is using the waste heat to generate steam and/or power by means of a waste heat recovery system (WHRS). Main engine exhaust gas energy is by far the most attractive among the waste heat sources of a ship because of the heat flow and temperature. Moreover, the exhaust gas heat dissipation accounts for about half of

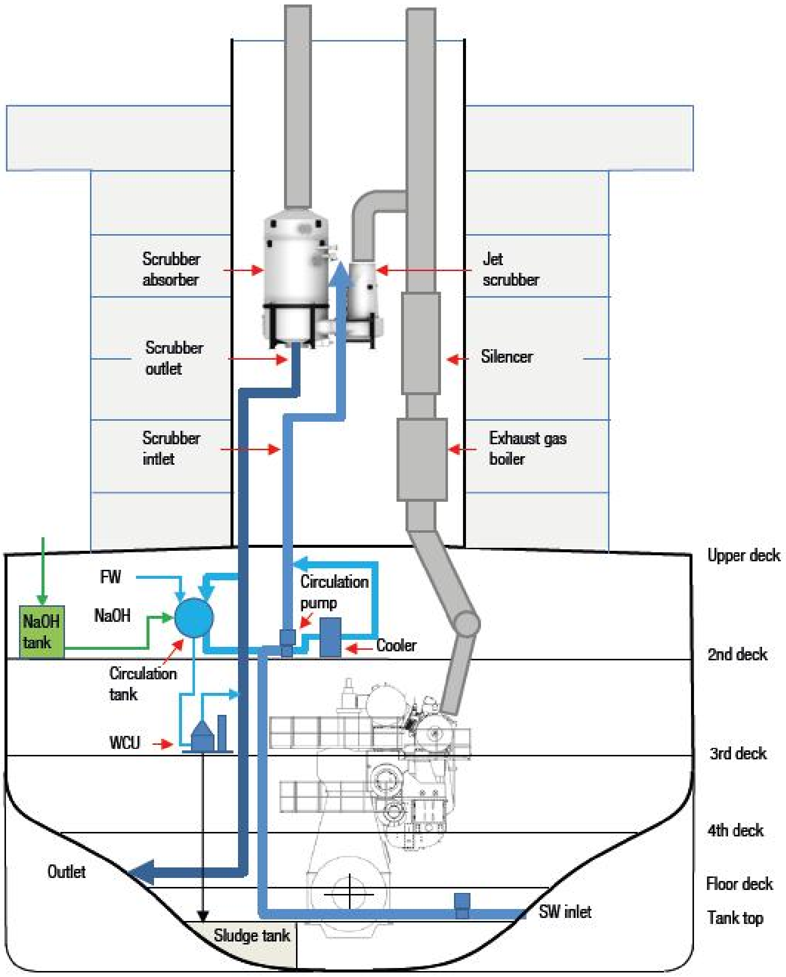
Scrubber absorber
Jet scrubber
Scrubber outlet
Silencer
Scrubber intlet
Exhaust gas boiler
Upper deck
FW
Circulation pump
NaOH
NaOH tank
Cooler
2nd deck
Circulation tank
WCU
3rd deck
4th deck
Outlet
Floor deck
SW inlet
Tank top
Sludge tank

Figure 2.10: Engine room arrangement with a hybrid system of SO_x scrubber.

the total waste heat, which is about one-fourth of the total fuel energy. In many cases, a WHRS is able to supply the ship's total need of electricity as a standalone power source, but it can also run in parallel with a shaft generator, shaft motor and auxiliary diesel generating sets. This type of advanced power system requires though an advanced power management system [49].

Different principles of WHRS are readily available depending on the level of complexity acceptable to the owner and shipyard and the actual electrical power consumption on-board. Ordinarily, an exhaust gas boiler is used to provide heating steam for ship services, but also there are manners to benefit from that waste heat to provide power. This can be achieved by a power turbine (PT), a steam turbine (ST) or even a combination of both, as shown in Fig. 2.11 (adapted from [49]).

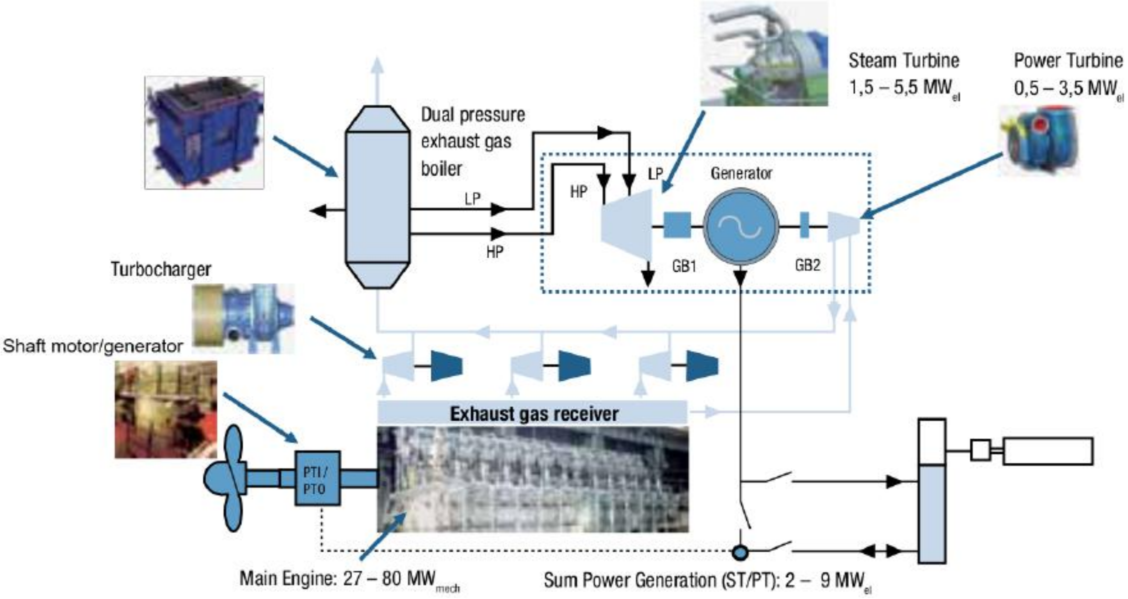
Steam Turbine
1,5 – 5,5 MW$_{el}$
Power Turbine
0,5 – 3,5 MW$_{el}$
Dual pressure
exhaust gas
boiler
LP
HP
HP
LP
Generator
GB1
GB2
Turbocharger
Shaft motor/generator
Exhaust gas receiver
PTI/
PTO
Main Engine: 27 – 80 MW$_{mech}$
Sum Power Generation (ST/PT): 2 – 9 MW$_{el}$

Figure 2.11: Main WHRS principles.

The PT principle consists in an exhaust gas driven turbine connected to a generator via a gearbox. The power turbine is installed on a separate exhaust gas pipe from the exhaust gas receiver, which bypasses the turbochargers. Power equivalent to approximate 3.1% of the main engine shaft power can be on average achieved by this principle. Similarly, the ST principle consists in a steam driven turbine connected to a generator via a gearbox. The steam is produced in a large exhaust gas driven boiler installed on the main engine exhaust gas piping system. This principle is more efficient and reaches about 5.6 to 6.9% of the main engine shaft power. On the other hand, an electrical output of over 11% of the main engine power can only be achieved by utilising a WHRS comprising both steam and power turbines and combined with utilising scavenge air energy for exhaust boiler feed-water heating.

Chapter 3

Developed engine model

This chapter proposes a simple and fast model to be used in the selection optimisation of marine slow speed two-stroke dual-fuel Diesel engines. To avoid consulting the catalogue data for every engine, every time the iterative process is carried out, the engine operational features are normalised and the deriving trends are approximated by polynomials.

3.1 Methodology

The algorithms for developing the proposed model were implemented in MatLab environment. Owing to the data availability of the web-based application CEAS-ERD, only engines provided by MAN Diesel & Turbo and covered by this application were studied [45]. Lower heating value has been taken as 42.7 MJ/kg and 50 MJ/kg for liquid fuel and gaseous fuel, respectively. Standard ambient conditions provided by the International Organisation for Standardisation (ISO) and sulphur content of 3.5% were also assumed.

Although engine type designation refers to the number of cylinders, stroke/bore ratio, diameter of piston, engine concept, mark number, fuel injection concept and Tier III technology, narrow engine configurations are studied here. Since all the addressed engines are not equipped with Tier III technology, they hold the same fuel injection concept (GI)[1] and engine concept (ME-C)[2]; these appointments are not always repeated. Furthermore, only standard configurations of engines were taken.

---

[1] Gas injection methane

[2] Electronically controlled

3.1.1 Engine layout diagrams

All necessary information to plot the layout diagrams for the 16 engines considered herein is presented in Tab. 3.1. Brake power per cylinder on the four points of the envelope ($P_{Bc,L1}$, $P_{Bc,L2}$, $P_{Bc,L3}$ and $P_{Bc,L4}$), speed limits (n_{min} and n_{max})[3] and limitations on the number of cylinders ($Z_{c,min}$ and $Z_{c,max}$) are also listed in the table. As it may be noticed, only engines of type G (green ultra-long stroke) and S (super long stroke) were studied.

Table 3.1: Available ME-GI slow speed dual-fuel engines and their particulars to chart layout diagrams.

Engine	$P_{Bc,L1}$	$P_{Bc,L2}$	$P_{Bc,L3}$	$P_{Bc,L4}$	n_{min}	n_{max}	$Z_{c,min}$	$Z_{c,max}$
	kW/cylinder				rpm		cylinder	
G95-9.5	6870	5170	6010	4520	70	80	5	12
G90-10.5	6240	4670	5350	4010	72	84	5	12
S90-10.5	6100	4880	5230	4180	72	84	5	12
S90-9.5	5810	4650	4700	3760	68	84	5	12
G80-9.5	4710	3550	3800	2860	58	72	6	9
S80-9.5	4510	3610	4160	3330	72	78	6	9
G70-9.5	3640	2740	2720	2050	62	83	5	8
S70-8.5	3270	2610	2620	2100	73	91	5	8
S65-8.5	2870	2290	2330	1860	77	95	5	8
G60-9.5	2680	2010	1990	1500	72	97	5	8
S60-8.5	2380	1900	1900	1520	84	105	5	8
G50-9.5	1720	1290	1360	1020	79	100	5	9
S50-9.5	1780	1420	1350	1080	89	117	5	9
S50-8.5	1660	1330	1340	1070	102	127	5	9
G45-9.5	1390	1045	1090	820	87	111	5	8
G40-9.5	1100	825	870	655	99	125	5	8

3.1.2 Specific fuel consumption at SMCR

Since specific fuel consumption at SMCR depends on its position on the engine layout diagram, the SMCR was placed on the points L1, L2, L3 and L4 and the operational features of every engine were analysed. Hence, the CEAS-ERD was run four times for every of the 16 engines, summing up 64 runs. Considering the propeller law with loads between 10 and 100% of SMCR, this application provides a table with specific fuel consumption [g/kWh], exhaust gas mass flow [kg/s], mixed exhaust gas temperature after turbocharger [°C] and a guiding steam production capacity of an exhaust gas boiler at 7.0 bar_a[4] [kg/h].

---

[3] Subscripts *max* and *min* stand respectively for maximum and minimum

[4] Absolute pressure

Firstly, exhaust gas mass flow (MF) and temperature (T) were divided by brake power to obtain specific mass flow (SMF), in kg/kWh, and specific temperature (ST), in °C/MW, as stated in Eq. 3.1 and 3.2, respectively. Then, all operational features at SMCR were divided by themselves at NMCR to obtain normalised specific fuel consumptions (SFOC$_N$, SGC$_N$ and SPOC$_N$)[5] and normalised specific exhaust gas data (SMF$_N$ and ST$_N$) regarding NMCR. Equation 3.3 illustrates this procedure for SFOC$_N$.In these equations, P_B is brake power [kW]; the index i varies between 1 and 19 representing engine loads between 10 and 100% with a step of 5% of the SMCR; j varies between 1 and 4 representing the SMCR position (L1, L2, L3 and L4) and k varies between 1 and 16 representing the engines.

$$SMF_{ijk} = \frac{MF_{ijk}}{P_{B,ijk}} \cdot 3600 \tag{3.1}$$

$$ST_{ijk} = \frac{T_{ijk}}{P_{B,ijk}} \cdot 1000 \tag{3.2}$$

$$SFOC_{N,jk} = \frac{SFOC_{SMCR,jk}}{SFOC_{NMCR,k}} \tag{3.3}$$

Polynomial surfaces about specific fuel consumptions at SMCR normalised with respect to NMCR and their percentage errors of regression are illustrated in Fig. 3.1, whilst normalised exhaust gas polynomial surfaces and percentage errors are shown in Fig. 3.2. In both figures, regressions were performed as function of mean effective pressure and engine speed normalised with respect to NMCR (MEP$_N$ and n_N), as defined by Eq. 3.4 and 3.5, respectively.

$$MEP_N = \frac{MEP_{SMCR}}{MEP_{NMCR}} \tag{3.4}$$

$$n_N = \frac{n_{SMCR}}{n_{NMCR}} \tag{3.5}$$

Table 3.2 provides the coefficients (p) for every polynomial surfaces formulated as in Eq. 3.6, where z represents SPOC$_N$, SGC$_N$, SFOC$_N$, SMF$_N$ and ST$_N$, x is n_N and y is MEP$_N$.

$$z = p_{00} + p_{10} \cdot x + p_{01} \cdot y + p_{20} \cdot x^2 + p_{11} \cdot x \cdot y + p_{02} \cdot y^2 \tag{3.6}$$

Mean effective pressure may also be written as in Eq. 3.7 [39]. Since number of cylinders (Z_c), revolutions of crankshaft per complete working cycle (r) and cylinder swept volume (V_S) are engine constants, MEP$_N$ could also be written as in Eq. 3.8. Hence, n_N and MEP$_N$ could be calculated with support of Tab. 3.1.

---

[5] Subscript N stands for normalised with respect to NMCR

Table 3.2: Coefficients of the polynomial surfaces.

Coefficients	SPOC_N	SGC_N	SFOC_N	SMF_N	ST_N
p_{00}	2.297	0.7858	0.8326	1.118	7.320
p_{10}	-0.003505	-0.0003174	-0.0004246	-0.3700	-5.328
p_{01}	-1.295	0.2143	0.1675	0.1291	-5.883
p_{20}	0	0	0	0.1533	1.552
p_{11}	0	0	0	-0.03078	1.548
p_{02}	0	0	0	0	1.791

$$MEP = \frac{r}{Z_c \cdot V_S} \cdot \frac{P_B}{n} \tag{3.7}$$

$$MEP_N = \frac{P_{SMCR}}{n_{SMCR}} \cdot \frac{n_{NMCR}}{P_{NMCR}} \tag{3.8}$$

As illustrated in Fig. 3.1, normalised specific fuel consumptions vary almost linearly with respect to MEP_N and are practically not influenced by n_N, hence they could be approached by plans. In contrast, exhaust gas parameters vary with respect to both MEP_N and n_N, such that plans are not the best approach. Although specific fuel consumptions differ in gas and diesel modes, exhaust gas features are quite similar, thus only one trend of SMF_N and ST_N are shown in Fig. 3.2. Moreover, either engines of type G or S did not present substantial differences and, for this reason, they were analysed together.

It draws attention that the two largest deviations regarding SFOC_N (Fig. 3.1) are around 1.4%, whilst all others do not even reach 0.3%. This is due to engine G40ME-C9.5-GI, which is the only standard fitted with conventional turbocharger instead of high-efficiency turbocharger. On the other hand, the error regarding SPOC_N peaks at 1.8% and its average is comparably higher. Just as the SFOC_N, SGC_N presents only two increased deviations, not above 1.5%, whilst others do not reach 0.3%, which is also due to that engine. On the other hand, only minor deviations peaking at about 0.2% are noticed regarding SMF_N in Fig. 3.2. Similarly, the largest deviation regarding ST_N is under 0.7%.

3.1.3 Specific fuel consumption at part load

In this case, after obtaining the specific operational features in different engine loads, they were divided by themselves at SMCR. Hence, the normalised specific fuel consumptions (SFOC_S, SGC_S, SPOC_S)[6] and the normalised specific exhaust gas parameters (SMF_S and ST_S) with respect to SMCR were acquired. Equation

---

[6] Subscript S stands for normalised with respect to SMCR

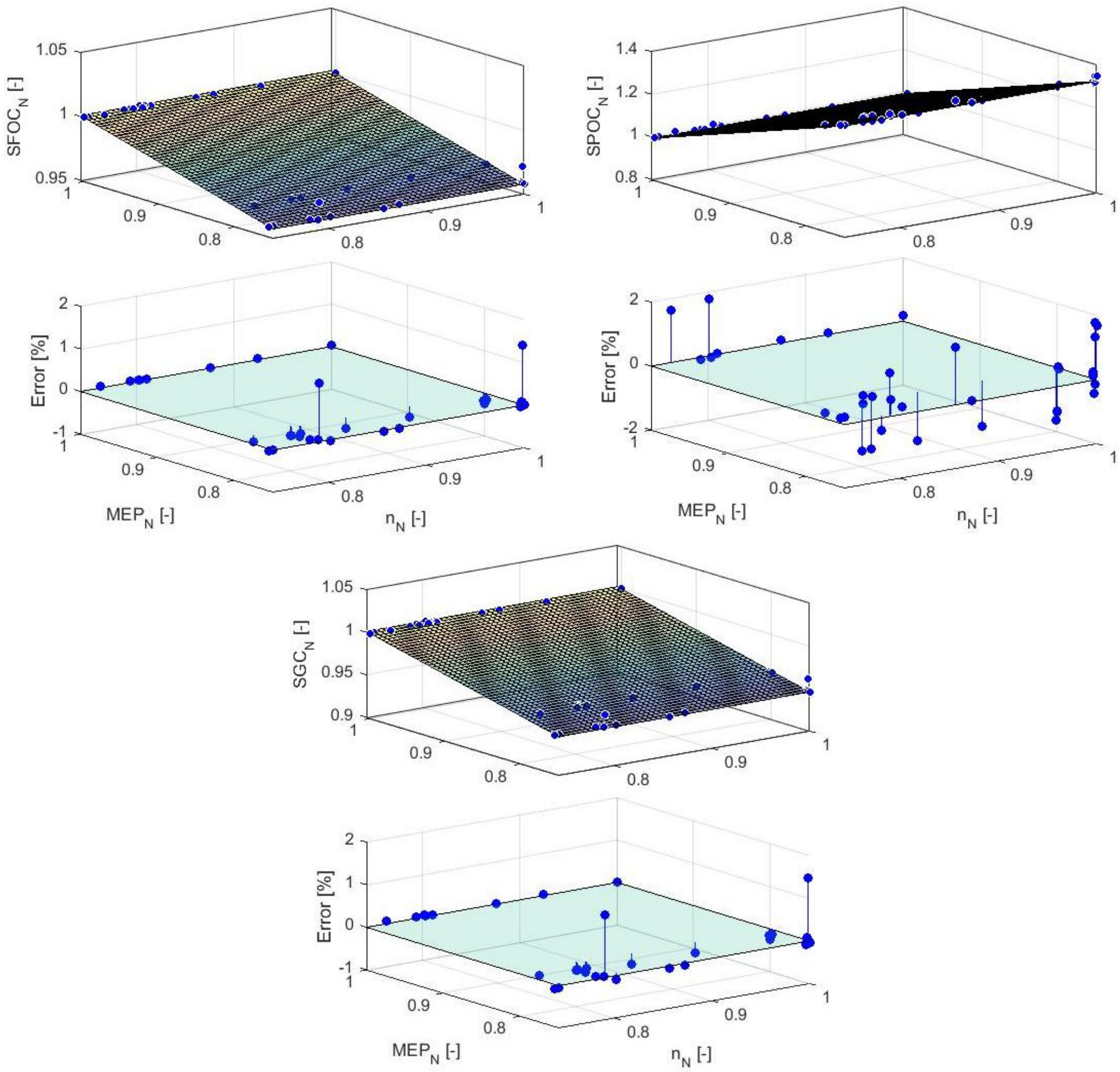

Figure 3.1: Polynomial surfaces of the specific fuel consumptions normalised with respect to NMCR and respective percentage errors of regression.

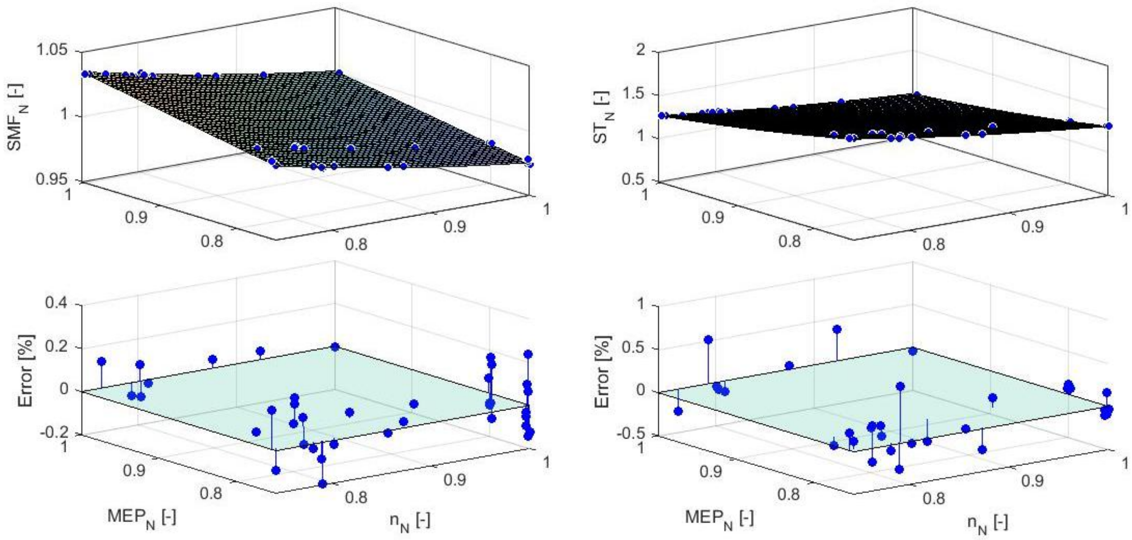

Figure 3.2: Polynomial surfaces of the exhaust gas parameters normalised with respect to NMCR and respective percentage errors of regression.

3.9 exemplifies this procedure for SFOC$_S$, where the index i varies between 1 and 19 representing engine loads between 10 to 100%; j varies between 1 and 4 representing the SMCR position and k varies between 1 and 16 representing the engines.

$$SFOC_{S,ijk} = \frac{SFOC_{ijk}}{SFOC_{SMCR,jk}} \tag{3.9}$$

Table 3.3 provides the coefficients for every polynomial curves formulated as in Eq. 3.10, in which y represents SPOC$_S$, SGC$_S$, SFOC$_S$, SMF$_S$ and ST$_S$, and x is engine load. Every curve was obtained by using centring and scaling transformation to improve the numerical properties of both polynomial and fitting algorithm, hence x is normalised by the mean (μ) and standard deviation (σ) given in Tab. 3.3.

$$y = p_0 + p_1 \cdot x + p_2 \cdot x^2 + p_3 \cdot x^3 + ... + p_8 \cdot x^8 \tag{3.10}$$

Since some datasets were approached by more than one polynomial, the letters in Tab. 3.3 (a, b and c) indicate the load range where the polynomial is suitable. Regarding SGC$_N$, letters indicate respectively ranges from 80 to 100%, 35 to 75% and 10 to 35% load. About SMF$_N$ and ST$_N$, “a” indicates a range from 35 to 100% and “b” from 10 to 30% load. In addition, Intervals not covered by polynomials could be approximated through linear interpolation.

Table 3.3: Coefficients of the polynomial curves.

Co.	SPOC$_N$	SGC$_N$			SFOC$_N$	SMF$_N$		ST$_N$	
		a	b	c		a	b	a	b
p_0*	1485	984.1	956.8	973.6	991.1	1117	1564	1357	4596
p_1*	-486.0	9.381	-8.131	-8.866	-37.61	-72.29	-167.1	-443.1	-1349
p_2*	255.6	1.295	2.578	4.834	15.05	-4.884	73.82	205.3	169.8
p_3*	-133.9	0	1.244	0	20.71	3.002	-56.51	-69.99	0
p_4*	-46.64	0	0	0	-1.715	0	34.01	25.05	0
p_5*	35.38	0	0	0	-10.17	0	0	-4.821	0
p_6*	49.72	0	0	0	2.932	0	0	0	0
p_7*	-26.17	0	0	0	0.7298	0	0	0	0
p_8*	0	0	0	0	-0.1642	0	0	0	0
μ	55.00	90.00	55.00	22.50	55.00	67.50	20.00	67.50	20.00
σ	27.39	7.082	12.92	8.550	27.39	20.16	7.077	20.16	7.077

*All coefficient values are multiplied by 1000.

Polynomial curves for the specific fuel consumptions normalised with respect to SMCR and their percentage errors of regression are shown in Fig. 3.3, whereas normalised exhaust gas polynomial curves and percentage errors are shown in Fig. 3.4. In both figures, regressions were performed as a function of brake power given in percentage of SMCR ($P_B[\%SMCR]$), which is the same as engine load.

Figure 3.3 shows that SFOC_S presented the minimum value for engine load of 70%. Although there are 64 datasets, they are mostly superimposed such that there are basically four data streams for brake power below 70% of SMCR. Moreover, the mismatches rise as engine load decreases, such that the greatest error is 1.8% for 10% load. Differently, SPOC_S grows steadily as load declines and its error is quite dispersed with a maximum about 1.9% for 80% load. Meanwhile, four polynomials were needed to approximate more accurately the behaviour of SGC_S, which also presented a global minimum for 70% load. However, two data streams stand out and the deviation peaks at -3.3%, whilst all the others reach at most -1.3%. This is again due to engine G40ME-C9.5-GI, which is the only one fitted with a conventional turbocharger.

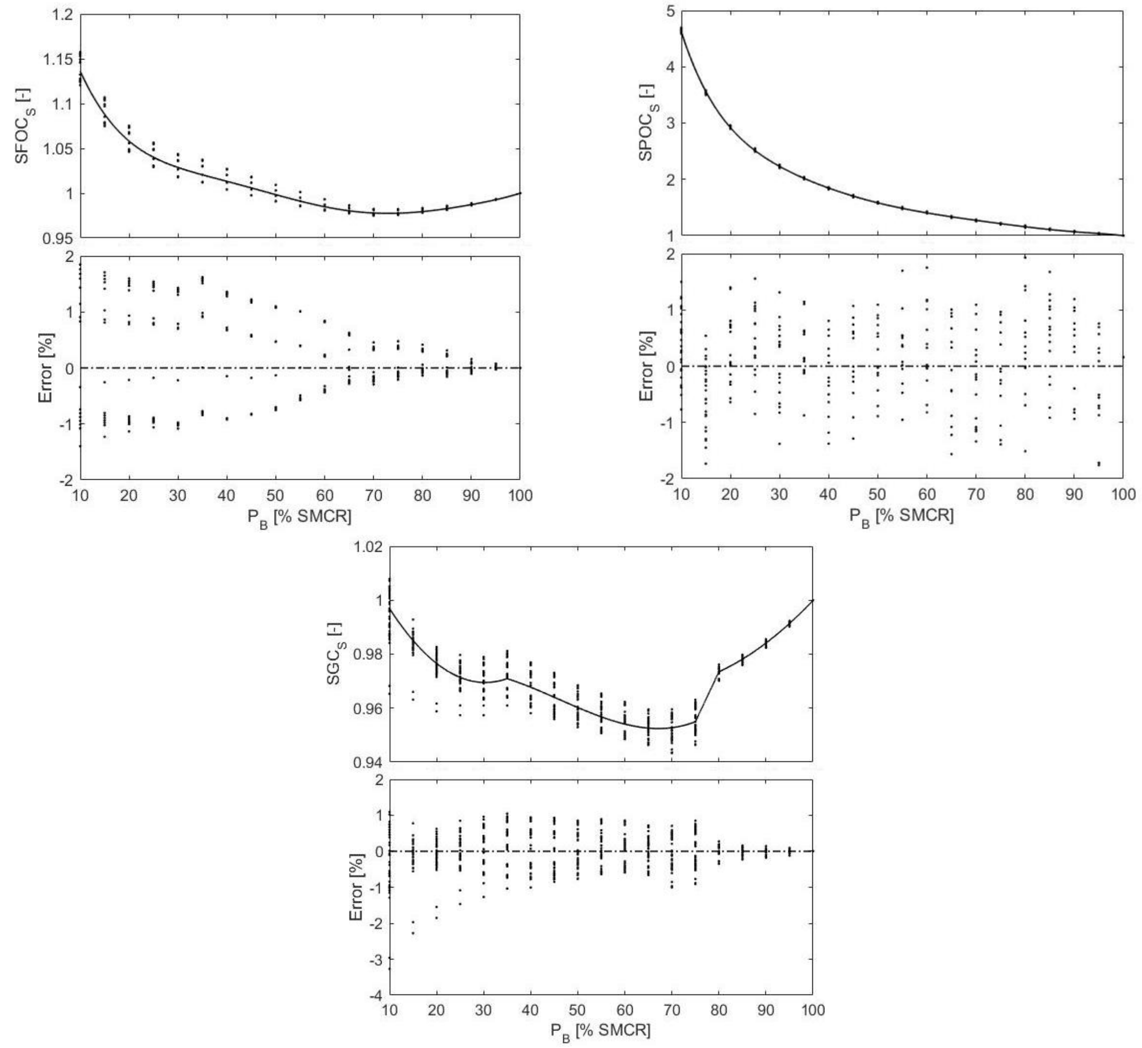

Figure 3.3: Polynomial curves of the specific fuel consumptions normalised with respect to SMCR and respective percentage errors of regression.

In order to approach specific exhaust gas mass flow and temperature normalised with respect to SMCR (SMF_S and ST_S), three polynomials were applied, as shown in Fig. 3.4. In both cases, wider percentage errors happened for lower loading conditions, such that for 20% load the error reached 1.5% and for 10% load the error peaked at 5.4%, respectively about SMF$_S$ and ST$_S$.

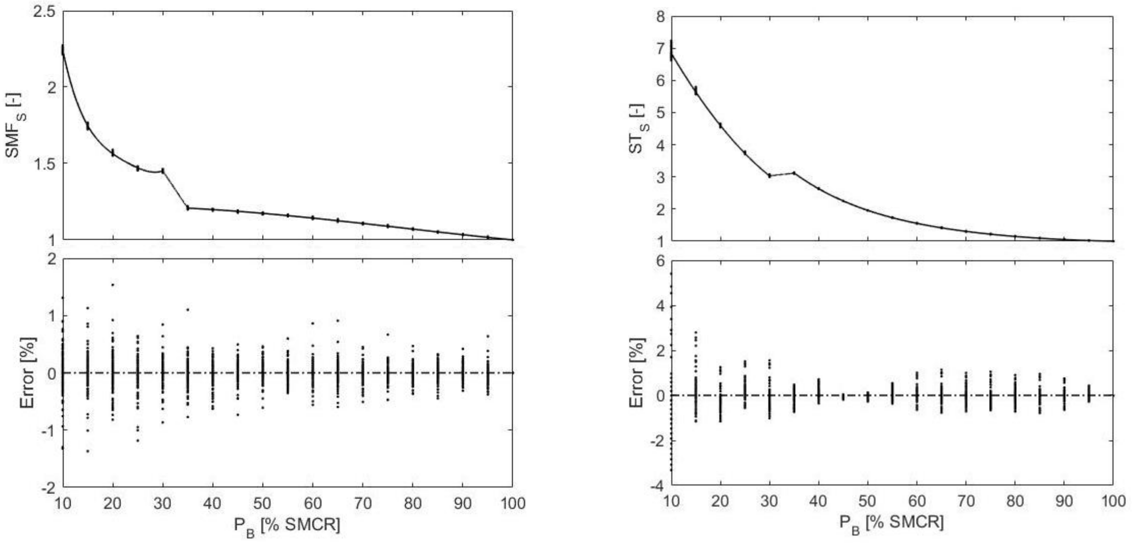

Figure 3.4: Polynomial curves of the exhaust gas parameters normalised with respect to SMCR and respective percentage errors of regression.

3.2 Statement of the model

The model consists of computing the specific fuel consumptions for any operating point, that is, at any engine speed and brake power, by equations such as Eq. 3.11 and 3.12, which exemplify the procedure for SFOC and exhaust gas MF. Any specific fuel consumption can be calculated analogously to SFOC whereas the exhaust gas temperature can be calculated analogously to MF. As one can notice, the procedure to evaluate exhaust gas parameters is different because they were formerly converted into specific variables (divided by brake power). Thus, Eq. 3.12 takes into account brake power at SMCR ($P_{B,SMCR}$) and load fraction (f_{SMCR}). Besides the polynomials previously acquired, the parameter of interest must be known at NMCR in both equations. Thus, Tab. 3.4 lists all necessary information for every engine either in gas or diesel operating mode.

$$SFOC = SFOC_{NMCR} \cdot SFOC_N \cdot SFOC_S \tag{3.11}$$

$$MF = SMF_{NMCR} \cdot SMF_N \cdot SMF_S \cdot P_{B,SMCR} \cdot f_{SMCR} \tag{3.12}$$

Table 3.4: Specific features at NMCR for gas and diesel mode.

Engine	Gas mode				Diesel mode		
	SPOC	SGC	SMF	ST	SFOC	SMF	ST
	g/kWh		kg/kWh	°C/MW	g/kWh	kg/kWh	°C/MW
G95-9.5	5.0	136.7	7.943	2.863	166.0	7.965	2.911
G90-10.5	4.9	135.9	7.942	3.152	165.0	7.966	3.205
S90-10.5	5.0	136.7	7.943	3.224	166.0	7.967	3.279
S90-9.5	5.0	136.7	8.040	3.385	166.0	8.065	3.442
G80-9.5	5.0	136.7	7.745	5.567	166.0	7.762	5.662
S80-9.5	5.0	136.7	8.239	5.814	166.0	8.266	5.913
G70-9.5	5.0	137.5	7.739	7.933	167.0	7.764	8.070
S70-8.5	5.0	139.2	8.243	8.830	169.0	8.271	8.983
S65-8.5	5.0	139.2	8.639	10.06	169.0	8.671	10.24
G60-9.5	5.0	137.5	7.942	10.77	167.0	7.959	10.96
S60-8.5	5.0	139.2	8.641	12.13	169.0	8.660	12.34
G50-9.5	5.0	138.3	7.744	14.92	168.0	7.767	15.18
S50-9.5	5.0	139.2	7.640	14.42	169.0	7.663	14.67
S50-8.5	5.1	140.0	8.651	15.46	170.0	8.675	15.73
G45-9.5	5.1	140.0	7.640	21.22	170.0	7.673	21.58
G40-9.5	5.2	144.1	7.364	29.09	175.0	7.364	29.55

3.3 Validation of the model

Two engines of intermediary NMCR were simulated and the results were compared against catalogue data (CEAS-ERD). Since the polynomials were reached considering SMCR on L1, L2, L3 and L4, it is necessary to investigate the model accuracy in intermediate points. Therefore, SMCR was additionally placed in the centre of the engine layout diagram (LC), such that the engine 8G70ME-C9.5-GI was examined for 22.3 MW and 73 rpm, as well as the engine 8S70ME-C8.5-GI was examined for 21.1 MW and 82 rpm.

Figures 3.5 and 3.6 show fuel consumption and exhaust gas parameters from the model compared with catalogue data for the engine 8G70ME-C9.5-GI and 8S70ME-C8.5-GI, respectively. Noticeably, the model is able to predict the behaviour of specific fuel consumptions and exhaust gas with only minor mismatches, even when SMCR is on LC. Although exhaust gas mass flow coincides in diesel and gas mode (MF and MF_g[7]), the temperature in gas mode (T_g) is lower than in diesel mode (T) and presents an almost constant difference.

Figures 3.7 and 3.8 illustrate the percentage errors of the model in diesel and gas mode for the engines 8G70ME-C9.5-GI and 8S70ME-C8.5-GI, respectively. The

---

[7] Subscript g stands for gas mode

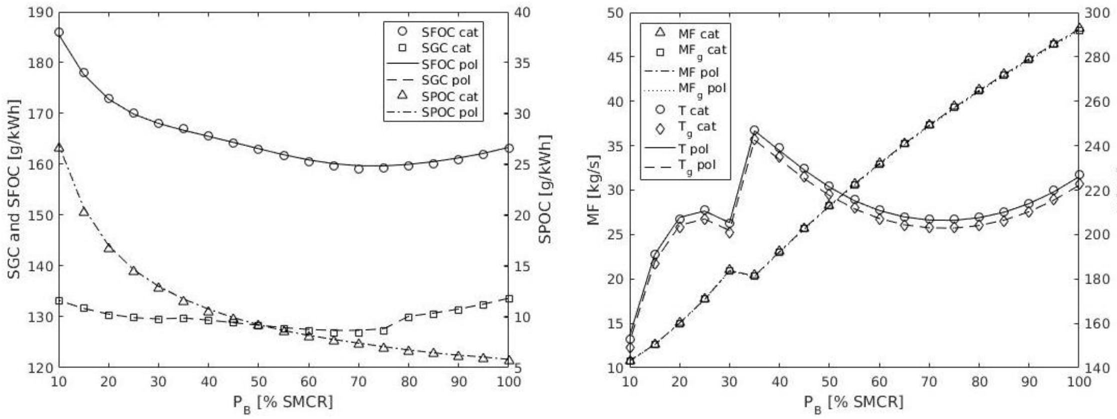

Figure 3.5: Fuel consumption and exhaust gas parameters from the model compared with catalogue data for the engine 8G70ME-C9.5-GI.

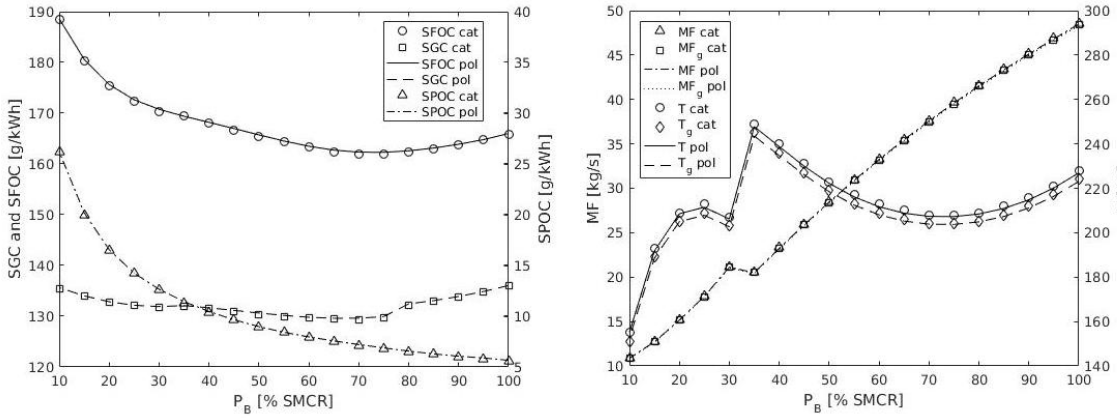

Figure 3.6: Fuel consumption and exhaust gas parameters from the model compared with catalogue data for the engine 8S70ME-C8.5-GI.

largest deviations about specific fuel oil consumption (SFOC$_e$[8]) and exhaust gas temperature (T_e) occurs for the engine 8G70ME-C9.5-GI when the load is 10%. The former is approximately 1.6% when SMCR is either on L2 or L4, and the latter is -2.4% when SMCR is on L3, as shown in Fig. 3.7a. The engine 8S70ME-C8.5-GI holds the highest exhaust gas mass flow error (MF$_e$), which also come about 10% load, for SMCR on L3, and accounts for -0.6% in Fig. 3.8a.

The biggest errors in gas mode, about specific gas consumption (SGC$_e$), exhaust gas mass flow (MF$_e$) and temperature (T_e), occur for 10% of SMCR whilst the greatest deviation regarding specific pilot oil consumption (SPOCe) takes place when the engine load is 95%. The engine 8G70ME-C9.5-GI holds the highest SPOC$_e$ and T_e, which are around -2.5 and -3.4%, as well as happen when SMCR is on LC and L3, respectively (3.7b). On the other hand, 8S70ME-C8.5-GI holds the highest SGC$_e$ and MF$_e$, respectively around -1.1 and 0.6%, and these values happen respectively when SMCR is on L2 and LC, as shown in Fig. 3.8b.

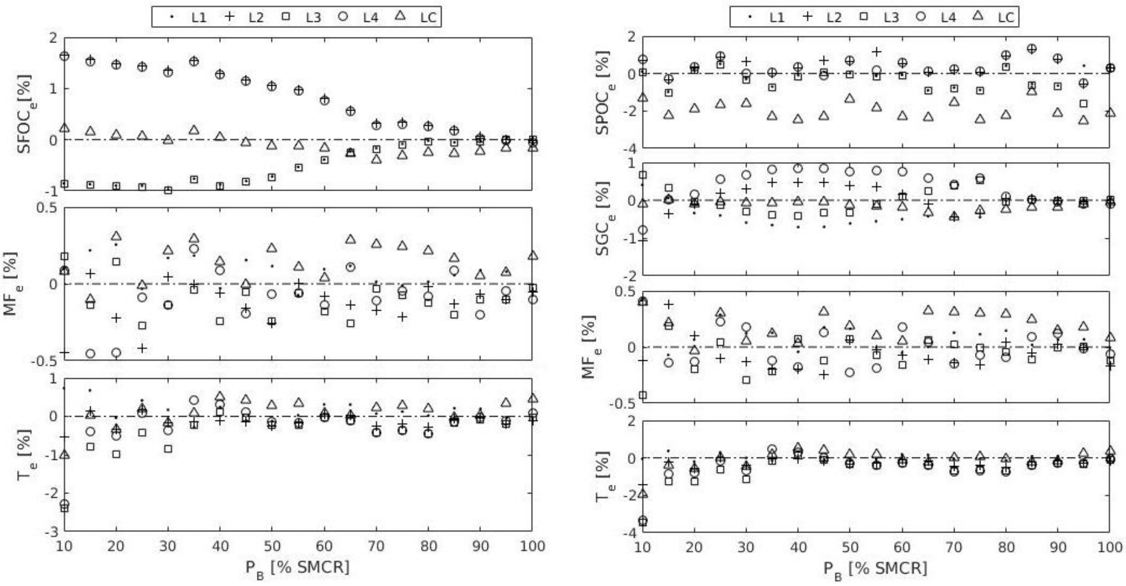

(a) Diesel mode (b) Gas mode

Figure 3.7: Modelling errors for the engine 8G70ME-C9.5-GI.

The results' assessment revealed that the model was not only capable to represent adequately the behaviour of the variables but also presented acceptable percentage errors. The majority of the biggest deviations regarding the two simulated engines occurred for engine load of 10% and they did not exceed -3.4%, even when SMCR was placed on the centre of layout diagram. Having this figure as quite acceptable, the model may be utilised successfully when one is interested in exhaust gas mass flow and temperature, as well as specific fuel consumptions. Therefore, a simple and fast model to be applied in optimisation problems about the selection of marine

---

[8] Subscript e stands for error

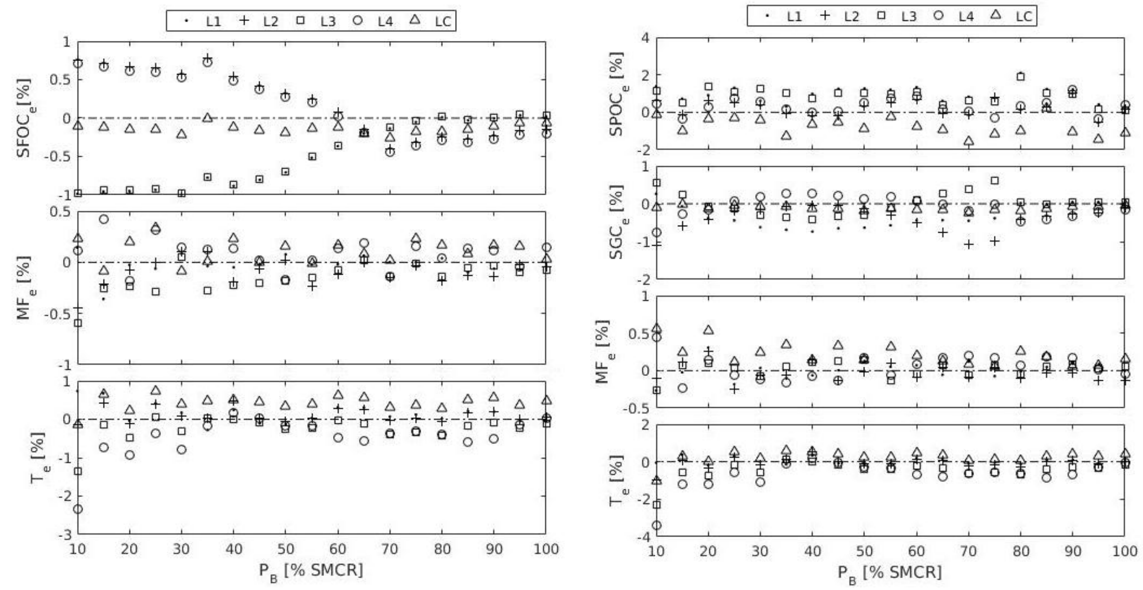

(a) Diesel mode (b) Gas mode

Figure 3.8: Modelling errors for the engine 8S70ME-C8.5-GI.

dual-fuel low-speed diesel engines can be considered developed.

3.4 Strengths of the model

The main strengths that make the model suitable for the present purpose are listed following.

+ Only a few input data are required to apply the model, namely: operating engine features in the NMCR, the polynomial surfaces and curves, as well as the power in the SMCR and a load fraction, in case of part load.

+ The model is capable to calculate specific fuel consumptions, exhaust gas mass flow and temperature for every engine working from 10% to 100% of SMCR, wherever this point is placed on the envelope.

+ The model presents just small deviations.

+ The processing time is under 0.4 seconds, thereby the model can be considered fast enough.

+ The model is simple and easy to implement, as well as an individual calibration for each engine is unnecessary.

3.5 Limitations of the model

Although that model is suitable for the present purpose, some improvements may be incorporated in the future. Thus, in order to guide future works, a list of limitations of the model is presented following.

- Only engines of the type ME-C-GI were used, that is, those whose fuel injection timing and actuation of exhaust valves, starting valves and cylinder lubrication are electronically controlled. Moreover, only engines fitted with high-efficiency turbochargers and without gas after-treatment devices were considered. In other words, only default configurations were used. Thus, Tier III technologies, varied fuel injection concepts, control types, and turbochargers, as well as other optimised load ranges, fuel sulphur contents and ambient conditions could have been taken into account.

- Only engines manufactured by MAN Diesel & Turbo were included in the study. A broader range of engines could have been used in case other manufacturers provide complete information of their engines.

- As the CEAS-ERD application correlates engine speed with power by the propeller law, the individual effect of them was not accounted. This is an interesting aspect to be enhanced in the future.

Chapter 4

Developed approach

Next, it is explained in detail a comprehensive early-stage approach to optimise the synthesis, design and operation of LNGC energy systems. The approach developed in this chapter considers economic and technical aspects, as well as weather conditions, seeking to be minimally complete.

4.1 Methodology

In order to set up a comprehensive approach to be used for shipowners and marine engineers, the proposed approach goes over technical and economic aspects as well as considers the weather along the route. Since the net present value (NPV) is a common economic measure of merit, the method consists in an optimisation process whose objective function to be maximised is the NPV and the design variables are propulsion parameters and service speeds. Thus, the purpose is finding the synthesis of components, their design characteristics and the operational profile that maximise the NPV of an LNGC.

Herein, synthesis of components refers to the condition of the propulsion system to hold one or two main engines, each one driving a propeller, and the existence of shipboard re-liquefaction. The components design characteristics refer to the propeller and engine specification. The operational profile refers to the service speed and the fuel to be burnt in each part of the journey, namely the fuel profile. Once a computational environment became necessary, all the computations were performed in MatLab. The proposed approach was explained hereinafter by means of flowcharts and then an overview of each model was addressed.

Figure 4.1 illustrates the proposed approach towards the optimisation of synthesis, design and operation for an LNGC energy system. This figure shows the different computations that were followed, as well as their input and output data. Given a guess of optimisation design variables, that is, propulsion parameters and service speed, the first step is estimating the brake power and shaft speed in service for each route-track, as detailed in Fig. 4.2. The next steps are computing the specified maximum continuous rating (SMCR) and then determining the suitable engines, still considering the initial guess of design variables. The fourth step is assessing the NPV for each suitable engine considering the different fuel profiles, as detailed in Fig. 4.3. Having accomplished this, it is performed a simple search for the matching of engine and fuel profile that holds the maximum NPV, which is the optimum for that guess of design variables.

All these steps are executed iteratively by the optimisation algorithm, and convergence is verified at the end of each run. If the algorithm converged, the optimum engine-propeller matching was reached; otherwise, a new guess of propulsion parameters is taken by the optimisation algorithm, as detailed in Fig. 4.4. Similarly, if there is no suitable engine among the available options during a run, that initial guess of design variables is considered infeasible, and the optimisation algorithm interrupts the run to guess new design variables and come back to the first step.

In order to estimate brake power and shaft speed in service for each route-track, the procedure shown in Fig. 4.2 was proposed. It starts by computing the total hydrodynamic resistance concerning specified weather conditions and then computing the total resistance in service conditions. Next comes the computation of propulsion factors, followed by calculation of propeller performance. Having accomplished this, technical constraints related to strength, cavitation and vibration are verified. If any of these criteria are not met, the design variables are considered infeasible and the run is interrupted; otherwise, the run proceeds to the computation of brake power in service.

The net present value (NPV) estimation for each matching of engine and fuel profile is achieved by following the procedure illustrated in Fig. 4.3, where is shown the computations and their input and output data. It consists of computing capital expenditures (CAPEX), operational expenditures (OPEX) and then the NPV.

Figure 4.4 shows the iterative procedure of the differential evolution optimisation algorithm applied. It is an evolutionary and stochastic algorithm; in other words, it attempts to mimic nature and does not make use of the gradient of the objective function as a direction of optimisation [50]. Firstly, one individual (design) is randomly created by the uniform distribution (continuous) approach [51] and its objective function is assessed. If design variables are infeasible, that individual is rejected and another is created to replace it; otherwise, this individual is kept in the population. This is done until a full population is created, such that there are only capable individuals (feasible design variables) in the initial population. Then, an offspring member is generated from the initial population and its objective function is assessed. If the offspring is better than its main progenitor, it replaces its main

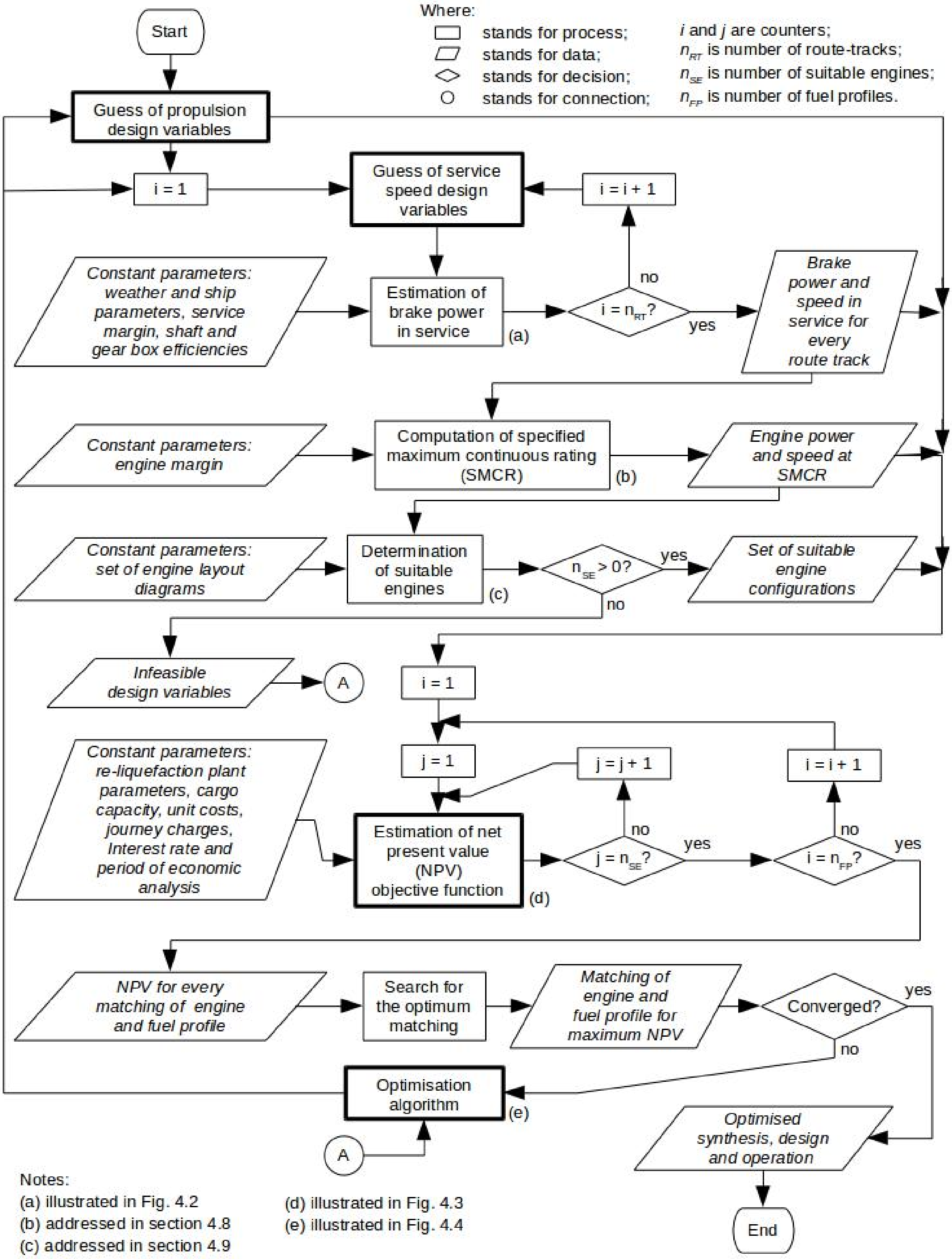
Where:
stands for process;
stands for data;
stands for decision;
stands for connection;
i and j are counters;
n_{RT} is number of route-tracks;
n_{SE} is number of suitable engines;
n_{FP} is number of fuel profiles.
Start
Guess of propulsion design variables
i = 1
Guess of service speed design variables
i = i + 1
Constant parameters: weather and ship parameters, service margin, shaft and gear box efficiencies
Estimation of brake power in service
(a)
$i = n_{RT}$?
no
yes
Brake power and speed in service for every route track
Constant parameters: engine margin
Computation of specified maximum continuous rating (SMCR)
(b)
Engine power and speed at SMCR
Constant parameters: set of engine layout diagrams
Determination of suitable engines
(c)
$n_{SE} > 0$?
yes
no
Set of suitable engine configurations
Infeasible design variables
A
i = 1
j = 1
j = j + 1
i = i + 1
Constant parameters: re-liquefaction plant parameters, cargo capacity, unit costs, journey charges, Interest rate and period of economic analysis
Estimation of net present value (NPV) objective function
(d)
$j = n_{SE}$?
no
yes
$i = n_{FP}$?
no
yes
NPV for every matching of engine and fuel profile
Search for the optimum matching
Matching of engine and fuel profile for maximum NPV
Converged?
yes
no
Optimisation algorithm
(e)
A
Optimised synthesis, design and operation
End
Notes:
(a) illustrated in Fig. 4.2
(b) addressed in section 4.8
(c) addressed in section 4.9
(d) illustrated in Fig. 4.3
(e) illustrated in Fig. 4.4

Figure 4.1: Optimisation approach towards synthesis, design and operation of an LNGC energy system.

]

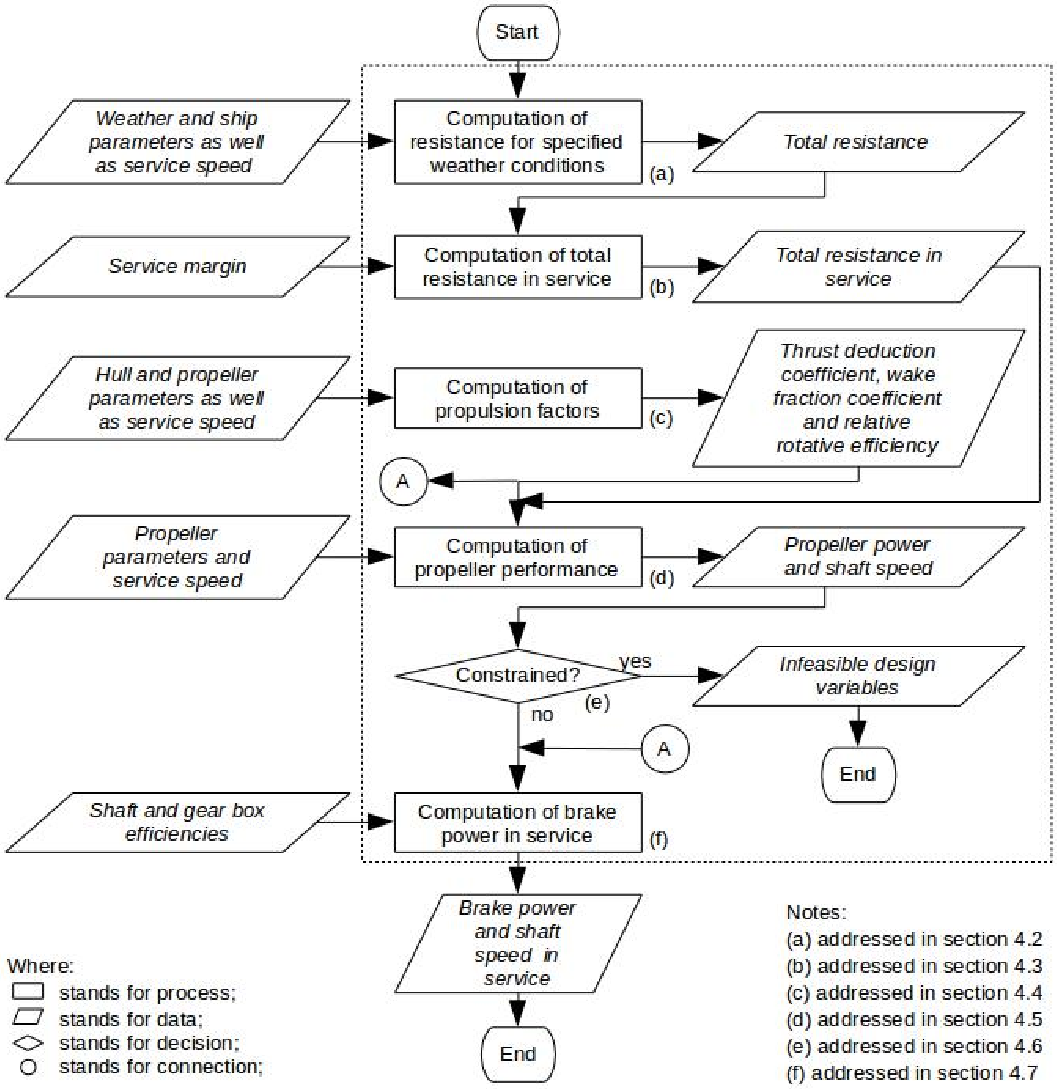
Start
Weather and ship parameters as well as service speed
Computation of resistance for specified weather conditions
(a)
Total resistance
Service margin
Computation of total resistance in service
(b)
Total resistance in service
Hull and propeller parameters as well as service speed
Computation of propulsion factors
(c)
Thrust deduction coefficient, wake fraction coefficient and relative rotative efficiency
A
Propeller parameters and service speed
Computation of propeller performance
(d)
Propeller power and shaft speed
Constrained?
yes
no
(e)
Infeasible design variables
A
End
Shaft and gear box efficiencies
Computation of brake power in service
(f)
Brake power and shaft speed in service
End
Where:
▭ stands for process;
▱ stands for data;
◇ stands for decision;
○ stands for connection;
Notes:
(a) addressed in section 4.2
(b) addressed in section 4.3
(c) addressed in section 4.4
(d) addressed in section 4.5
(e) addressed in section 4.6
(f) addressed in section 4.7

Figure 4.2: Brake power and shaft speed estimation in service for each route-track.

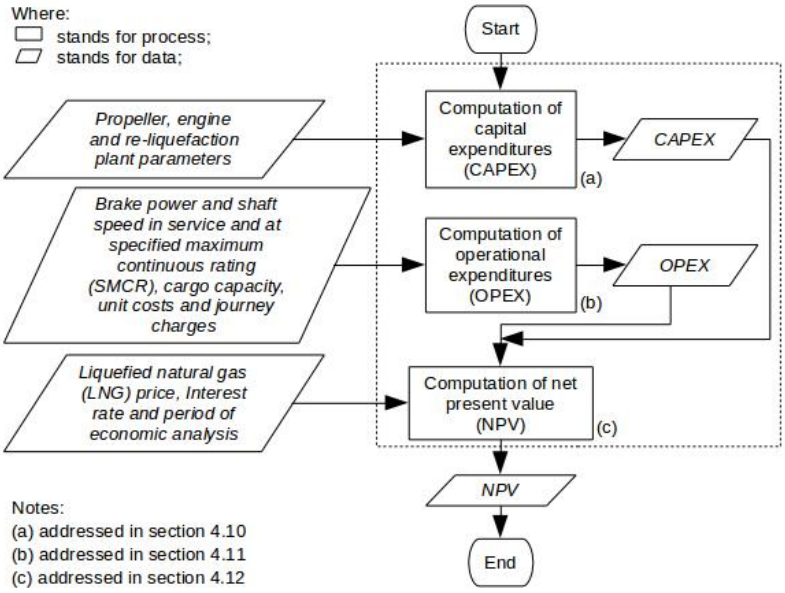
Where:
stands for process;
stands for data;
Start
Propeller, engine and re-liquefaction plant parameters
Computation of capital expenditures (CAPEX)
(a)
CAPEX
Brake power and shaft speed in service and at specified maximum continuous rating (SMCR), cargo capacity, unit costs and journey charges
Computation of operational expenditures (OPEX)
(b)
OPEX
Liquefied natural gas (LNG) price, Interest rate and period of economic analysis
Computation of net present value (NPV)
(c)
NPV
End
Notes:
(a) addressed in section 4.10
(b) addressed in section 4.11
(c) addressed in section 4.12

Figure 4.3: Net present value estimation for each matching of engine and fuel profile.

progenitor in the population; otherwise, the offspring is rejected. This proceeds until every member of the initial population has been the main progenitor of an offspring, that is, until a generation has elapsed. The best member of the population after a predetermined number of generations is considered the optimum design.

4.2 Computation of resistance for specified weather conditions

According to CARLTON [52], many approaches can be used to compute total ship resistance in still water, as well as to estimate added resistance due to rough weather. Regarding still water, the usual approach whenever algebraic models are required is the well-known Holtrop-Mennen model [53] [54], which is a statistical power prediction method based on a regression analysis of random model experiments and full-scale test data. Based on geometric parameters and speed, this model provides an approximated value of the total propulsion resistance in still water ($R_{T,sw}$).

Owing to the occurrence of rough weather during voyages, the resistance changes and affects the behaviour of the vessel. In order to predict the added resistance, semi-empirical approaches are more suitable than others more complexes in cases where a high computational time is a trouble [25]. The Kwon's model [55] is an approximate method for predicting speed loss of a displacement type ship due to added resistance in weather conditions (irregular waves and wind). The advantage of this method is that it is easy and practical to use once it is based on the Eq. 4.1, where v_{rw} is service speed in rough weather, v_{sw} is service speed in still water, C_β

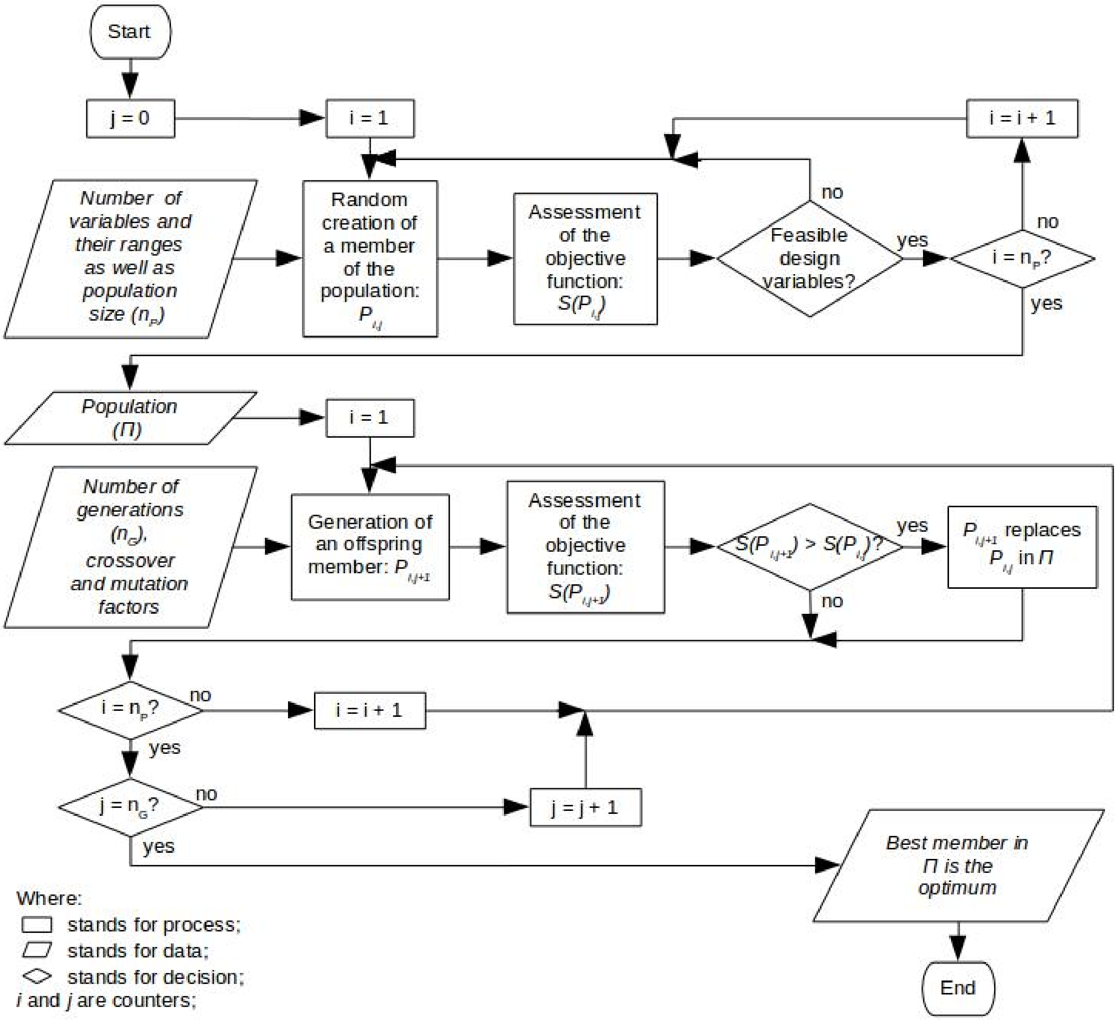
Start
j = 0
i = 1
i = i + 1
Number of variables and their ranges as well as population size (n_P)
Random creation of a member of the population: $P_{i,j}$
Assessment of the objective function: $S(P_{i,j})$
Feasible design variables?
no
yes
$i = n_P$?
no
yes
Population (Π)
i = 1
Number of generations (n_G), crossover and mutation factors
Generation of an offspring member: $P_{i,j+1}$
Assessment of the objective function: $S(P_{i,j+1})$
$S(P_{i,j+1}) > S(P_{i,j})$?
yes
no
$P_{i,j+1}$ replaces $P_{i,j}$ in Π
$i = n_P$?
no
yes
i = i + 1
$j = n_G$?
no
yes
j = j + 1
Best member in Π is the optimum
End
Where:
stands for process;
stands for data;
stands for decision;
i and j are counters;

Figure 4.4: Iterative procedure of the differential evolution optimisation algorithm.

is a direction reduction coefficient, C_U is a speed reduction coefficient and C_{form} is a ship form coefficient.

$$\frac{v_{rw}}{v_{sw}} = 1 - \frac{C_\beta \cdot C_U \cdot C_{form}}{100} \tag{4.1}$$

Since v_{rw} is a design variable in the present work, v_{sw} was calculated by Eq. 4.1 and then the corresponding $R_{T,sw}$ was obtained by Eq. 4.2. In this equation R_F is frictional resistance, $1 + k_1$ is the form factor of the hull, R_{APP} is appendage resistance, R_W is wave resistance, R_B is additional pressure resistance of bulbous bow near the water surface, R_{TR} is additional pressure resistance due to transom immersion and R_A is the model-ship correlation resistance.

$$R_{T,sw} = R_F \cdot (1 + k_1) + R_{APP} + R_W + R_B + R_{TR} + R_A \tag{4.2}$$

Therefore, one considers that the ship is sailing at v_{rw}, which is generally lower than the corresponding v_{sw}, but the resistance is that one related to the corresponding v_{sw}.

In order to calculate those coefficients, it is necessary to know some parameters related to weather, such as weather direction angle with respect to the ship's bow and Beaufort Number (BN), besides ship parameters and service speed. Weather direction is assumed to be the same as wind (surface waves) and it is also known as encounter angle, such as illustrated in Fig. 4.5. Beaufort Number is used to represent a range of wave heights and sea conditions, which can be taken as a function of the wind speed in m/s at a height of 10 m above sea level (v_{10}), such as illustrated in Eq. 4.3 [56]. Therefore, the monthly means of daily means for zonal and meridional wind components (10 metre U wind component and 10 metre V wind component), as well as the absolute wind speed (10 metre wind speed) provided by the European Centre for Medium-Range Weather Forecasts [57] was used. There must be noticed that among the measured data supported by this server there are also interpolated data depending on the wished grid.

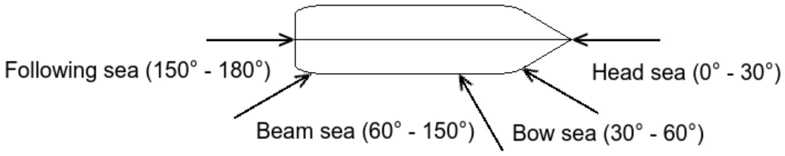

Figure 4.5: Encounter Angle.

$$BN = \sqrt[1.5]{\frac{v_{10}}{0.836}} \tag{4.3}$$

4.3 Computation of total resistance in service

A well-chosen design condition must be realistic and representative for the service conditions that the ship will encounter during its operational life. Therefore, the total resistance in service ($R_{T,ser}$) is related to the trial total resistance ($R_{T,tri}$) by the service margin (SM), as shown in Eq. 4.4. The service margin can be built up as a product of factors including effects of fouling (sm_f), hull form (sm_h), displacement (sm_d), weather (sm_w) and water depth (sm_{wd}), as illustrated in Eq. 4.5 [39].

$$R_{T,ser} = SM \cdot R_{T,tri} \tag{4.4}$$

$$SM = sm_f \cdot sm_h \cdot sm_d \cdot sm_w \cdot sm_{wd} \tag{4.5}$$

Herein the effects regarding hull form, displacement and weather have already been taken into account by the previous computation, as well as it is assumed that the ship sails in deep waters most of the time. Hence, the only factor with value different of one is that about fouling (sm_f), which is recommended to take as 3% of increase resistance per year [39].

4.4 Computation of propulsion factors

Only a part of the thrust produced by the propellers is used to overcome the pure towing resistance of a ship, the remaining part has to overcome the added resistance created by the presence of the propellers themselves. Furthermore, the propellers are located within a region where the water velocity is affected by the hull's presence (ship propeller wake). Thus, there must be considered the thrust deduction factor (t) for calculating the thrust (Th), and the wake factor (w) for calculating the advance velocity of the propeller (v_A). These calculations are shown respectively in Eq. 4.6, where Z_p is the number of propellers, and Eq. 4.7.

$$Th = \frac{R_{T,ser}}{Z_p \cdot (1 - t)} \tag{4.6}$$

$$v_A = (1 - w) \cdot v_{rw} \tag{4.7}$$

Equations given by Holtrop and Mennen [53] [54], which are based on ship and propeller parameters, as well as on service speed, were applied to obtain these propulsion factors and also the relative rotative efficiency (η_R). This latter is used subsequently to calculate brake power in service.

4.5 Computation of propeller performance

Over the years there have been a considerable number of standard series propellers tested in many establishments around the world and those most commonly used by propeller designers and analysts are referenced in [52]. Wageningen B-screw series, also known as Troost series, is perhaps the most extensive and widely used propeller series, as declared by the latter author, and for this reason, it was applied. The thrust and torque coefficients (K_T and K_Q) of the screws are expressed as polynomials in the advance ratio (J), the pitch ratio (P/D), the blade-area ratio (A_E/A_O) and the number of blades (Z). Additionally, the effect of the Reynolds number (R_n) is taken into account in the polynomials [58]. Thus, the relationships shown in Eq. 4.8 and 4.9 were used to calculate the non-dimensional thrust and torque provided by the propeller.

$$K_T = f_1(J, P/D, A_E/A_O, Z, R_n) \tag{4.8}$$

$$K_Q = f_2(J, P/D, A_E/A_O, Z, R_n) \tag{4.9}$$

On the other hand, by using open water diagram, the non-dimensional thrust required by the ship ($K_{T,s}$[1]) was calculated by Eq. 4.10. Once K_T must equal $K_{T,s}$, the issue is finding the value of J for that, which was made by solving an equation system. Then, shaft speed (n) and torque (Q) were calculated by Eq. 4.11 and Eq. 4.12, respectively, where ρ is the water density and D is the propeller diameter.

$$K_{T,s} = \frac{T}{\rho \cdot v_A^2 \cdot D^2} \cdot J^2 \tag{4.10}$$

$$n = \frac{v_A}{J \cdot D} \tag{4.11}$$

$$Q = K_Q \cdot \rho \cdot n^2 \cdot D^5 \tag{4.12}$$

Lastly, open water power (P_O) and efficiency (η_O) were obtained respectively from Eq. 4.13 and Eq. 4.14.

$$P_O = 2\pi \cdot Q \cdot n \tag{4.13}$$

$$\eta_O = \frac{1}{2\pi} \cdot \frac{J \cdot K_T}{K_Q} \tag{4.14}$$

---

[1] Subscript s stands for ship

4.6 Constraints

The propulsion design variables were only considered feasible if approved for all criteria, namely propeller blade resistance, cavitation, propeller peripheral velocity, and resonance. Each criterion was tested in that order and more details about them are given below.

4.6.1 Propeller blade strength

In order to constrain propellers with unsatisfactory strength properties, the inequality given in Eq. 4.15 was used. The blade thickness at 75% of the propeller radius ($t_{0.75R}$) must not be lesser than the minimum thickness required ($t_{0.75R,min}$). Approaches for $t_{0.75R}$ and $t_{0.75R,min}$ given by OOSTERVELD and OSSANNEN [58] were used, as written in Eq. 4.16. This equation is not dimensionally homogeneous, hence D is propeller diameter in ft, P_S is the power delivered by each blade in hp, S_C is the maximum allowable stress of the propeller material in psi and n is propeller speed in rpm.

$$t_{0.75R} \geq t_{0.75R,min} \tag{4.15}$$

$$\begin{aligned} \cancel{D} \quad \cdot \quad & (0.0185 - 0.00125 \cdot Z) \geq \cancel{D} \cdot \\ \cdot \quad & \left[0.0028 + 0.21 \cdot \sqrt[3]{\frac{(2375 - 1125 \cdot P/D) \cdot P_S}{4.123 \cdot n \cdot D^3 \cdot \left(\frac{S_C + D^2 \cdot n^2}{12{,}788}\right)}} \right] \end{aligned} \tag{4.16}$$

4.6.2 Cavitation

Cavitation on back of propeller blades was constrained according to the Burrill cavitation diagram for uniform flow [52] by the inequality given in Eq. 4.17. The thrust loading coefficient ($\tau_{c0.7R}$) must be at most equal to the maximum thrust loading coefficient ($\tau_{c0.7R,max}$), depending on the maximum cavitation level adopted. By assuming 5% cavitation as the maximum allowable, the exponential curve shown on the right side of Eq. 4.18 was approximated. On the left side of this equation is shown the definition of thrust loading coefficient. In Eq. 4.18 A_p is the projected area of the propeller and $\sigma_{0.7R}$ is the mean cavitation number, which is defined in Eq. 4.19. In this equation, p_0 is the static pressure at the shaft centre line and p_v is the water vapour pressure.

$$\tau_{c0.7R} \leq \tau_{c0.7R,max} \tag{4.17}$$

$$\frac{Th}{\frac{1}{2} \cdot \rho \cdot A_p \cdot [{v_A}^2 + (0.7\pi \cdot n \cdot D)^2]} \leq 0.2032 \cdot e^{0.3504 \cdot \sigma_{0.7R}} - 0.2311 \cdot e^{-3.194 \cdot \sigma_{0.7R}} \quad (4.18)$$

$$\sigma_{0.7R} = \frac{p_0 - p_v}{\frac{1}{2} \cdot \rho \cdot [{v_A}^2 + (0.7\pi \cdot n \cdot D)^2]} \quad (4.19)$$

4.6.3 Propeller peripheral velocity

The blade tip peripheral velocity (v_{tip}) should be as low as possible in order to reduce noise and vibrations. Its recommended upper level is 39 m/s [59], as shown in Eq. 4.20.

$$v_{tip} = \pi \cdot D \cdot n \leq 39 \quad (4.20)$$

4.6.4 Resonance

The coincidence of the natural frequency identified with some natural mode and the exciting frequency of some excitation component corresponds to a condition of resonance. Intending to reach ships with consistently acceptable vibration characteristics, it is essential to avoid resonances involving the active participation of major subsystems in frequency ranges where the dominant excitations are strongest [60]. For this reason, attention was given to the hull girder vertical vibration excited by the propeller. Equation 4.21, which is simplified and suitable for initial design stage of ships [61], was applied to calculate the first four orders vertical vibration natural frequencies. In this equation B is the moulded breadth, D_m is the moulded depth, Δ_V is the displacement including the virtual added mass of water, L_{pp} is the length between perpendiculars, and C_n is a coefficient dependent on vibration order and ship type. This coefficient was approximated as if the ship were a bulk carrier for the three first orders and an extrapolation was carried out to obtain it for the fourth order. The values used for C_n are listed in Tab. 4.1.

$$f_n = C_n \cdot \sqrt{\frac{B \cdot D_m^2}{\Delta_V \cdot L_{pp}^2}} \quad (4.21)$$

Table 4.1: Coefficient C_n of the hull girder vertical natural frequency.

Order	1^{st}	2^{nd}	3^{rd}	4^{th}
C_n	620.6	1212.2	1735.6	2186.6

On the other hand, the excitation frequencies due to the propeller (f) were calculated by Eq. 4.22, in which n_h is an integer related to the harmonics (1 for the first harmonic and so on).

$$f = n_h \cdot Z \cdot n \tag{4.22}$$

Thus, any propeller that holds excitation frequencies with less than a difference in relation to the hull girder vertical natural frequencies was constrained. Mathematically this corresponds to Eq 4.23.

$$0.90 \cdot f_n \leq f \leq 1.10 \cdot f_n \tag{4.23}$$

4.7 Computation of brake power in service

Calculating brake power (P_B) consists in considering losses to approximate the required power in the engine shaft based on the open water power (P_O), as shown in Eq. 4.24. In practice, when a propeller is behind a ship, the power actually delivered to the propeller is generally different from P_O as a result of the non-uniform velocity field in front of the propeller. This is offset by the relative rotative efficiency (η_R), whilst mechanical losses over the propulsion chain are expressed by shaft efficiency (η_S) and gearbox efficiency (η_{GB}).

$$P_B = \frac{P_O}{\eta_R \cdot \eta_S \cdot \eta_{GB}} \tag{4.24}$$

4.8 Computation of SMCR

The operating point with the maximum brake power required throughout the journey is taken as the maximum continuous rating (MCR) point. Trying to make sure the ship will be able to keep its service speed and the engine will be not fully loaded even in the hardest condition, margins are considered on the MCR power (P_{MCR}). Once the service margin (SM) has already been applied, the engine margin (EM), which often lies between 0.8 and 0.9 [39], is used to obtain the SMCR power (P_{SMCR}), as shown in Eq. 4.25. Meanwhile, the shaft speed at SMCR (n_{SMCR}) can be approximated from the shaft speed at MCR (n_{MCR}) by assuming the propeller law, as shown in Eq. 4.26.

$$P_{SMCR} = \frac{P_{MCR}}{EM} \tag{4.25}$$

$$n_{SMCR} = n_{MCR} \cdot \sqrt[3]{\frac{P_{SMCR}}{P_{MCR}}} \tag{4.26}$$

4.9 Determination of suitable engines

In order to determine the suitable engines, the standard selection of slow speed Diesel engines (Sec. 2.4) was followed. The first step is placing the SMCR point on the engine layout diagram programme to know which engines are able to supply the required power and speed. Next step is determining how many cylinders are necessary. Thus, a function was implemented to search the suitable engines regarding a given SMCR. To chart diagrams covering the entire capacity of engines, L1 and L3 corresponding to the maximum number of cylinders as well as L2 and L4 corresponding to the minimum number of cylinders were taken from Tab. 3.1. That function plots a chart with all the engine layout diagrams considered and the SMCR point, as sampled in Fig. 4.6.

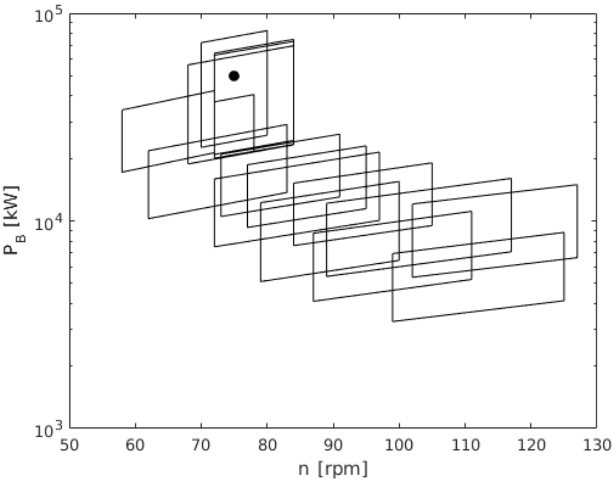

Figure 4.6: Engine layout diagrams considered and a SMCR of 50 MW and 75 rpm.

Then, another function tests every single engine for speed and those matching the speed are tested for power to predict the required number of cylinders. Thus, a list of suitable engines and their needed number of cylinders to meet the SMCR is provided. Table 4.2 shows the engines and their required number of cylinders for the case from Fig. 4.6. Each one of the four engines could meet the SMCR with different numbers of cylinders, totalling eleven alternatives to be considered.

Only engines covered by the CEAS-ERD [45] were applied herein. This application considers 16 engines (cylinder diameters from 400 to 950 mm) with a number of cylinders varying between 5 and 12. It represents a total of 83 because

Table 4.2: Suitable engines and number of cylinders.

Engine	Number of cylinders
G95-9.5	8, 9 or 10
G90-10.5	9, 10 or 11
S90-10.5	10 or 11
S90-9.5	10, 11 or 12

some engines hold fewer cylinders. All engines are electronically controlled (ME-C engine concept) and are not equipped with exhaust gas after-treatment.

4.10 Computation of CAPEX

Among capital expenditures, acquisition costs of the main engine, propeller, shaft and re-liquefaction plant are of primary interest for the present study. Nevertheless, obtaining cost and related data is not easy, as engine manufacturers consider this information confidential. Hence, WATSON [6] decided to use weight as the estimating parameter once it has the advantage to apply to almost all components of ship cost. This author also reached a curve of machinery weight-related cost (WRC_m), in American dollar [US$] per tonne [t], versus machinery weight (W_m), including materials, labour and overheads. This curve could be approximated by Eq. 4.27, where W_m must include the total machinery weight, which is the sum due to the main engine, propeller and shaft. Meanwhile, the re-liquefaction plant was taken as a cargo-related outfit whose weight-related cost (WRC_{rp}) is given as being 28500 US$/t. Therefore, machinery CAPEX ($CAPEX_m$) and re-liquefaction plant CAPEX ($CAPEX_{rp}$) were calculated respectively by Eq. 4.28 and 4.29, where W_{rp} is the re-liquefaction plant weight.

$$WRC_m = 9850 \cdot e^{-0.001457 \cdot W_m} + 10226 \cdot e^{-0.00007049 \cdot W_m} \tag{4.27}$$

$$CAPEX_m = WRC_m \cdot W_m \tag{4.28}$$

$$CAPEX_{rp} = WRC_{rp} \cdot W_{rp} \tag{4.29}$$

Once the costs given in [6] are on a 1993 basis, a correction concerning inflation became necessary. In this sense, with respect to oil and gas field machinery and equipment manufacturing, the producer price index industry data was applied [62]. Thus, in order to bring the total CAPEX from a 1993 to a 2015 basis, it was applied Eq. 4.30, where Z_p is the number of propulsion chains, PPI stands for producer price index and f_{ins} is an installation cost factor.

$$CAPEX = (CAPEX_m \cdot Z_p + CAPEX_{rp}) \cdot \frac{PPI_{2015}}{PPI_{1993}} \cdot f_{ins} \tag{4.30}$$

Main engine weight was achieved with CEAS-ERD whilst propeller weight (W_p) and shaft weight (W_s) were respectively approximated by Eq. 4.31 and 4.32, in which D is propeller diameter in m, L_s is shaft length in m, P_{NMCR} is power at NMCR in kW and n_{NMCR} is shaft speed at NMCR in rpm [56]. On the other hand, the re-liquefaction plant weight (W_{rp}) was assumed as 240 t, which is a figure respective to an LNG re-liquefaction system mark III by WARTSILA [63].

$$W_p = D^3 \cdot \left(0.18 \cdot A_E/A_O - \frac{Z-2}{100}\right) \tag{4.31}$$

$$W_s = 0.081 \cdot L_s \cdot \left(\frac{P_{NMCR}}{n_{NMCR}}\right)^{2/3} \tag{4.32}$$

4.11 Computation of OPEX

The most representative measures of operational expenditures for the present work are journey cost (C_{jou}), purchase cost of the LNG cargo (C_{LNG}), fuel cost related to propulsion ($C_{f,pro}$), fuel cost related to other consumers on board ($C_{f,oth}$), fuel cost related to BOG re-liquefaction ($C_{f,rel}$), and maintenance cost (C_m). Hence, the total OPEX in a round trip of the vessel is given by Eq. 4.33.

$$OPEX = C_{jou} + C_{LNG} + C_{f,pro} + C_{f,oth} + C_{f,rel} + C_m \tag{4.33}$$

Journey cost (C_{jou}) includes port fees and tolls. The purchase cost of the LNG cargo (C_{LNG}) was calculated by Eq. 4.34, in which FOB_{LNG} is the free-on-board LNG price, ρ_{LNG} is the LNG density and Vp_{LNG} is the cargo volume of LNG purchased at loading terminal. The latter was calculated by Eq. 4.35, where Vt_{LNG} is the ship's total cargo capacity in volume, n_{RTb} is the number of route-tracks in ballast, V_{BOG} is the total volume of LNG becoming BOG (including naturally and forced generated amounts), V_{rel} is the volume of LNG coming from BOG re-liquefaction, i is an index that refers to each route-track in ballast and V_h is the heel volume.

$$C_{LNG} = FOB_{LNG} \cdot Vp_{LNG} \cdot \rho_{LNG} \tag{4.34}$$

$$Vp_{LNG} = Vt_{LNG} - V_h + \sum_{i=1}^{n_{RTb}} \left[V_{BOG} - V_{rel}\right]_i \tag{4.35}$$

The total fuel costs, either $C_{f,pro}$, $C_{f,oth}$ or $C_{f,rel}$, must consider the portions referring to fuel oil ($C_{f,O}$), pilot oil ($C_{f,PO}$) and gaseous fuel ($C_{f,G}$), as in Eq. 4.36. The former is regarding dual-fuel engines when operating in diesel mode, whilst the two latter occur for gas mode. As the gaseous fuel comes from cargo (BOG), its cost is included in C_{LNG}, and thereby $C_{f,G}$ was neglected.

$$C_f = C_{f,O} + C_{f,PO} + C_{f,G} \tag{4.36}$$

Regarding fuel cost related to propulsion ($C_{f,pro}$), Eq. 4.37 could be applied to calculate both fuel oil and pilot oil cost. In this equation $C_{f,pL}$ stands for the total liquid fuel cost, c_{lf} is liquid fuel unit cost, SFC is the specific fuel consumption of the prime mover, δt is the duration of the condition and the index i refers to each route-track.

$$C_{f,pL} = c_{lf} \cdot \sum_{i=1}^{n_{RT}} \left[SFC \cdot P_B \cdot Z_p \cdot \delta t\right]_i \tag{4.37}$$

Since there must be a compression system to increase BOG pressure to feed prime mover, the electricity to power this system, other consumers and the re-liquefaction plant is supplied by dual-fuel generation sets. Hence, the cost of liquid fuels to feed other consumers could be calculated by Eq. 4.38, where SFC_{GE} is the specific fuel consumption of the generation engine, η_G is the generator's efficiency and P_{oth} is the electric power required by other consumers [23].

$$C_{f,oL} = c_{lf} \cdot \sum_{i=1}^{n_{RT}} \left[\frac{SFC_{GE}}{\eta_G} \cdot P_{oth} \cdot \delta t\right]_i \tag{4.38}$$

In order to calculate the liquid fuel cost for re-liquefying BOG, Eq. 4.39 was used. In this equation, SP_{BOG} is the power required to re-liquefy a mass flow unit of BOG, which is a measure of the specific power requirement of the re-liquefaction plant. Since BOG may be burnt in both prime mover and generation sets, only the surplus is re-liquefied. Therefore, the mass flow of BOG to be re-liquefied ($\dot{m}_{BOGr}$) in each route-track was calculated by Eq. 4.40. The flow of naturally generated BOG ($\dot{m}_{BOGg}$) and of total consumed BOG ($\dot{m}_{BOGc}$) are given by Eq. 4.41 and 4.42, respectively. In these equations, V_{LNG} is the volume of LNG in the tanks for each route-track, BOR is the boil-off rate and P_{com} is the electric power required by the BOG compression system. Such equations were solved iteratively because the BOG consumed to re-liquefy the surplus of BOG also reduces the amount of BOG to be re-liquefied.

$$C_{f,rL} = c_{lf} \cdot \sum_{i=1}^{n_{RT}} \left[\frac{SFC_{GE}}{\eta_G} \cdot SP_{BOG} \cdot \dot{m}_{BOGr} \cdot \delta t\right]_i \tag{4.39}$$

$$\dot{m}_{BOGr} = \dot{m}_{BOGg} - \dot{m}_{BOGc} \tag{4.40}$$

$$\dot{m}_{BOGg} = V_{LNG} \cdot \rho_{LNG} \cdot BOR \tag{4.41}$$

$$\dot{m}_{BOGc} = SGC \cdot P_B \cdot Z_p + \frac{SGC_{GE}}{\eta_G} \cdot (P_{oth} + P_{com} + SP_{BOG} \cdot \dot{m}_{BOGr}) \tag{4.42}$$

Noticeably, all fuel costs are strongly dependent on the specific fuel consumption of the prime mover and generation sets. To assess the specific fuel consumption of the dual-fuel low-speed Diesel engines, the engine model herein-before developed in Chap. 3 is used. More precisely, the statement of the model is addressed in Sec. 3.2.

The total maintenance cost (C_m) includes propeller and prime mover. However, as the maintenance cost of a propeller is significantly lower than that of an engine, only the engine maintenance cost ($C_{m,E}$) was taken into account. To calculate it, one used Eq. 4.43.

$$C_m \approx C_{m,E} = c_m \cdot \sum_{i=1}^{n_{RT}} \left[P_{NMCR} \cdot Z_p \cdot \delta t\right]_i \tag{4.43}$$

4.12 Computation of NPV

As implied by its name, NPV is simply the present value of the projected cash flow including the investments. It requires an estimate of future revenues and it assigns an interest rate for discounting future, usually after-tax, cash flows [7]. Thus, NPV was calculated by Eq. 4.44, where n_y is the period of economic analysis in years (the ship's lifetime), Fy is the annual net cash flow, r_d is the discount rate and i is an index that refers to each year of economic analysis.

$$NPV = \sum_{i=1}^{n_y} \left[\frac{Fy}{(1+r_d)^i} - CAPEX\right]_i \tag{4.44}$$

The annual net cash flow Fy is given by the difference between income and OPEX, being calculated by Eq. 4.45, in which n_{rnd} is the number of round trips a year, CIF_{LNG} is the cost-insurance-freight LNG price and Vd_{LNG} is the volume of LNG delivered at unloading terminal. The latter was calculated by Eq. 4.46, where n_{RTl} is the number of route-tracks in laden and the index i refers to each route-track in laden.

$$Fy = \sum_{i=1}^{n_{rnd}} \left[CIF_{LNG} \cdot Vd_{LNG} \cdot \rho_{LNG} - OPEX\right]_i \tag{4.45}$$

$$Vd_{LNG} = Vt_{LNG} - V_h - \sum_{i=1}^{n_{RTl}} \left[V_{BOG} - V_{rel}\right]_i \tag{4.46}$$

4.13 Differential evolution optimisation algorithm

In this algorithm the generation of an offspring member ($P_{i,j+1}$) is given by Eq. 4.47, where $P_{i,j}$ is the i^{th} individual of the j^{th} generation of the population Π; α, β and γ are three randomly chosen members of the population Π; F is a weight constant, which defines the mutation ($0.5 \leq F \leq 1.0$); δ_1 and δ_2 are two functions related to crossover. Depending on the value of a random number R (between 0 and 1) and of the crossover factor CR ($0.5 \leq CR \leq 1.0$), δ_1 and δ_2 take different values, such as shown in Eq. 4.48.

$$P_{i,j+1} = \delta_1 \cdot P_{i,j} + \delta_2 \cdot \left[P_{\alpha,j} + F \cdot (P_{\beta,j} - P_{\gamma,j})\right] \tag{4.47}$$

$$\text{if } R \leq CR \begin{cases} \delta_1 = 0 \\ \delta_2 = 1 \end{cases}, \text{ otherwise} \begin{cases} \delta_1 = 1 \\ \delta_2 = 0 \end{cases} \tag{4.48}$$

The random generation of integers was achieved by considering uniformly distributed pseudo-random integers. Meanwhile, the generation of floats was done by considering uniformly distributed random numbers [51].

Chapter 5

Case study

This chapter addresses the ship and energy system parameters adopted to test the relevance of the developed approach. Details about the route, operational profiles, as well as economic and optimisation issues, are also included.

5.1 Ship

The case study of an LNGC with a cargo capacity of 175,000 m^3 was proposed and its hull for the specific situation of two propellers is illustrated in Fig. 5.1. This ship holds the parameters listed in Tab. 5.1. As one may notice, various parameters are different for laden and ballast operation whilst others do not vary.

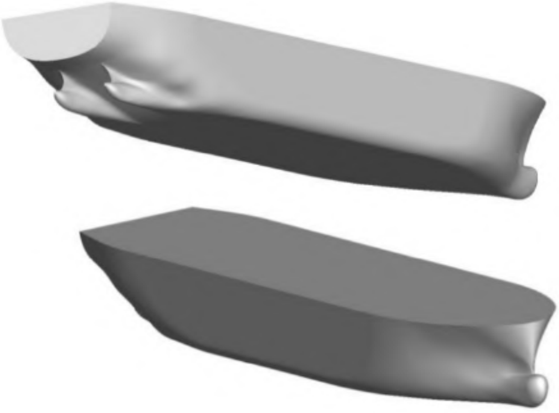

Figure 5.1: LNGC for the case study.

The energy system of the ship is schematically shown in Fig. 5.2, where it can be noticed that BOG can feed the GCU, the dual-fuel generation sets, the BOG compression system and the re-liquefaction plant. On the other hand, dual-fuel generation sets provide electricity to re-liquefaction plant, other consumers and BOG compression system. The existence of a re-liquefaction system is not mandatory,

Table 5.1: Ship parameters.

Parameter	Symbol	Unit	Laden	Ballast
Length on waterline	L	m	292.7	282.3
Length between perpendiculars	L_{pp}	m	293.7	
Moulded breadth	B	m	49.00	
Moulded draught	T_m	m	11.50	9.500
Moulded depth	D_m	m	23.00	
Moulded displacement volume	∇	m^3	118,464	95,511
Longitudinal centre of buoyancy	LCB	%	-1.951	0.1984
Transverse bulb area	A_{BT}	m^2	25.00	
Centre of bulb area above keel line	h_B	m	5.300	
Midship section coefficient	C_M	-	0.9856	0.9825
Water-plane area coefficient	C_{WP}	-	0.8160	0.8125
Stern shape parameter	C_{stern}	-	-25	

such that the ship can hold it or not. Likewise, the ship can have two propulsion chains or only one, as shown in that figure.

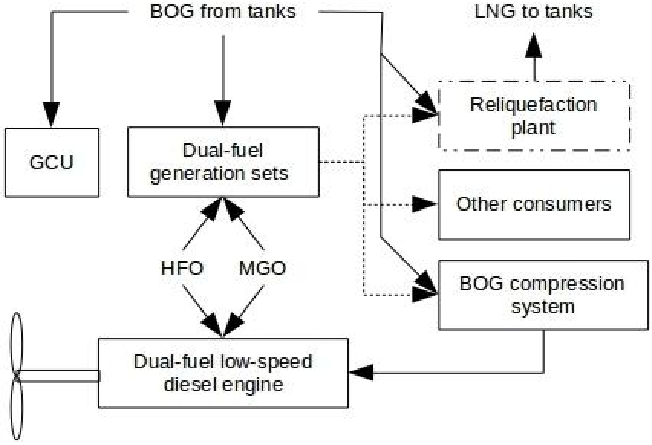
BOG from tanks
LNG to tanks
Reliquefaction plant
GCU
Dual-fuel generation sets
Other consumers
HFO
MGO
BOG compression system
Dual-fuel low-speed diesel engine

Figure 5.2: Energy system scheme.

Table 5.2 lists the energy system parameters for the studied ship. Some data, namely SP_{BOG}, P_{oth} and P_{com}, were achieved by regression from [23]. The $SFOC_{GE}$, SGC_{GE}, $SPOC_{GE}$ and η_G were achieved by considering generation sets with engines W34DF of 435 kW per cylinder [64]. Since the composition of BOG is time-dependent, an average value for LHV_{BOG} was taken from [2].

The values of all specific fuel consumptions, including those from the engine model developed herein-before (Chap. 3), were taken regarding standard lower heating values of 42,700 kJ/kg and 50,000 kJ/kg, respectively for liquid (LHV_l) and gaseous fuel (LHV_g). They must thereby be rectified regarding LHV_{HFO} and LHV_{BOG}. Assuming the engine efficiency as a constant regarding fuels of the

Table 5.2: Energy system parameters.

Parameter	Symbol	Unit	Value
Centre of propeller shaft above keel line	h_s	m	4.250
Shaft length from engine to propeller	L_s	m	30.00
Total cargo capacity	Vt_{LNG}	m^3	175,000
Shaft efficiency	η_S	%	99.00
Fouling factor	sm_f	-	1.075
Engine margin	EM	%	90.00
Re-liquefaction plant weight	W_{rp}	t	240.0
Boil-off rate	BOR	%	0.150
Heel volume fraction	r_h	%	5.000
LNG density	ρ_{LNG}	$\mathrm{t/m}^3$	0.427
Re-liquefaction specific power (laden)	$\mathrm{SP}_{BOG,l}$	kWh/t	831.6
Re-liquefaction specific power (ballast)	$\mathrm{SP}_{BOG,b}$	kWh/t	4550
Electric power of other consumers	P_{oth}	kW	2121
Electric power of BOG compression	P_{com}	kW	1630
SFOC of generation engines	SFOC_{GE}	g/kWh	189.0
SGC of generation engines	SGC_{GE}	g/kWh	152.6
SPOC of generation engines	SPOC_{GE}	g/kWh	2.000
Generator efficiency	η_G	%	96.00
HFO lower heating value	LHV_{HFO}	kJ/kg	40,500
MGO lower heating value	LHV_{MGO}	kJ/kg	42,700
BOG lower heating value	LHV_{BOG}	kJ/kg	46,000

same phase (gaseous or liquid), the specific fuel consumption becomes inversely proportional to the LHV. Hence, Eq. 5.1 was used to find the specific heavy fuel oil consumption ($SFOC_{HFO}$) from the specific fuel oil consumption (SFOC) for LHV$_l$. The specific pilot heavy fuel oil consumption ($SPOC_{HFO}$) was analogously calculated. Similarly, the specific BOG consumption (SGC_{BOG}) was calculated from the specific gas consumption (SGC) for LHV$_g$ using Eq. 5.2.

$$SFOC_{HFO} = SFOC \cdot \frac{LHV_l}{LHV_{HFO}} \tag{5.1}$$

$$SGC_{BOG} = SGC \cdot \frac{LHV_g}{LHV_{BOG}} \tag{5.2}$$

5.2 Route

This ship travels in laden from Lake Charles to Tokyo Bay via Panama Canal, and returns in ballast, following the great circle route, as shown in Fig. 5.3. This is the shortest course between two points on the surface of a sphere and that is why it was used. The topology of the monthly average wind speed for December 2015 is presented in the same figure. Twenty way-points were considered, dividing the route into 19 tracks. Table 5.3 presents the route parameters of interest for each route-track (RT), where S is the route-track length whilst BN and θ_l are 2015 average values respectively concerning Beaufort Number and encounter angle for the laden trip. It is worthwhile to notice that the encounter angle for ballast trip is the supplementary angle of θ_l.

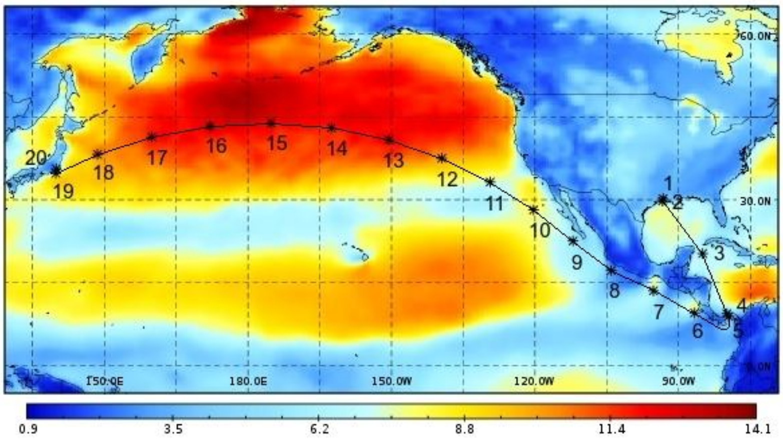

Figure 5.3: Route between Lake Charles and Tokyo Bay via Panama Canal and the topology of absolute wind speed [m/s] for December 2015.

Table 5.3: Route parameters.

RT	S [km]	BN	θ_l [°]
1 - 2	59.0	3	64.78
2 - 3	1339	4	47.70
3 - 4	1339	4	83.55
4 - 5	77.0	3	132.4
5 - 6	1015	3	58.33
6 - 7	1015	3	142.8
7 - 8	1015	2	42.50
8 - 9	1015	3	52.42
9 - 10	1015	4	40.52
10 - 11	1015	4	48.76
11 - 12	1015	4	65.82
12 - 13	1015	4	50.10
13 - 14	1015	5	36.69
14 - 15	1015	5	7.438
15 - 16	1015	5	0.561
16 - 17	1015	5	12.30
17 - 18	1015	5	23.21
18 - 19	1015	5	50.71
19 - 20	93.0	3	74.54

5.3 Operational profile

The ship keeps a different operational profile regarding service speed and fuel to burn depending on the stage of the route, as presented in Tab. 5.4. Three levels of service speed were identified to reduce pollution, such that the smaller the distance from a continent, the slower the speed. Thus, the three levels were: low for $v_{rw} \leq 12.0$ knots [kn], intermediary for $v_{rw} \leq 16.0$ kn and high for $v_{rw} \leq 19.5$ kn. Moreover, since cleaner fuels must be burnt between way-points 1 and 5, as well as between 19 and 20 due to environmental rules, four fuel profiles (FPs) were proposed:

1. Prime mover and generation sets burn HFO wherever possible and MGO only where is necessary, such that BOG is completely re-liquefied.

2. Prime mover and generation sets burn HFO wherever possible and BOG only where is necessary, such that only the remaining BOG is re-liquefied. In this case, wherever BOG is applied the pilot oil is MGO.

3. Prime mover and generation sets burn only BOG in laden whilst in ballast they burn HFO wherever possible and MGO where is necessary, such that only the remaining BOG is re-liquefied. In this case, pilot oil is always MGO for the generation sets whilst the prime mover uses HFO wherever is possible and MGO only where cleaner fuels are required.

4. Prime mover and generation sets only burn BOG during the entire voyage, such that there is no re-liquefaction plant and the remaining BOG is burnt in a gas combustion unit (GCU). Pilot oil is always MGO for the generation sets whilst the prime mover uses HFO wherever is possible and MGO only where cleaner fuels are required.

Table 5.4: Operational profile.

RT	$\frac{v_{rw}}{\text{kn}}$	FP_1	FP_2	FP_3	FP_4
1 - 5	≤ 12.0	MGO	BOG/MGO	BOG/MGO	BOG/MGO
5 - 11	≤ 16.0	HFO	HFO	BOG/HFO(MGO)	BOG/HFO(MGO)
11 - 18	≤ 19.5	HFO	HFO	BOG/HFO(MGO)	BOG/HFO(MGO)
18 - 19	≤ 16.0	HFO	HFO	BOG/HFO(MGO)	BOG/HFO(MGO)
19 - 20	≤ 12.0	MGO	BOG/MGO	BOG/MGO	BOG/MGO
20 - 19	≤ 12.0	MGO	BOG/MGO	MGO	BOG/MGO
19 - 18	≤ 16.0	HFO	HFO	HFO	BOG/HFO(MGO)
18 - 11	≤ 19.5	HFO	HFO	HFO	BOG/HFO(MGO)
11 - 5	≤ 16.0	HFO	HFO	HFO	BOG/HFO(MGO)
5 - 1	≤ 12.0	MGO	BOG/MGO	MGO	BOG/MGO

Note: the ship sails in laden from 1 to 20 and in ballast from 20 to 1.

Although the total time of a round trip depends mainly on the service speeds, a constant standing period of 24 hours in each port for loading and unloading was also considered. Moreover, this ship has an idle time of 14 days for dry-docking or afloat repairs every 2.5 years, which is important to calculate the average number of round trips a year (n_{rnd}) and to estimate the fouling service margin (sm_f).

5.4 Economic and optimisation parameters

Table 5.5 presents the economic parameters, where C_{jou} includes only the port fees and Panama Canal tolls over a round trip. The optimisation variables and their ranges are listed in Tab. 5.6. The last five rows contain the only discrete variables whereas the others are continuous. Moreover, the last three variables are the only secondary ones, such that they are not input data, they are dependent on the others and are achieved by running the optimisation algorithm although they are also optimised. Besides the optimisation variables, it is important to mention the factors related to mutation (F) and crossover (CR), which equal 0.8 and 0.5, respectively.

Table 5.5: Economic parameters.

Parameter	Symbol	Unit	Value
Producer price index 1993	PPI_{1993}	-	138.4
Producer price index 2015	PPI_{2015}	-	267.9
Installation cost factor	f_{ins}	-	2.0
HFO unit cost	c_{HFO}	US$/t	314.2
MGO unit cost	c_{MGO}	US$/t	547.3
Cost-insurance-freight LNG price	CIF_{LNG}	US$/t	550.8
Free-on-board LNG price	FOB_{LNG}	US$/t	371.8
Maintenance unit cost	c_m	US$/kWh	$1.6 \cdot 10^{-3}$
Journey cost a round trip	C_{jou}	US$	979,724
Discount rate	r_d	%	9.0
Period of economic analysis	n_y	y	20

Table 5.6: Optimisation variables.

Variable	Symbol	Unit	Range
Low service speed (laden)	$v_{rw,ll}$	kn	10.0 - 12.0
Intermediary service speed (laden)	$v_{rw,il}$	kn	12.0 - 16.0
High service speed (laden)	$v_{rw,hl}$	kn	16.0 - 19.5
Low service speed (ballast)	$v_{rw,lb}$	kn	10.0 - 12.0
Intermediary service speed (ballast)	$v_{rw,ib}$	kn	12.0 - 16.0
High service speed (ballast)	$v_{rw,hb}$	kn	16.0 - 19.5
Propeller diameter	D	m	6.50 - 8.50
Expanded area ratio	A_E/A_O	-	0.30 - 1.05
Pitch ratio	P/D	-	0.50 - 1.40
Number of blades	Z	-	2 - 7
Number of propulsion chains	Z_p	-	1 - 2
Engine identification	E_{ID}	-	1 - 16
Number of cylinders	Z_c	-	5 - 12
Fuel profile identification	FP_{ID}	-	1 - 4

Chapter 6

Results and discussion

Next, it is presented the influence of the optimisation algorithm parameters on the NPV along the generations. The evolution of each variable and the effectiveness of the constraints are assessed as well as the engine and fuel profile selection effect. Ultimately, the weather condition effect is discussed.

6.1 Optimization algorithm parameters

Firstly, it was necessary to verify if the population size (n_P) and the number of generations (n_G) used were suitable. The convergence of optimisation is heavily dependent on these parameters and their ideal values are specific to every single case. Therefore, three combinations of these parameters were assessed by plotting the maximum, mean and minimum of the objective function throughout the generations, as shown in Fig. 6.1.

By comparing Fig. 6.1a and Fig. 6.1b, one can notice that doubling the number of generations had a small effect on the objective function. Even less influential was to double the population size, as can be seen when comparing Fig. 6.1b and Fig. 6.1c. Thus, a population of 120 individuals and 120 generations (Fig. 6.1c) were considered suitable. The processing times for a computer fitted with a processor Intel Core i7-5930K of 3.50 GHz and 16 GB of RAM were 1.6, 2.7 and 5.9 h, respectively for the case (a), (b) and (c). The worst individual of the final population, in comparison with the worst individual of the initial population, had the objective function (NPV) increased by 21%, 20% and 22% respectively for the case (a), (b) and (c).

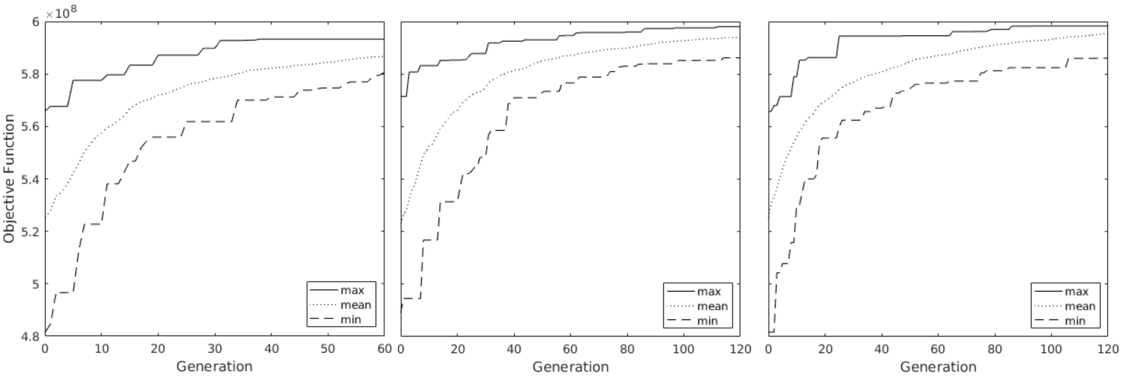

(a) $n_P = 60$; $n_G = 60$ (b) $n_P = 60$; $n_G = 120$ (c) $n_P = 120$; $n_G = 120$

Figure 6.1: Optimisation algorithm convergence for different values of n_P and n_G.

6.2 Optimisation summary

Table 6.1 shows the optimisation summary, where one can see the effectiveness of the constraints and a number of computations performed by the algorithm. Remarkably, almost 48% of the 15,023 configurations assessed by the algorithm were constrained. The peripheral velocity constraint was responsible for over 33% of the rejected designs whereas cavitation was responsible for over 31%, engine for 18%, strength for 13% and the resonance constraint was responsible for under 4%. This table shows also some remarks about the optimisation process.

Overall, 623 designs were assessed to create the initial population, which means that 1 out of each 5.192 was feasible, and each offspring member took on average 1.4 s to be generated. Furthermore, some particularities were noticed about the designs rejected due to each constraint. Over 75% of the designs rejected due to the strength constraint presented in combination: high service speed ($v_{rw,h}$), number of blades (Z) greater than or equal to six and only one propulsion chain (Z_p). Nevertheless, as 99% of these rejected designs presented $Z \geq 6$, the number of blades was the most influential parameter. Similar remarks are presented for each constraint in Tab. 6.1. Since 64% of the designs rejected due to the cavitation constraint had $A_E/A_O < 0.675$ and almost 80% of those rejected due to peripheral velocity had $A_E/A_O > 0.675$, there is no general advice about the best value for expanded area ratio. The same occurs for other parameters, such that there is no general advice about the propeller configuration, which highlights the usefulness of the proposed approach.

Figure 6.2 shows the evolution of the fourteen optimisation variables for the best individual of each generation. As one may observe, almost all parameters presented a significant variation range and all of them were steady from the 86^{th} generation until the end. Various engines ($2 \leq E_{ID} \leq 13$) with various numbers of cylinders ($5 \leq Z_c \leq 9$) were the best one depending on the generation. On the other hand, fuel profile (FP_{ID}) was the only variable that remained steady throughout

Table 6.1: Optimisation summary.

Designs	Used/Rejected	Remarks
623	used to create initial population	feasibility ratio of 1 to 5.192
14,400	used to generate all offspring generations	generation ratio of 1 offspring member to each 1.413 s
931	rejected due to strength constraint	829 designs for $v_{rw,h}$, 923 for $Z \geq 6$, 811 for $Z_p = 1$ and 701 combined these aspects
2252	rejected due to cavitation constraint	1443 designs for $A_E/A_O < 0.675$
2428	rejected due to peripheral velocity constraint	2159 designs for $v_{rw,h}$, 1940 for $A_E/A_O > 0.675$, 2351 for $P/D < 0.95$ and 1667 combined these aspects
275	rejected due to resonance constraint	269 designs for $v_{rw,l}$, 263 for $Z \leq 3$, 236 for $P/D > 0.95$, 218 for $Z_p = 2$ and 171 combined these aspects
1286	rejected due to engine constraint	no

the generations. This is due to the strong relationship between fuel profile and fuel unit cost, which was not changed. Since in the FP_2 the ship uses the fuel of lowest unit cost (HFO) wherever possible and the second cheaper fuel (BOG) only where is necessary, this fuel profile was always optimum.

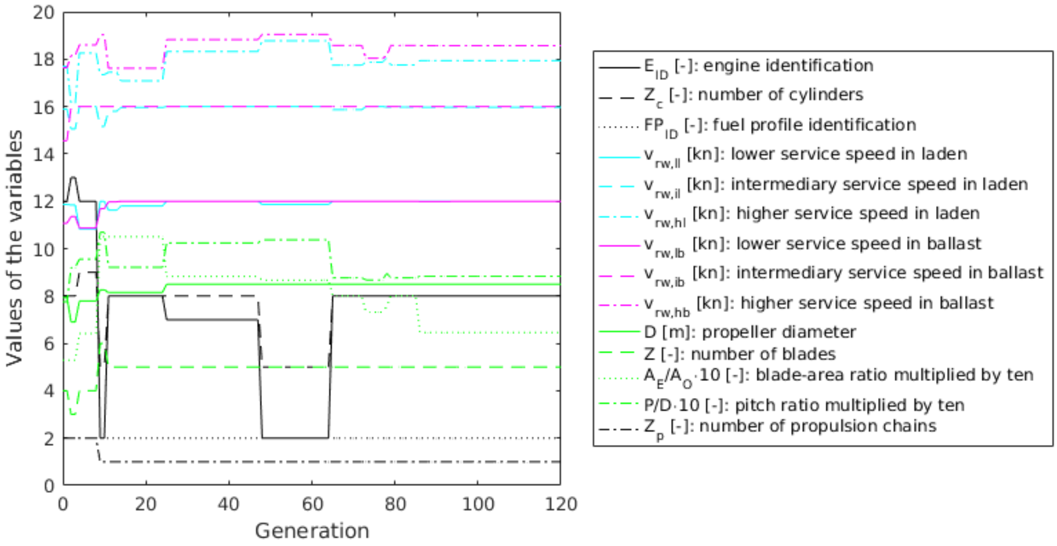

Figure 6.2: Evolution of the optimisation variables throughout the generations.

Table 6.2 presents average (μ) and standard deviation (σ) for the optimisation variables and also four alternatives of synthesis, design and operation (SDO) from the final population. The variables $v_{rw,ll}$, $v_{rw,il}$, $v_{rw,lb}$, $v_{rw,ib}$ and D presented average values close to their upper limits and low σ, indicating a trend. Similarly, Z_p trended to its lower limit, that is, one engine driving directly one propeller. FP_{ID} presented σ equals zero because there was no variation regardless the other variables, as previously explained and illustrated in Fig. 6.2.

The SDO_1 and SDO_4 in Tab. 6.2 are respectively the best (optimum) and the worst alternative, whereas the others are randomly chosen intermediates. E_{ID} 7, 8 and 12 stand respectively for the engines G70-9.5, S70-8.5 and G50-9.5 [65], thus a considerable diversity in size, weight and power per cylinder is observed in the final population. Although there are quite distinct individuals, the optimisation results for each SDO are close, indicating that the population is well-converged.

In order to assess propeller and engine performance, Eq. 6.1 and Eq. 6.2 were used to calculate an average open water efficiency ($\eta_{O,avg}$) and an average engine efficiency ($\eta_{E,avg}$), respectively. Remarkably, the best design does not hold the most efficient either propeller or engine. Contrarily, the SDO_4 holds the highest $\eta_{O,avg}$ and the SDO_1 holds the lowest $\eta_{E,avg}$. The SDO_4 presented $\eta_{O,avg}$ over 17% higher than SDO_1, whilst the SDO_2 had $\eta_{E,avg}$ 1.4% higher than SDO_1.

$$\eta_{O,avg} = \frac{\sum_{i=1}^{n_{RT}} \left[\eta_O \cdot \delta s\right]_i}{\sum_{i=1}^{n_{RT}} \delta s_i} \tag{6.1}$$

$$\eta_{E,avg} = \frac{\sum_{i=1}^{n_{RT}} \left[\eta_E \cdot \delta s\right]_i}{\sum_{i=1}^{n_{RT}} \delta s_i} \tag{6.2}$$

The SDO_4 presents the highest amount of LNG delivered per round trip (m_{LNG}) but, in contrast, the lowest annual income because it takes longer to accomplish a round trip (Δt_{rnd}), accomplishing fewer round trips per year (n_{rnd}). The SDO_1 presents the highest income and the lowest CAPEX but, in contrast, the highest OPEX. Thus, these economic measures of merit must be analysed in a combined way, such as performed by NPV. The NPV for the SDO_1 is US$ 12.3 million larger than for the SDO_4, accounting for a 2.1% gain. As noted, one of the strengths of the applied optimisation algorithm is achieving a population with various different improved designs, instead of only one. This is important for taking into account last subjective considerations and making the final decision.

6.3 Engine and fuel profile effect

Table 6.3 lists average engine efficiency ($\eta_{E,avg}$), average annual income and OPEX, as well as CAPEX and NPV for every matching of engine configuration and fuel profile (FP) suitable for SDO_2. There are five suitable engine configurations and four fuel profiles totalling 20 matchings. In order to facilitate the analysis, the

Table 6.2: Improved synthesis, design and operation (SDO) from the final population.

Feature	Unit	μ	σ	SDO_1	SDO_2	SDO_3	SDO_4
$v_{rw,ll}$	kn	11.99	0.0266	12.00	12.00	12.00	11.97
$v_{rw,il}$	kn	15.98	0.0262	15.97	15.99	16.00	16.00
$v_{rw,hl}$	kn	18.04	0.4381	17.94	17.91	17.54	17.74
$v_{rw,lb}$	kn	12.00	0.0084	12.00	12.00	12.00	12.00
$v_{rw,ib}$	kn	15.99	0.0175	16.00	16.00	16.00	15.97
$v_{rw,hb}$	kn	18.41	0.4062	18.57	18.38	17.91	17.49
D	m	8.460	0.2429	8.500	8.217	8.500	8.500
A_E/A_O	-	0.7488	0.1001	0.6460	0.7570	0.7849	0.4196
P/D	-	0.9277	0.0776	0.8837	1.0195	0.9301	0.8233
Z	-	5.0917	0.6859	5	6	4	3
Z_p	-	1.0333	0.1803	1	1	1	2
E_{ID}	-	7.167	2.247	8	7	8	12
Z_c	-	7.592	1.008	8	7	8	8
FP_{ID}	-	2.000	0.000	2	2	2	2
$\eta_{O,avg}$	%	-	-	64.09	63.17	63.74	75.11
$\eta_{E,avg}$	%	-	-	50.29	51.00	50.80	50.85
m_{LNG}	t	-	-	70,737	70,737	70,737	70,741
Δt_{rnd}	d	-	-	50.43	50.51	50.92	51.06
n_{rnd}	-	-	-	7.128	7.116	7.058	7.039
Income	US$·$10^6$	-	-	277.7	277.2	275.0	274.3
OPEX	US$·$10^6$	-	-	204.8	204.5	202.6	201.8
CAPEX	US$·$10^6$	-	-	67.24	69.61	67.93	75.68
NPV	US$·$10^6$	-	-	598.3	594.8	592.8	586.0

Notes: μ is average; σ is standard deviation; SDO_1 is the best (optimum) and SDO_4 is the worst.

influence of engine configuration and fuel profile for the SDO_2 is also shown as bar charts in Fig. 6.3.

As one may observe, $\eta_{E,avg}$ is always the highest for FP_4 and the lowest for FP_1, whereas it is the same intermediate value for FP_2 and FP_3. This is due to the assumption that engine efficiency depends only on the fuel phase (liquid or gaseous), made in Eq. 5.1 and 5.2, being independent of the fuel composition. Engine configuration is more influential on CAPEX whereas income and OPEX are more affected by the fuel profile. The FP_{ID} ranking in descending order of NPV was 2-1-3-4 for every engine. Since the best FP_{ID} does not occur for the highest efficiency or income, nor for the lowest expenditures, these merit measures analysed individually do not indicate the best project.

Among all five suitable engines, the best alternative regarding NPV was the 4^{th} one: engine 7G70-9.5 ($E_{ID} = 7$, 7 cylinders, "green" ultra-long stroke, 700 mm of piston diameter, mark number 9.5), whilst the worst one was the 2^{nd} one: engine 5S90-10.5 ($E_{ID} = 3$, 5 cylinders, super long stroke, 900 mm of piston diameter, mark number 10.5). For the best engine, the FP_2 led to an increase of US$ 22.6 million on NPV in comparison with the FP_4. This means that a simple search for the best fuel profile provided a gain of over 3.9%. Comparing the highest and the worst NPV among all matchings, the gain peaked at US$ 29.1 million, accounting for over 5.1%, which illustrates the combined effect of a simple search for the best matching of engine and fuel profile. Additionally, even for the best engine (7G70-9.5), NPV would be lower than the worst one in Tab. 6.2 (SDO_4) if either FP_3 or FP_4 were chosen.

6.4 Weather effect

In order to evaluate the influence of weather conditions, Fig. 6.4 shows the total resistance during laden and ballast trips for rough weather and still water. Weather effect for the laden trip was stronger between way-points 14 and 18, where the total resistance in rough weather ($R_{T,rw}$) was around 139 kN higher than for still water ($R_{T,sw}$), accounting for an increase of over 9.6%. However, the largest total resistance for rough weather occurred in ballast, between way-points 13 and 14, and peaked at 1601 kN. In this case, the added resistance was only 50 kN, representing a 3.2% increase.

The propeller's open water efficiency was also affected by weather conditions, as shown for the SDO_1 in Fig. 6.5. The strongest influence for the laden trip resulted in a decrease of 2.0 percentage points, accounting for under 3.1%, between way-points 14 and 18. For the ballast condition, the effect was most significant between way-points 4 and 5, where there was a drop of 1.5 percentage points,

Table 6.3: Influence of the matchings of engine configuration and fuel profile for the SDO_2.

E_{ID}	Engine	Z_c	FP_{ID}	$\eta_{E,avg}$	Income	OPEX	CAPEX	NPV
				%	US$·$10^6$			
2	G90-10.5	5	1	52.91	278.2	205.6	75.05	587.6
			2	53.04	277.3	204.3	75.05	591.1
			3	53.04	271.3	200.4	75.05	572.3
			4	53.64	267.5	200.1	48.57	566.9
3	S90-10.5	5	1	52.42	278.2	205.7	76.10	586.0
			2	52.56	277.3	204.3	76.10	589.6
			3	52.56	271.3	200.4	76.10	570.6
			4	53.13	267.5	200.1	49.62	565.7
4	S90-9.5	5	1	52.05	278.2	205.7	75.90	585.9
			2	52.21	277.3	204.4	75.90	589.6
			3	52.21	271.2	200.4	75.90	570.5
			4	52.80	267.5	200.1	49.42	566.0
7	G70-9.5	7	1	50.77	278.2	205.9	69.61	591.0
			2	51.00	277.2	204.5	69.61	594.8
			3	51.00	271.1	200.4	69.61	575.4
			4	51.66	267.5	200.1	43.13	572.2
7	G70-9.5	8	1	51.85	278.2	205.8	73.14	588.4
			2	52.00	277.3	204.4	73.14	592.1
			3	52.00	271.2	200.4	73.14	573.0
			4	52.61	267.5	200.1	46.66	568.6

Notes: the maximum NPV occurs for the matching 7G70-9.5 and FP_2, and the minimum one occurs for 5S90-10.5 and FP_4.

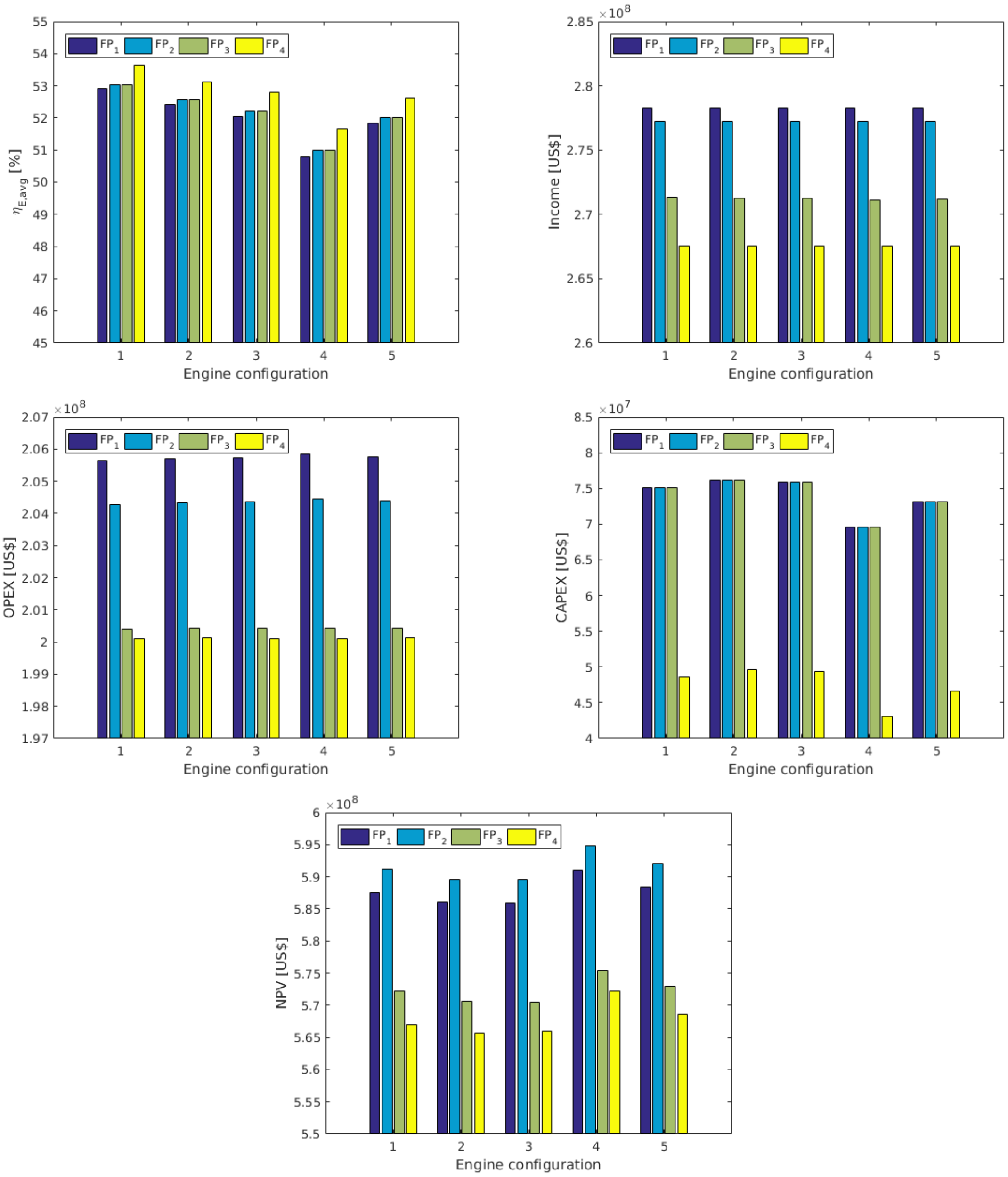

Figure 6.3: Engine configuration and fuel profile effects for the SDO$_2$.

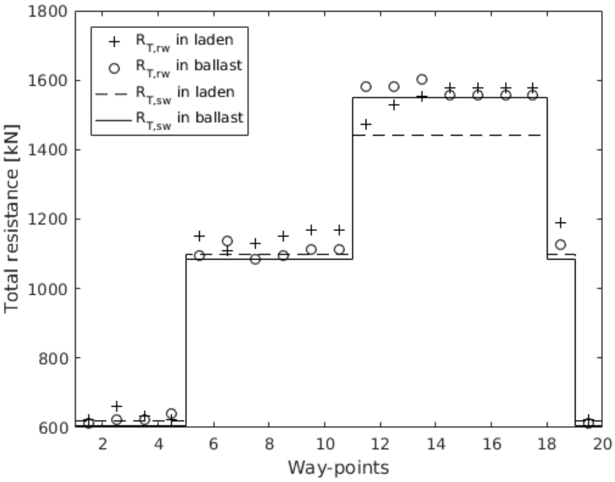

Figure 6.4: Total resistance throughout the voyage.

accounting for a 2.2% drop. Moreover, one can see clearly that the propeller's open water efficiency for still water does not present a trend regarding the service speed.

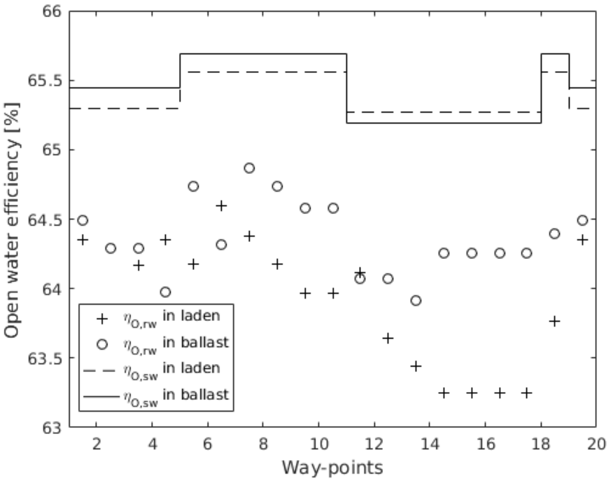

Figure 6.5: Propeller's open water efficiency throughout the voyage for the SDO_1.

The required shaft speed throughout the voyage for the SDO_1 are shown in Fig. 6.6. The shaft speed for the entire voyage was higher in rough weather (n_{rw}) than in still water (n_{sw}). The increase of n_{rw} in laden condition reached 3.9 rpm between way-points 14 and 18, a 4.8% increase. However, the highest value of n_{rw} occurred in ballast condition, peaking at about 86 rpm between way-points 13 and 14, a 3% increase.

The required brake power throughout the voyage for the SDO_1 are shown in Fig. 6.7. The brake power in rough weather ($P_{B,rw}$) and laden condition reached

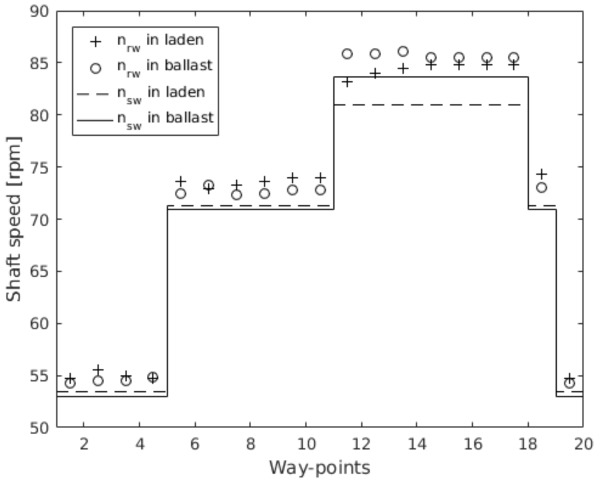

Figure 6.6: Required shaft speed throughout the voyage for the SDO_1.

an increase of over 3.9 MW between way-points 14 and 18, an increase of almost 22% in comparison with still water ($P_{B,sw}$). The highest $P_{B,rw}$ occurred, though, in ballast condition, peaking at 23 MW between way-points 13 and 14, an increase about 13%.

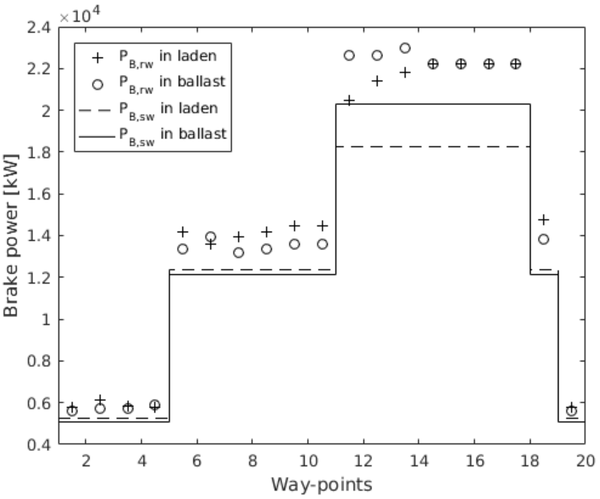

Figure 6.7: Required brake power throughout the voyage for the SDO_1.

Owing to the overlap of all those effects, the brake power in rough weather ($P_{B,rw}$) was appreciably increased in comparison to the brake power in still water ($P_{B,sw}$). Therefore, the operating point of the engine-propeller matching is primarily affected by the variation in brake power, and secondarily by the variation in shaft speed.

For the purpose of studying the effect of different weathers on the optimisation, June and December 2015 conditions were also considered. June is a milder month whereas December presents an extremer weather. Table 6.4 lists Beaufort Number (BN) and encounter angle for the laden trip (θ_l) along the route-tracks (RT) for June, December and 2015 average. Encounter angle for the ballast trip is the supplementary angle of θ_l. More expressive variations in θ_l can be observed whilst BN varies just slightly with respect to its average.

Table 6.4: Varying weather conditions for 2015.

RT	S [km]	Jun		Dec		Avg	
		BN	θ_l [°]	BN	θ_l [°]	BN	θ_l [°]
1 - 2	59.0	3	15.27	4	45.66	3	64.78
2 - 3	1339	3	31.01	4	42.42	4	47.70
3 - 4	1339	4	74.09	4	83.12	4	83.55
4 - 5	77.0	2	131.4	3	128.9	3	132.4
5 - 6	1015	2	69.77	2	98.05	3	58.33
6 - 7	1015	3	142.1	3	125.2	3	142.8
7 - 8	1015	3	140.5	2	38.71	2	42.50
8 - 9	1015	3	10.04	4	59.27	3	52.42
9 - 10	1015	4	30.04	4	50.95	4	40.52
10 - 11	1015	4	41.17	4	51.89	4	48.76
11 - 12	1015	4	78.50	5	17.04	4	65.82
12 - 13	1015	4	88.67	6	36.56	4	50.10
13 - 14	1015	4	61.06	6	27.53	5	36.69
14 - 15	1015	4	43.90	6	12.37	5	7.438
15 - 16	1015	4	20.90	6	0.055	5	0.561
16 - 17	1015	4	32.11	6	13.93	5	12.30
17 - 18	1015	4	78.02	5	31.07	5	23.21
18 - 19	1015	4	93.72	5	62.08	5	50.71
19 - 20	93.0	2	150.8	3	42.17	3	74.54

Table 6.5 presents the variable optimal values for weather conditions from June, December and 2015 average. Power and rotational speed for SMCR are presented as well as NPV. The different weather conditions caused some variations on service speed and blade area ratio whilst all the other variables had quite discreet changes. Therefore, the SMCR point and the NPV were slightly affected.

Although more significant influences could be expected, the limited number of engines considered might have forced similar solutions, as shown in Fig. 6.8. As can be seen, the SMCR points are placed on the edge of the E_8 layout diagram and there are no other engines of larger power for near rotational speeds. Another consideration is that the weather conditions used were approximated from monthly means of daily means. Hence, the occasional most severe weather conditions were balanced by milder conditions, affecting insignificantly the mean. That is why the three conditions assessed are not so different.

Table 6.5: Optimal synthesis, design and operation for varying adverse weather conditions.

Feature	Unit	Jun	Dec	Avg
$v_{rw,ll}$	kn	12.00	12.00	12.00
$v_{rw,il}$	kn	16.00	15.95	15.97
$v_{rw,hl}$	kn	18.14	17.91	17.94
$v_{rw,lb}$	kn	12.00	12.00	12.00
$v_{rw,ib}$	kn	16.00	15.92	16.00
$v_{rw,hb}$	kn	18.64	18.52	18.57
D	m	8.424	8.500	8.500
A_E/A_O	-	0.6863	0.7533	0.6460
P/D	-	0.8803	0.8788	0.8837
Z	-	5	5	5
Z_p	-	1	1	1
E_{ID}	-	8	8	8
Z_c	-	8	8	8
FP_{ID}	-	2	2	2
P_{SMCR}	MW	25.60	25.60	25.52
n_{SMCR}	rpm	90.92	89.78	89.22
NPV	US$·$10^6$	600.4	596.3	598.3

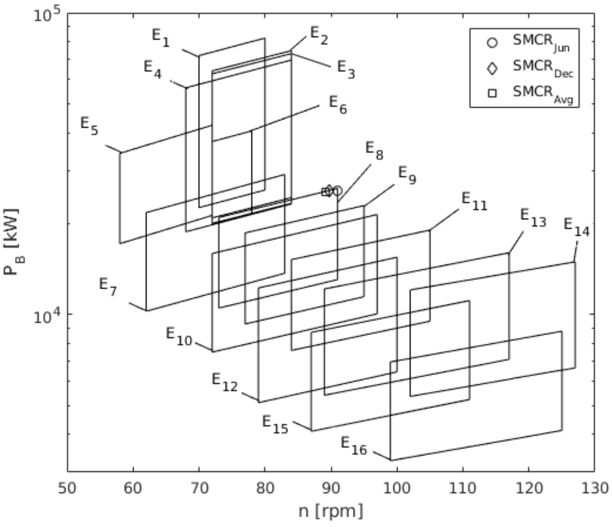

Figure 6.8: SMCR points for weather conditions from different months.

6.5 Economic scene effect

There is a strong relationship between the optimum fuel profile and the fuel and LNG prices, as previously mentioned. In order to assess the influence of different economic scenes on the optimum synthesis, design and operation, a data collection about fuels and LNG prices were carried out. Figure 6.9 shows the annual average prices of fuels and LNG for the period between 2000 and 2015, as well as the averages for this entire interval. Although there are appreciable alterations every year, the global average MGO price ($c_{MGO,avg}$) is almost coincident with the average LNG cost, insurance and freight ($CIF_{LNG,avg}$). Likewise, the global average HFO price ($c_{HFO,avg}$) is almost coincident with the average LNG free on board ($FOB_{LNG,avg}$).

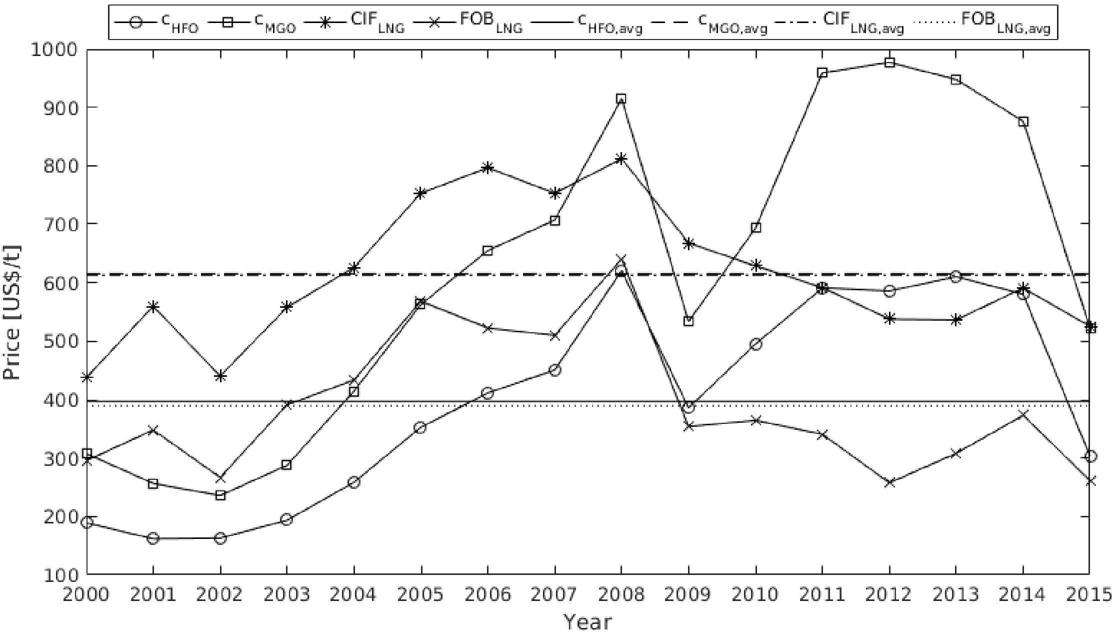

Figure 6.9: Fluctuation in fuel and LNG prices.

Table 6.6 shows five economic scenes and the global average (Avg). These scenes were selected as they are completely distinct from one another, being quite influential on the optimisation. Therefore, the optimisation process was run for each one of the economic scenes whilst the other input data were kept as stated in Chap. 5. Figure 6.10 illustrates the evolution of the optimisation variables along the generations whilst Tab. 6.7 lists the optimal synthesis, design and operation variables, as well as the NPV, for those selected economic scenes.

The optimisation variables were seen to evolute differently along the generations for each economic scene in Fig. 6.10. The optimal configurations were also different, evidencing the influence of the economic scene on the synthesis, design and operation of the system. As previously noticed, the best configuration presents a steady value of fuel profile (FP_{ID}) along the generations, independently of the economic scene.

Table 6.6: Selected economic scenes.

Year	c_{HFO} [US\$/t]	c_{MGO} [US\$/t]	CIF_{LNG} [US\$/t]	FOB_{LNG} [US\$/t]
2003	193.6	287.7	557.7	391.0
2006	411.3	655.0	796.7	522.5
2008	620.7	914.7	812.0	640.7
2012	585.7	976.8	537.8	257.6
2015	303.0	522.2	525.2	260.9
Avg	397.0	615.6	613.4	389.7

However, the optimum FP_{ID} was FP_1 for the 2003 scene; FP_2 for the 2006, 2008, 2015 and average scene; and FP_4 for the 2012 scene. The FP_3, though, was not the optimum for any of the selected economic scenes.

Remembering the description of the fuel profiles (Sec. 5.3), it is acceptable to assume that the FP_1 was the optimum only for the 2003 scene as it was the only time that c_{HFO} and c_{MGO} were both lower than FOB_{LNG}. In this case, it is more advantageous to burn HFO and MGO, and to sell all the LNG cargo. The FP_4 was the optimum only for the 2012 scene as it was the only time that FOB_{LNG} and CIF_{LNG} were both lower than c_{HFO}. In this case, the income from the LNG supposedly sold, instead of burnt, would not compensate for the cost of HFO theoretically used. For the years 2006 and 2008, the use of HFO instead of BOG is predictable because c_{HFO} is lower than FOB_{LNG}. The same does not occur in 2015 and in the average scene, in which, although c_{HFO} is between FOB_{LNG} and CIF_{LNG}, FP_2 was the best one. In this case, the use of BOG as fuel would decrease OPEX but it would also decrease incomes more sharply.

As can be seen in Tab. 6.7, the various economic scenes provided quite different configurations with expressive variations on NPV. The high service speeds varied either in laden or ballast ($v_{rw,hl}$ or $v_{rw,hb}$) whilst the most of the others remained steady. In five out of the six cases, the diameter of the propeller was its only parameter converging to the same value. The different diameter coincided with the only variation in the number of propulsion chains (Z_p). The NPV for 2012 scene and FP_4 was 36% higher than for the average (Avg) scene and FP_2. Furthermore, a remarkable difference of over 120% was found by comparing the NPV for the 2012 scene and FP_4 with the 2008 scene and FP_2, highlighting the influence of the economic scene and fuel profile on the synthesis, design and operation of the system.

6.6 Strengths of the approach

A list summarising the main strengths of the approach may be found below.

+ The total processing time to run all the cases presented herein was under 52

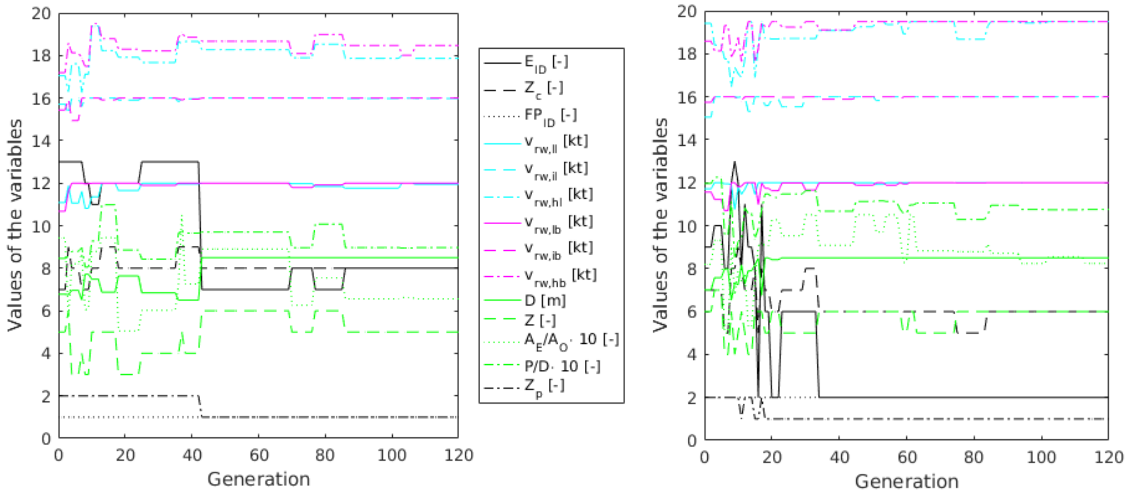

(a) For the scene from 2003

(b) For the scene from 2006

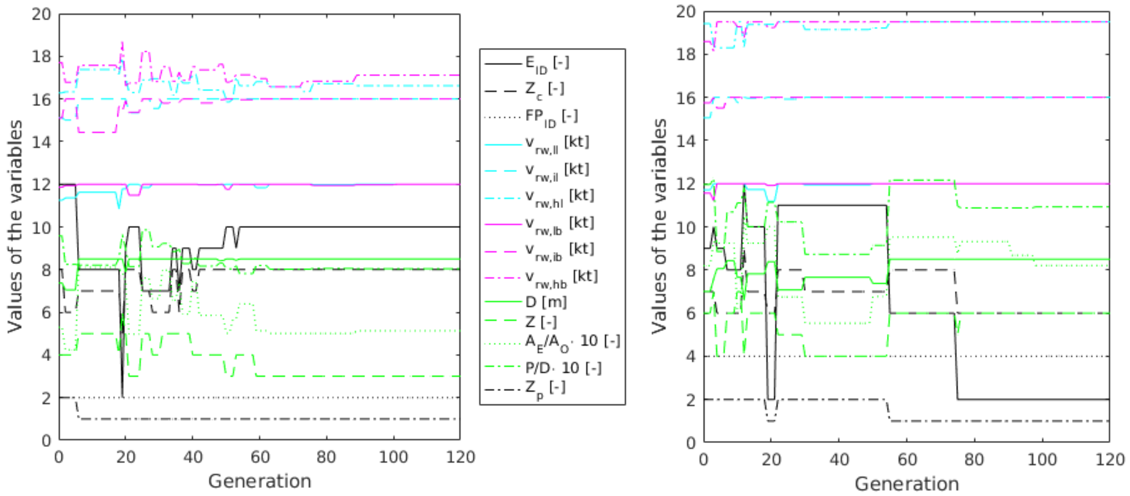

(c) For the scene from 2008

(d) For the scene from 2012

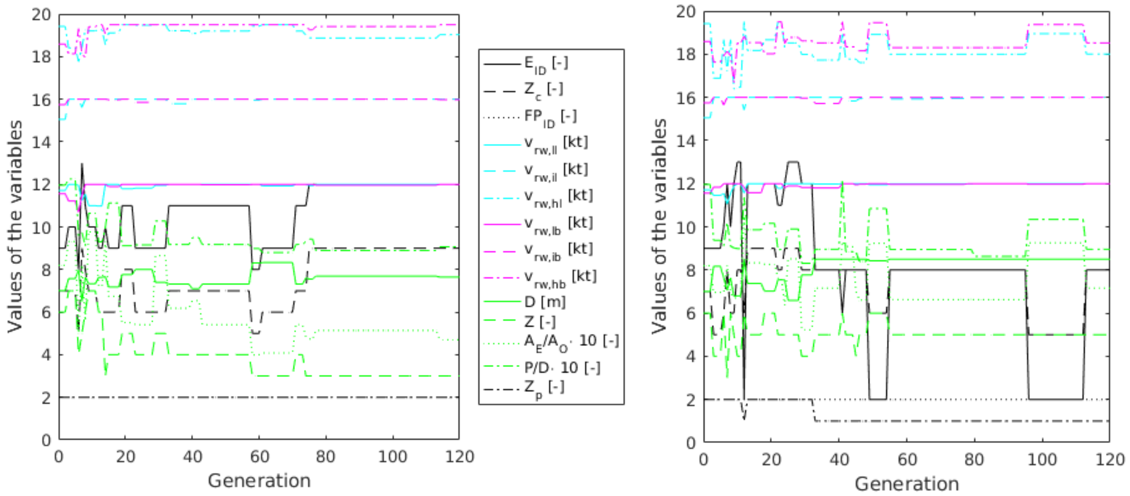

(e) For the scene from 2015

(f) For the average scene

Figure 6.10: Evolution of the optimisation variables for the selected economic scenes.

Table 6.7: Optimal synthesis, design and operation for the selected economic scenes.

Feature	Unit	2003	2006	2008	2012	2015	Avg
$v_{rw,ll}$	kn	11.95	12.00	12.00	12.00	12.00	12.00
$v_{rw,il}$	kn	15.98	16.00	16.00	16.00	16.00	16.00
$v_{rw,hl}$	kn	17.86	19.50	16.62	19.50	19.03	18.01
$v_{rw,lb}$	kn	12.00	12.00	12.00	12.00	12.00	12.00
$v_{rw,ib}$	kn	16.00	16.00	16.00	16.00	15.97	16.00
$v_{rw,hb}$	kn	18.47	19.50	17.12	19.50	19.50	18.52
D	m	8.500	8.500	8.500	8.500	7.648	8.500
A_E/A_O	-	0.6561	0.8238	0.5128	0.8208	0.4702	0.7158
P/D	-	0.8969	1.0751	0.8037	1.0924	0.9070	0.8958
Z	-	5	6	3	6	3	5
Z_p	-	1	1	1	1	2	1
E_{ID}	-	8	2	10	2	12	8
Z_c	-	8	6	8	6	9	8
FP$_{ID}$	-	1	2	2	4	2	2
NPV	US\$$\cdot 10^6$	573.8	1011.5	483.3	1065.6	1001.4	783.7

hours, thereby the approach can be considered fast enough for an early-stage optimisation.

- + Technical constraints were taken into account to avoid propeller configurations that might present problems related to strength, cavitation, vibration and noise.
- + The approach searches for the best engine-propeller matching amongst all the technical possibilities.
- + Different sea conditions can be considered for each route-track and the weather conditions required by the Kwon's added resistance method are only Beaufort Number and encounter angle.
- + Different parameters can be set up in each route-track and this enables various operational profiles to be considered to seek the highest net present value.

6.7 Limitations of the approach

Since an early-stage design optimisation approach must be fast, only simpler models were used. However, the simpler, the more limited they are. Each one of the models has its own limitations that, in turn, become limitations of the overall approach. Thus, the main limitations of the approach, besides those, are listed following.

- The influences of the water depth were not considered at all, such that the service margin component due to water depth was based on deep water. Therewith, the approach is inappropriate for shallow water.

- Appendages were neglected in the resistance calculation that considers merely form parameters, not the hull design itself.

- Neither a waste heat recovery system nor a gas after-treatment equipment was incorporated in the approach. Likewise, a re-liquefaction plant was not modelled and thereby the BOG properties were considered constant as well as its evaporation rate.

- Noxious emissions were considered neither to constraint the service speed nor to include additional fees. Similarly, no design index were considered either as a constraint or an additional objective function.

- A constant weather condition along the ship's life-cycle is a simplifying hypothesis. Severe sea conditions might cause overload on the engine and propeller, as well as might cause cavitation increase, which affects the behaviour of the propeller. The propeller might even emerge from the water and the engine might not be able to keep the ship service speed. Those situations were not taken into account.

- The Kwon's model does not consider wave amplitude, wavelength or frequency, such that if a more detailed model were used, the reliability of the approach could increase.

Chapter 7

Conclusion

This work has proposed a comprehensive early-stage approach to perform the optimisation of synthesis, design and operation for an LNGC under rough weather. Since an engine model suitable for optimisation problems was not found, developing such a model has been the first step of this work. It has been considered fixed pitch propellers directly driven by dual-fuel low-speed Diesel engines. Constraints have been incorporated to the approach in order to avoid propellers that could present issues concerning strength, cavitation and vibration. Different fuel profiles and service speeds have also been assessed. The approach proposed herein has used a differential evolution optimisation algorithm to optimise fourteen parameters. The objective function to be maximised by the algorithm has been the net present value for the ship's lifetime.

The computation of 15,023 input data sets have been run in 5.9 hours and almost 48% of the configurations have been constrained, the peripheral velocity being responsible for most rejections. The worst individual of the final population has had the objective function increased by 22% in comparison to the worst individual of the initial population. The final population has included rather distinct designs with a variation of only 2.1% in the objective function, which is a strength of the approach. Thus, subjective considerations may be taken into account before the final decision with only minor concerns.

Analysing the rejected configurations and why they have been rejected, there have not been general recommendations about configuration so that the propellers could escape the constraints. The best design has not held the most efficient either propeller or engine but the highest OPEX, which emphasises that these measures of merit must not be considered separately. An appropriate objective function must consider them in combination, such as done by the net present value. A simple search for the best matching of fuel profile and engine has provided a gain of over 5.1%.

The average weather condition for 2015 have led to almost 22% increase in brake power and 4.8% increase in shaft speed, emphasizing the effect on the engine and propeller operating points. On the other hand, the assessment of weather conditions from different months in 2015 did not show significant effects. One reason for this was the limited number of engines considered that forced the convergence to similar SMCR points. Another reason is that the weather conditions used were approximated from monthly means of daily means, being not so different one another.

The optimisation variables were seen to evolute differently along the generations for each one of the six economic scenes studied. The optimal configurations were also affected. It was seen that the use of BOG as fuel would decrease OPEX but it would also decrease incomes more sharply, depending on the economic scene. A remarkable difference of over 120% was found by comparing the NPV for the best economic scene with the worst one. Thus, the combined influence of economic scene and fuel profile on the synthesis, design and operation of the system was underlined.

Ultimately, the approach has shown significant gains and highlighted the need for exploring a broad range of propellers and engines, as well as considering the weather conditions in an integrated way. Assessing various profiles of fuel and service speed, as well as different economic scenes, was shown meaningful to found the configuration that maximises the NPV. Although an LNGC has been considered, this approach could be applied to other types of ships with only minor adjustments.

Chapter 8

Written articles and future work

This chapter sums up the articles written during the doctoral period and gives some possible courses of action to seek improvements in the developed approach.

8.1 Written articles

Some articles have been written and submitted to congresses and journals during the doctoral period. All of them are listed and their publication is briefly described below. Besides, the first page of each article is attached as appendix.

1. Literature review of an LNG carrier machinery system (Sec. A.1) – this paper was presented at the 16^{th} International Congress of the International Maritime Association of the Mediterranean (IMAM 2015), from 21 to 24 September 2015, in Pula, Croatia, and then it was published as a chapter in the book Towards Green Marine Technology and Transport.

2. Optimised selection of marine dual-fuel low-speed Diesel engines: introducing relative specific fuel consumptions (Sec. A.2) – this paper was submitted to the journal Marine Systems & Ocean Technology on 14 March 2016 and accepted on 7 September 2016.

3. A model to optimise the selection of marine dual-fuel low-speed Diesel engines (Sec. A.3) – this paper was presented at the 26^{th} National Congress on Maritime Transportation, Ship and Offshore Construction (SOBENA 2016), from 8 to 10 November 2016, in Rio de Janeiro, Brazil. Afterwards, the paper was encouraged to be sent to the journal Marine Systems & Ocean Technology, being submitted on 29 November 2016 and accepted on 30 May 2017.

4. An approach to optimise the selection of LNG carriers' propulsion system (Sec. A.4) – this paper was presented at the VII Seminar and Workshop

in Ocean Engineering (SEMENGO 2016), from 23 to 25 November 2016, in Rio Grande, Brazil. Afterwards, the paper was encouraged to be sent to the journal Thermal Engineering (RETERM), being submitted on 11 May 2017 and accepted on 6 July 2017.

5. Matching engine to propeller for an LNGC under rough weather (Sec. A.5) – this paper was presented at the 17^{th} International Congress of the International Maritime Association of the Mediterranean (IMAM 2017), from 9 to 11 October 2017, in Lisbon, Portugal. The paper is likely to become a chapter in the book Maritime Transportation and Harvesting of Sea Resources, which is expected to be published in 2018.
6. Optimising the engine-propeller matching for a liquefied natural gas carrier under rough weather (Sec. A.6) – this paper was submitted to the journal Applied Energy on 13 July 2017 but is still under review.

8.2 Future work

Only articles addressing partially the approach developed and the results found herein have been written so far. Hence, the first future work to be performed is a paper covering entirely the approach and results. Afterwards, the following list of future works can be performed in any order.

- Since different input data have not been simulated, the sensitivity of the net present value to input data, as ship and energy system parameters for instance, may be studied. Thus, ships of various geometries and cargo capacities can be assessed in order to find out which one holds the highest net present value. Furthermore, the ship's geometric parameters can be taken as design variables. In this case, a relation between cargo capacity and geometry would be need so that the best geometry could be found.
- Various routes could be studied in order to find the one maximising the NPV. The optimum design, synthesis and operation of the ship energy system depend on the weather condition of each route. Therefore, perhaps lengthier routes whose weather is less rough provide higher NPV than the shortest route (great circle route).
- As the best parameter values of the optimisation algorithm depend on every single problem, they could be optimised to enhance the algorithm performance. Moreover, other stochastic optimisation algorithms, such as simulated annealing and particle swarm, for instance, could be adopted. Thus,

their performances could be compared to each other to figure out the best algorithm to use in this case.

- If fuel and LNG prices, as well as weather conditions, follow typical patterns, they could be explained by deterministic functions. However, these parameters are also influenced by uncertain factors, which are the drivers of stochastic components. Hence, the simulation of these parameters should take into account both deterministic and stochastic components. In future works, they may be considered as probability distributions or treated by models as the geometric Brownian motion or mean-reversion model. In this sense, the robustness of solution is a substantial measure that was not treated in the present study. The degree of robustness to be supplied for a satisfactory solution is related to the system variations most likely to occur.

- Since the weather condition, as well as the fuel and LNG prices, are time-dependent parameters, the problem could be modelled as a dynamic optimisation problem (DOP). The goal of methods dealing with DOPs is no longer to locate a stationary optimal solution but to track its movement through the solution and time spaces as close as possible. Evolutionary techniques and their variants have been the most widely used methods to solve DOPs, but other approaches are gaining ever more attention in the past years [66].

References

[1] MOKHATAB, S., MAK, J. Y., VALAPPIL, J. V., et al. *Handbook of Liquefied Natural Gas.* New York, USA, Elsevier BV, 2014. doi: 10.1016/b978-0-12-404585-9.05001-7. Available at: <`http://dx.doi.org/10.1016/b978-0-12-404585-9.05001-7`>.

[2] DIMOPOULOS, G. G., FRANGOPOULOS, C. A. "A Dynamic Model for Liquefied Natural Gas Evaporation During Marine Transportation", *International Journal of Thermodynamics*, v. 11, n. 3, pp. 123–131, sep 2008.

[3] MIANA, M., DEL HOYO, R., RODRIGÁLVAREZ, V., et al. "Calculation models for prediction of Liquefied Natural Gas (LNG) ageing during ship transportation", *Applied Energy*, v. 87, n. 5, pp. 1687–1700, may 2010. doi: 10.1016/j.apenergy.2009.10.023. Available at: <`http://dx.doi.org/10.1016/j.apenergy.2009.10.023`>.

[4] KUMAR, S., KWON, H.-T., CHOI, K.-H., et al. "LNG: An eco-friendly cryogenic fuel for sustainable development", *Applied Energy*, v. 88, n. 12, pp. 4264–4273, dec 2011. doi: 10.1016/j.apenergy.2011.06.035. Available at: <`http://dx.doi.org/10.1016/j.apenergy.2011.06.035`>.

[5] WOODYARD, D. *Pounder's Marine Diesel Engines and Gas Turbines.* Oxford, UK, Elsevier BV, 2009. doi: 10.1016/b978-0-7506-8984-7.00002-3. Available at: <`http://dx.doi.org/10.1016/b978-0-7506-8984-7.00002-3`>.

[6] WATSON, D. G. M. *Practical Ship Design.* Oxford, UK, Elsevier, 2002. doi: 10.1016/s1571-9952(98)x8001-3. Available at: <`http://dx.doi.org/10.1016/s1571-9952(98)x8001-3`>.

[7] LAMB, T. *Ship Design and Construction.* New York, USA, The Society of Naval Architects and Marine Engineers (SNAME), 2003.

[8] BULUT, E., DURU, O., KOÇAK, G. "Rotational priority investigation in fuzzy analytic hierarchy process design: An empirical study on the marine

engine selection problem", *Applied Mathematical Modelling*, v. 39, n. 2, pp. 913–923, jan 2015. doi: 10.1016/j.apm.2014.07.018. Available at: <`http://dx.doi.org/10.1016/j.apm.2014.07.018`>.

[9] SOLEM, S., FAGERHOLT, K., ERIKSTAD, S. O., et al. "Optimization of diesel electric machinery system configuration in conceptual ship design", *Journal of Marine Science and Technology*, v. 20, n. 3, pp. 406–416, feb 2015. doi: 10.1007/s00773-015-0307-4. Available at: <`http://dx.doi.org/10.1007/s00773-015-0307-4`>.

[10] SKOGLUND, L., KUTTENKEULER, J., ROSÉN, A., et al. "A comparative study of deterministic and ensemble weather forecasts for weather routing", *Journal of Marine Science and Technology*, v. 20, n. 3, pp. 429–441, nov 2014. doi: 10.1007/s00773-014-0295-9. Available at: <`https://doi.org/10.1007%2Fs00773-014-0295-9`>.

[11] CHALFANT, J. "Early-Stage Design for Electric Ship", *Proceedings of the Institute of Electrical and Electronics Engineers (IEEE)*, v. 103, n. 12, pp. 2252–2266, dec 2015.

[12] BENVENUTO, G., CARRERA, G., RIZZUTO, E. "Dynamic Simulation of Marine Propulsion Plants". In: *Proceedings of the International Conference on Ship and Marine Research*, Rome, Italy, oct 1994.

[13] KYRTATOS, N. P., THEODOSSOPOULOS, P., THEOTOKATOS, G., et al. "Simulation of the overall ship propulsion plant for performance prediction and control". In: *Proceedings of the Conference on Advanced Marine Machinery Systems with Low Pollution and High Efficiency*, London, UK, mar 1999.

[14] MICHALSKI, J. "A method for selection of parameters of ship propulsion system fitted with compromise screw propeller", *Polish Maritime Research*, v. 14, n. 4, jan 2007. doi: 10.2478/v10012-007-0032-y. Available at: <`http://dx.doi.org/10.2478/v10012-007-0032-y`>.

[15] CHEN, J.-H., SHIH, Y.-S. "Basic design of a series propeller with vibration consideration by genetic algorithm", *Journal of Marine Science and Technology*, v. 12, n. 3, pp. 119–129, sep 2007. doi: 10.1007/s00773-007-0249-6. Available at: <`https://doi.org/10.1007%2Fs00773-007-0249-6`>.

[16] DIMOPOULOS, G. G., KOUGIOUFAS, A. V., FRANGOPOULOS, C. A. "Synthesis design and operation optimization of a marine energy system", *Energy*, v. 33, n. 2, pp. 180–188, feb 2008. doi: 10.1016/j.energy.2007.09.

004. Available at: <`http://dx.doi.org/10.1016/j.energy.2007.09.004`>.

[17] DIMOPOULOS, G. G., FRANGOPOULOS, C. A. "Synthesis, Design and Operation Optimization of the Marine Energy System for a Liquefied Natural Gas Carrier", *International Journal of Thermodynamics*, v. 11, n. 4, pp. 203–211, dec 2008.

[18] DIMOPOULOS, G. G., FRANGOPOULOS, C. A. "Thermoeconomic Simulation of Marine Energy Systems for a Liquefied Natural Gas Carrier", *International Journal of Thermodynamics*, v. 11, n. 4, pp. 195–201, dec 2008.

[19] THEOTOKATOS, G. P. "Ship Propulsion Plant Transient Response Investigation using a Mean Value Engine Model", *International Journal of Energy*, v. 2, pp. 66–74, 2008.

[20] ALDOUS, L., SMITH, T. "Speed Optimisation for Liquefied Natural Gas Carriers: A Techno-Economic Model". In: *Proceedings of the International Conference on Technologies, Operations, Logistics & Modelling for Low Carbon Shipping*, Newcastle, UK, sep 2012.

[21] THEOTOKATOS, G., TZELEPIS, V. "A computational study on the performance and emission parameters mapping of a ship propulsion system", *Proceedings of the Institution of Mechanical Engineers Part M: Journal of Engineering for the Maritime Environment*, v. 229, n. 1, pp. 58–76, sep 2013. doi: 10.1177/1475090213498715. Available at: <`https://doi.org/10.1177%2F1475090213498715`>.

[22] DIMOPOULOS, G. G., GEORGOPOULOU, C. A., STEFANATOS, I. C., et al. "A general-purpose process modelling framework for marine energy systems", *Energy Conversion and Management*, v. 86, pp. 325–339, oct 2014. doi: 10.1016/j.enconman.2014.04.046. Available at: <`http://dx.doi.org/10.1016/j.enconman.2014.04.046`>.

[23] MAN. "LNG Carriers with ME-GI Engine and High Pressure Gas Supply System". Printed, Denmark, sep 2014.

[24] CICHOWICZ, J., THEOTOKATOS, G., VASSALOS, D. "Dynamic energy modelling for ship life-cycle performance assessment", *Ocean Engineering*, v. 110, pp. 49–61, dec 2015. doi: 10.1016/j.oceaneng.2015.05.041. Available at: <`https://doi.org/10.1016%2Fj.oceaneng.2015.05.041`>.

[25] LU, R., TURAN, O., BOULOUGOURIS, E., et al. "A semi-empirical ship operational performance prediction model for voyage optimization towards energy efficient shipping", *Ocean Engineering*, v. 110, pp. 18–28, dec 2015. doi: 10.1016/j.oceaneng.2015.07.042. Available at: <`http://dx.doi.org/10.1016/j.oceaneng.2015.07.042`>.

[26] YANG, M.-H., YEH, R.-H. "Thermodynamic and economic performances optimization of an organic Rankine cycle system utilizing exhaust gas of a large marine diesel engine", *Applied Energy*, v. 149, pp. 1–12, jul 2015. doi: 10.1016/j.apenergy.2015.03.083. Available at: <`http://dx.doi.org/10.1016/j.apenergy.2015.03.083`>.

[27] SCHULTEN, P. J. M. *The interaction between diesel engines, ship and propellers during manoeuvring.* Tese de Doutorado, Delft University of Technology, Delft, The Netherlands, 2005.

[28] MEDICA, V., RACIC, N., RADICA, G. "Performance simulation of marine slow-speed diesel propulsion engine with turbocharger under aggravated conditions", *Strojarstvo*, v. 51, n. 3, pp. 199–212, 2009.

[29] PAYRI, F., OLMEDA, P., MARTÍN, J., et al. "A complete 0D thermodynamic predictive model for direct injection diesel engines", *Applied Energy*, v. 88, n. 12, pp. 4632–4641, dec 2011. doi: 10.1016/j.apenergy.2011.06.005. Available at: <`https://doi.org/10.1016%2Fj.apenergy.2011.06.005`>.

[30] GUAN, C., THEOTOKATOS, G., CHEN, H. "Analysis of Two Stroke Marine Diesel Engine Operation Including Turbocharger Cut-Out by Using a Zero-Dimensional Model", *Energies*, v. 8, n. 6, pp. 5738–5764, jun 2015. doi: 10.3390/en8065738. Available at: <`https://doi.org/10.3390%2Fen8065738`>.

[31] MALKHEDE, D. N., SETH, B., DHARIWAL, H. "Mean Value Model and Control of a Marine Turbocharged Diesel Engine". In: *SAE Technical Paper Series*. SAE International, oct 2005. doi: 10.4271/2005-01-3889. Available at: <`https://doi.org/10.4271%2F2005-01-3889`>.

[32] THEOTOKATOS, G. "On the cycle mean value modelling of a large two-stroke marine diesel engine", *Proceedings of the Institution of Mechanical Engineers, Part M: Journal of Engineering for the Maritime Environment*, v. 224, n. 3, pp. 193–205, mar 2010. doi: 10.1243/14750902jeme188. Available at: <`https://doi.org/10.1243%2F14750902jeme188`>.

[33] GUAN, C., THEOTOKATOS, G., ZHOU, P., et al. "Computational investigation of a large containership propulsion engine operation at slow steaming conditions", *Applied Energy*, v. 130, pp. 370–383, oct 2014. doi: 10.1016/j.apenergy.2014.05.063. Available at: <`https://doi.org/10.1016%2Fj.apenergy.2014.05.063`>.

[34] BALDI, F., THEOTOKATOS, G., ANDERSSON, K. "Development of a combined mean value–zero dimensional model and application for a large marine four-stroke Diesel engine simulation", *Applied Energy*, v. 154, pp. 402–415, sep 2015. doi: 10.1016/j.apenergy.2015.05.024. Available at: <`https://doi.org/10.1016%2Fj.apenergy.2015.05.024`>.

[35] STEFANOPOULOU, A., SMITH, R. "Maneuverability and smoke emission constraints in marine diesel propulsion", *Control Engineering Practice*, v. 8, n. 9, pp. 1023–1031, sep 2000. doi: 10.1016/s0967-0661(00)00024-1. Available at: <`https://doi.org/10.1016%2Fs0967-0661%2800%2900024-1`>.

[36] BENVENUTO, G., CAMPORA, U. "A Gas Turbine Modular Model for Ship Propulsion Studies". In: *Proceedings of the Symposium on High Speed Marine Vehicles*, Naples, Italy, sep 2005.

[37] ALTOSOLE, M., FIGARI, M. "Effective simple methods for numerical modelling of marine engines in ship propulsion control systems design", *Journal of Naval Architecture and Marine Engineering*, v. 8, n. 2, dec 2011. doi: 10.3329/jname.v8i2.7366. Available at: <`https://doi.org/10.3329%2Fjname.v8i2.7366`>.

[38] MARTELLI, M. *Marine Propulsion Simulation: Methods and Results.* Berlin, Germany, DE GRUYTER OPEN, 2014. doi: 10.2478/9783110401509.3. Available at: <`https://doi.org/10.2478%2F9783110401509.3`>.

[39] WOUD, H. K., STAPERSMA, D. *Design of Propulsion and Electric Power Generation Systems.* London, UK, IMarEST, 2013.

[40] CHANG, D., RHEE, T., NAM, K., et al. "A study on availability and safety of new propulsion systems for LNG carriers", *Reliability Engineering & System Safety*, v. 93, n. 12, pp. 1877–1885, dec 2008. doi: 10.1016/j.ress.2008.03.013. Available at: <`https://doi.org/10.1016%2Fj.ress.2008.03.013`>.

[41] LNGWS. "LNG carriers favour two-stroke dual-fuel propulsion systems". jan 2016. Available at: <`http://www.lngworldshipping.com/news/view,`

lng-carriers-favour-twostroke-dualfuel-propulsion-systems_41323.htm>.

[42] WARTSILA. "Wartsila Low-Speed Dual-Fuel Solution". 2015. Available at: <https://www.wartsila.com/docs/default-source/product-files/engines/ls-x-engine/brochure-o-e-wartsila-dual-fual-low-speed.pdf?sfvrsn=4>.

[43] MAN. "ME-GI Dual Fuel MAN B&W Engines: A Technical, Operational and Cost-effective Solution for Ships Fuelled by Gas". Printed, Denmark, aug 2014.

[44] MAN. "MAN B&W ME-GI Dual fuel low speed engine". Printed, Denmark, sep 2012.

[45] MAN. "Computerised Engine Application System-Engine Room Dimensioning (CEAS-ERD)". dec 2015. Available at: <http://marine.man.eu/two-stroke/ceas>.

[46] MORAN, M. J., SHAPIRO, H. N., BOETTNER, D. D., et al. *Fundamentals of Engineering Thermodynamics*. New York, USA, John Wiley & Sons, 2011.

[47] IMO. "Resolution MEPC.176(58): Amendments to the Annex of the Protocol of 1997 to Amend the International Convention for the Prevention of Pollution from Ships, 1973, as Modified by the Protocol of 1978 Relating Thereto". oct 2008. Available at: <http://www.imo.org/en/KnowledgeCentre/IndexofIMOResolutions/Marine-Environment-Protection-Committee-%28MEPC%29/Documents/MEPC.176%2858%29.pdf>.

[48] MAN. "Emission Project Guide: MAN B&W Two-stroke Marine Engines". Printed, Denmark, mar 2014.

[49] MAN. "Waste Heat Recovery System (WHRS) for Reduction of Fuel Consumption, Emission and EEDI". Printed, Denmark, aug 2014.

[50] COLAÇO, M. J., ORLANDE, H. R. B., DULIKRAVICH, G. S. "Inverse and optimization problems in heat transfer", *Journal of the Brazilian Society of Mechanical Sciences and Engineering*, v. 28, n. 1, pp. 1–24, mar 2006. doi: 10.1590/s1678-58782006000100001. Available at: <https://doi.org/10.1590%2Fs1678-58782006000100001>.

[51] MATHWORKS. "Support Documentation". jun 2016. Available at: <`https://www.mathworks.com/help/matlab/index.html`>.

[52] CARLTON, J. S. *Marine Propellers and Propulsion.* Oxford, UK, Elsevier BV, 2012. doi: 10.1016/b978-0-08-097123-0.00012-5. Available at: <`http://dx.doi.org/10.1016/b978-0-08-097123-0.00012-5`>.

[53] HOLTROP, J., MENNEN, G. G. J. "An approximate power prediction method", *International Shipbuilding Progress*, v. 29, pp. 166–170, 1982.

[54] HOLTROP, J. "A statistical re-analysis of resistance and propulsion data", *International Shipbuilding Progress*, v. 31, pp. 272–276, 1984.

[55] KWON, Y. J. "Speed loss due to added resistance in wind and waves 3", *Naval Architecture*, v. 3, pp. 14 – 16., 2008.

[56] SCHNEEKLUTH, H., BERTRAM, V. *Ship Design for Efficiency and Economy.* Oxford, UK, Elsevier BV, 1998. doi: 10.1016/b978-075064133-3/50006-2. Available at: <`http://dx.doi.org/10.1016/b978-075064133-3/50006-2`>.

[57] FOR MEDIUM-RANGE WEATHER FORECASTS ECMWF, E. C. "ERA Interim". jun 2016. Available at: <`http://apps.ecmwf.int/datasets/data/interim-full-moda/levtype=sfc/`>.

[58] OOSTERVELD, M. W. C., OSSANNEN, P. V. "Further computer-analysed data of the Wageningen B-screw series", *International Shipbuilding Progress*, v. 22, pp. 3–14, 1975.

[59] HOLDEN, K. O., FAGERJORD, O., FROSTAD, R. "Early Design-Stage Approach to Reducing Hull Surface Forces Due to Propeller Cavitation", *SNAME Transactions*, v. 88, pp. 403 – 442, 1980.

[60] VORUS, W. S. "Vibration". In: Paulling, J. R. (Ed.), *The Principles of Naval Architecture Series*, The Society of Naval Architects and Marine Engineers, New Jersey, USA, 2010.

[61] YIN, Y., CUI, H., ZHAO, D., et al. "Predicting Method of Natural Frequency for Ship's Overall Vertical Vibration", *Brodogradnja/Shipbuilding*, v. 65, n. 3, pp. 49 – 58, 2014.

[62] OF LABOR STATISTICS, B. "Producer Price Index Industry Data". jun 2016. Available at: <`http://data.bls.gov/timeseries/PCU333132333132`>.

[63] WARTSILA. "Fuel Gas Handling System and BOG Reliquefaction for LNG Carrier". nov 2013. Available at: <`http://cdn.wartsila.com/docs/default-source/product-files/ogi/lng-solutions/presentation-o-ogi-ppt-df-2-stroke-gas-handling.pdf?sfvrsn=6`>.

[64] WARTSILA. "Wartsila 34DF Product Guide". dec 2015. Available at: <`http://www.wartsila.com/products/marine-oil-gas/engines-generating-sets/dual-fuel-engines/wartsila-34df`>.

[65] MARQUES, C. H., BELCHIOR, C. R. P., CAPRACE, J. D. J. E. M. "A model to optimise the selection of marine dual-fuel low-speed diesel engines", *Marine Systems & Ocean Technology*, jun 2017. doi: 10.1007/s40868-017-0030-6. Available at: <`https://doi.org/10.1007%2Fs40868-017-0030-6`>.

[66] CRUZ, C., GONZÁLEZ, J. R., PELTA, D. A. "Optimization in dynamic environments: a survey on problems, methods and measures", *Soft Computing*, v. 15, n. 7, pp. 1427–1448, dec 2011. doi: 10.1007/s00500-010-0681-0. Available at: <`https://doi.org/10.1007%2Fs00500-010-0681-0`>.

Appendix A

Linked articles

Next, it is attached the first page of each article written along the doctoral period. All have been published, except the last article (A.6), which is still under review.

A.1 First article

Towards Green Marine Technology and Transport – Guedes Soares, Dejhalla & Pavletić (Eds)
© 2015 Taylor & Francis Group, London, ISBN 978-1-138-02887-6

Literature review of a LNG carrier machinery system

C.R.P. Belchior
Department of Oceanic and Naval Engineering, Federal University of Rio de Janeiro, Rio de Janeiro, Brazil

C.H. Marques
School of Engineering, Federal University of Rio Grande, Rio Grande do Sul, Brazil

ABSTRACT: The present study aims to inform about some important subjects to take into account when it is beginning to work with liquefied natural gas carrier machinery systems. Firstly, some general information about liquefied natural gas and ships that carry it were presented. Then, reasons why the traditional steam turbine propulsion plant was abandoned, as well as alternative propulsion plants were addressed. Two-stroke slow speed diesel engines without reliquefaction plant, as well as dual-fuel diesel electric and dual-fuel direct drive propulsion plants were discussed. Further, basic knowledge about reliquefaction plant was presented and a way to evaluate its viability was explained. Taking into account the environmental concern, some alternatives for ballast operation and some issues about gaseous emissions were discussed, as well as manners to reduce these emissions were addressed. Lastly, options to increase the overall propulsion plant efficiency using the exhaust gas waste heat were presented.

1 INTRODUCTION

LNG carriers are specialized ships designed to transport Liquefied Natural Gas (LNG).They are fitted with insulated double-hulled tanks, designed to contain the cargo slightly above atmospheric pressure at a cryogenic temperature of approximately −169°C. An average LNG carrier presents tank capacity about 160,000 m^3 and typically, the storage tanks operate at 0.3 bar_g with a design pressure of 0.7 bar_g. LNG presents typically density between 430 and 470 kg/m^3, depending on its composition and state. The LNG is composed predominantly by methane (CH_4), as well as ethane (C_2H_6), propane (C_3H_8), butane (C_4H_{10}) and nitrogen (N_2). (Mokhatab et al. 2014)

Despite the high degree of insulation in the tank walls, it is impossible to avoid the heat transfer from the surroundings, so that some vaporization will be always present during LNG transportation by ships. This occurs mainly due the thermal conductivity through the tank walls and the movement of the liquid. That LNG evaporated is called Boil-off Gas (BOG) and its evaporation rate is called Boil-off Rate (BOR). The natural BOR from a typical LNG carrier tank is about 0.10 to 0.15% in volume per day, depending on the thermal insulation system (Mokhatab et al. 2014). Vaporization induces an increase in pressure in the tank, such that a certain amount of the vapour phase should be taken out of the tank to avoid dangerous overpressure. Usually, this outlet gas flow is used as fuel by the propulsion system of the ship to reduce its fuel consumption. (Miana et al. 2010)

One of the major advantages of using steam propulsion plant in LNG carriers has been its capability to burn the unavoidable BOG directly in the power boiler, which has made it practically an exclusive option for many years. However, as environmental, economic and technical expectations have increased, the drawbacks of the steam turbine power plant have made it a less attractive option. Among these drawbacks are the comparative low efficiency of the plant, its high fuel consumption, which in turn translates into high exhaust emissions and its large engine room space requirement. Advances in the design of dual-fuel diesel engines, shipboard LNG reliquefaction plants and marine gas turbines, provide meaningful alternatives to the traditional steam power plant for LNG vessels. (Gilmore et al. 2005)

Regarding to environmental concern, controls on exhaust gas emissions continue to tighten regionally and internationally dictating further responses from engine designers. Carbon dioxide (CO2), nitrogen oxides (NO_X), sulphur oxides (SO_X) and Particulate Materials (PM) are the gaseous emissions of most concern. Thereby, in-engine measures to decrease these emissions, including common rail fuel systems, emulsified fuel, direct water injection and charge air humidification, have been studied. In addition, exhaust gas after-treatment, such as Selective Catalytic Reduction (SCR) and Exhaust Gas Recirculation (EGR)

A.2 Second article

Mar Syst Ocean Technol (2017) 12:1–12
DOI 10.1007/s40868-016-0019-6

Optimised selection of marine dual-fuel low-speed diesel engines: introducing relative specific fuel consumptions

Crístofer H. Marques[1,2] · **Carlos R. P. Belchior**[2]

Received: 14 March 2016 / Accepted: 7 September 2016 / Published online: 20 September 2016
© Sociedade Brasileira de Engenharia Naval 2016

Abstract Low-speed diesel engines are the most used ones in large ships as main propulsion, and due to severe environmental rules, there has been an intensive search for using alternative fuels which generate less emissions in these engines. In this context, dual-fuel diesel engines have been developed and their employment keeps growing. Therefore, the present study aimed to elaborate a simple and fast approach to assist the selection of the optimal marine dual-fuel low-speed diesel engine concerning fuel consumption to be fitted as primary mover. Relative specific fuel consumptions were introduced to develop unified expressions, and a polynomial approach was applied in order to fit curves. The accuracy of the method was verified through comparisons with a web-based application provided by an engine manufacturer and the highest deviation peaked at about 2.7 %. A practical liquefied natural gas carrier design of matching propeller/ship and engine was performed so that the convenience of the method could be explored. Thus, through the proposed optimisation methodology, annual savings of over 8.1 and 9.6 % were reached regarding heavy fuel oil and boil-off gas, respectively. At last, it was found that the optimal matching might not be due to the most efficient either propeller or engine.

Keywords Optimisation · Selection · Dual-fuel diesel engine · Low-speed diesel engine · Marine propulsion · Prime mover

1 Introduction

Prime mover selection is one of the major steps in merchant ship building projects. Since this machine is usually operated until the end of the ship's lifetime, its selection is made taking into account its durability. The importance of each selection criteria differs from one to another ship type. In some ships, only a few of the criteria need to be considered, in others all must be taken into account although with different degrees of emphasis. The most applied prime mover in merchant transportation of large scale has been the low-speed diesel engine, and factors influencing its selection can be classified into two categories: technical aspects and financial aspects. Noise, vibration, emissions, size, weight and efficiency are only some examples of the former whilst capital expenditures and operational expenditures summarise the latter.

Criteria designation is a highly difficult problem due to the fact that many products are not provided with detailed information about their performance and particulars. On the other hand, some indicators may provide information about the engine's performance, such as, time used in the existing fleet, previous damage records, and so forth. Although a complete criteria list for choosing main machinery are given by Watson [1] and many considerations are done by Lamb [2], Bulut et al. [3] based on interviews with a group of technical experts and managers of selected shipping companies defined the following six major selection criteria: power, acquisition cost, fuel

---

✉ Crístofer H. Marques
cristoferhood@oceanica.ufrj.br

[1] School of Engineering, Federal University of Rio Grande, Rio Grande 96203-900, Brazil

[2] Present Address: Department of Oceanic and Naval Engineering, Federal University of Rio de Janeiro, Rio de Janeiro 21945-970, Brazil

A.3 Third article

Mar Syst Ocean Technol (2017) 12:138–149
DOI 10.1007/s40868-017-0030-6

A model to optimise the selection of marine dual-fuel low-speed diesel engines

Crístofer Hood Marques[1,2] · **Carlos Rodrigues Pereira Belchior**[2] · **Jean David Job Emmanuel Marie Caprace**[2]

Received: 29 November 2016 / Accepted: 30 May 2017 / Published online: 5 June 2017
© Sociedade Brasileira de Engenharia Naval 2017

Abstract This study aimed to address the state of the art of marine diesel engines computer simulation models and the main computer applications. There are simple models based on transfer function or more complex models based on computational fluid dynamics. The models may be either implemented through basic programming languages or simulated through dedicated packages of internal combustion engine simulation. Owing to the recent interest to reduce the gas emission, dual-fuel engines are increasingly being used as primary propulsion in merchant ships. In this context, a simplified model of marine dual-fuel low-speed diesel engine has been developed. Through the normalisation of specific fuel consumption and exhaust gas data, clear trends approachable by polynomial curves or surfaces were revealed. Thus, by using the proposed model and knowing the characteristics of an engine at its nominal maximum continuous rating, it is possible to predict the engine operation in any design point on the engine layout diagram, even at part load. The maximum deviations regarding the two simulated engines did not exceed −3.4%. Summarising, the developed model is a simple and effective tool for optimising the selection of dual-fuel low-speed diesel engines to be applied in ship propulsion systems.

Keywords Marine propulsion · Prime mover · Optimisation · Prediction model · Selection

1 Introduction

The earliest engine models were based on ideal (air standard) cycles [1] and are currently the most widely taught in undergraduate courses. Although these were very simplistic, they helped the engineers to understand engine operation. The first of these models is supposed to have been developed in the late 1800s [2].

On the other hand, internal combustion engine simulations itself have been developed and applied since the 1960s. It consists in reproducing mathematically the significant processes and predicting the performance and operation details. In the beginning, the simulations were fairly elementary and limited by both computing capabilities and a lack of knowledge concerning some key sub-models. Nowadays, many of these simulations contain advanced and detailed sub-models about fluid mechanics, heat transfer, friction, combustion and chemical kinetics, being performed by sophisticated computer programs [3].

The earliest works on compression ignition engines are perhaps due to McAulay et al. [4], as well as Krieger and Borman [5]. Their simulations were fairly complete, but a major weakness was the lack of a comprehensive description of the complex diesel engine combustion process.

The development of engine cycle simulations is a challenging task largely because of turbulent and unsteady flow, non-uniform mixture composition, highly exothermic chemical reactions, two or three phase compositions, as well as pollutant species. In addition, the important time scales have a large dynamic range of between 1 µs and 1 s, and the important length scales range roughly between 1 µm and 1 m.

According to Schulten [6], five main sorts of engine model might be recognised: computational fluid dynamics

---

✉ Crístofer Hood Marques
cristoferhood@oceanica.ufrj.br

[1] Federal University of Rio Grande – FURG, Rio Grande, Brazil

[2] Federal University of Rio de Janeiro – COPPE/UFRJ, Rio de Janeiro, Brazil

A.4 Fourth article

Tecnologia/Technology

AN APPROACH TO OPTIMISE THE SELECTION OF LNG CARRIERS' PROPULSION SYSTEM

C. H. Marques[a],
C. R. P. Belchior[b],
and J. -D. Caprace[b]

[a] Universidade Federal do Rio Grande
Escola de Engenharia
Avenida Itália, km 8, CP. 474
Rio Grande, RS, Brasil
cristoferhood@oceanica.ufrj.br
[b] Universidade Federal do Rio de Janeiro
Departamento de Engenharia Naval e Oceânica
Avenida Horácio Macedo, 2030, CP. 68508
Ilha do Fundão, Rio de Janeiro, RJ, Brasil

Received: May 11, 2017
Revised: June 12, 2017
Accepted: July 06, 2017

ABSTRACT

Marine transport of natural gas, mostly in its liquid phase, is of growing importance in the global energy markets. The fleet of liquefied natural gas carriers is thereby increasing and being upgraded to enhance its performance. Since there is no well-defined procedure about how to perform the selection of the propulsion system considering the peculiarities of this kind of vessel, this work intend to fill this gap. In other words, the present article aims to propose an approach so that one can perform the optimised selection of liquefied natural gas carriers' propulsion system mainly concerning financial aspects. Firstly, some fundamentals about liquefied natural gas and its transport are presented followed by reasons why the traditional steam turbine propulsion plant was abandoned and dual-fuel diesel engines have been applied instead. Then, a list of criteria is discussed and studies that inspired this work are summarised. A case study of a ship with cargo capacity of 174,000 m³ operating between Lake Charles and Tokyo Bay via Panama Canal is selected. Owing to this route and environmental rules, the ship has to travel at three different levels of service speed unlike ordinary ones, which usually keep a steady speed throughout voyage. Maximising the net present value of the project is the objective function that is intended to be achieved by optimising eleven variables regarding synthesis, design and operation of the propulsion system. Finally, it is suggested that this work may assist marine engineers and ship-owners to design and outline the operation of liquefied natural gas carriers.

Keywords: propulsion, dual-fuel engine, prime mover, optimisation, LNG

NOMENCLATURE

$1+k_1$	form factor of the hull, N
A_E/A_O	blade-area ratio
C_{form}	ship form coefficient
C_n	coefficients of the Troost series polynomials
C_U	speed reduction coefficient
C_β	direction reduction coefficient
D	propeller diameter, m
F	net cash flow, US$
i	discount rate
J	advance ratio
K_Q	non-dimensional torque coefficient
K_T	non-dimensional thrust coefficients
n	number of terms in Troost series polynomials
n_e	engine speed, rpm
P/D	pitch ratio
P_B	brake power, W
P_E	effective power, W
R_A	model-ship correlation resistance, N
R_{APP}	appendage resistance, N
R_B	additional pressure resistance of bulbous bow near the water surface, N
R_F	frictional resistance, N
R_T	total resistance, N
R_{TR}	additional pressure resistance due to transom immersion, N
R_W	wave resistance, N
s_n	exponents of J (Troost series polynomials)
t	total time of project, year
t_n	exponents of P/D (Troost series polynomials)
u_n	exponents of A_E/A_O (Troost series polynomials)
v_n	exponents of Z (Troost series polynomials)
V_{rw}	service speed in rough weather, m/s
V_{sw}	service speed in still water, m/s
y	time of cash flow, year
Z	blade number of the propeller
Z_c	number of cylinders
Z_p	number of propellers and engines
η_H	hull efficiency
η_O	open water propeller efficiency
η_R	relative rotative efficiency
η_{TRM}	transmission efficiency

Subscripts

r	normalised in relation to nominal maximum continuous rating

Abbreviations

BOG	boil-off gas
BOR	boil-off rate
CAPEX	capital expenditure, US$
EM	engine margin
FP	fuel profile
GCU	gas combustion unit
HFO	heavy fuel oil
ID	engine identification
ITTC	International Towing Tank Conference

A.5 Fifth article

Maritime Transportation and Harvesting of Sea Resources – Guedes Soares & Teixeira (Eds)
© 2018 Taylor & Francis Group, London, ISBN 978-0-8153-7993-5

Matching engine to propeller for an LNGC under rough weather

C.H. Marques
Engineering School, Federal University of Rio Grande (FURG), Rio Grande, Brazil Currently at UFRJ

C.R.P. Belchior & J.-D. Caprace
Department of Marine and Ocean Engineering, Federal University of Rio de Janeiro (UFRJ),
Rio de Janeiro, Brazil

ABSTRACT: The present work aims to provide a comprehensive approach to perform the engine to propeller matching for a Liquefied Natural Gas Carrier (LNGC) under rough weather. A weather condition was included in the assessment of total resistance, and thereby affected the propeller's open water efficiency, shaft speed and brake power. Constraints were included to the approach in order to avoid propellers that could present issues concerning strength, cavitation and vibration. The case study was designed using an LNGC of 175,000 m^3 holding three service speeds. Thus, the propeller to engine matchings were addressed for 10 randomly chosen propulsion installations. The lowest total required power was over 14% lower than the highest. Brake power for rough weather was over 18% higher than for still water. Therefore, the approach proved useful and highlighted the need to explore a broad range of propellers and engines, as well as to consider weather conditions.

1 INTRODUCTION

Liquefied natural gas carriers (LNGCs) are specialised ships designed to transport liquefied natural gas. They are fitted with insulated double-hulled tanks, designed to contain the cargo slightly above atmospheric pressure at a cryogenic temperature without any means of external refrigeration. Despite the high degree of insulation, some vapourisation will occur due to the unavoidable heat transfer from the surroundings to the cargo. Since vapourisation induces a pressure increase in the tank, a certain amount of the vapour phase should be taken out of the tank to avoid dangerous overpressure (Mokhatab et al. 2014). Usually, this outlet gas flow is used as fuel by the marine energy system of the ship to reduce its main fuel consumption (Miana et al. 2010).

For many years steam propulsion plants were practically an exclusive option for LNGCs due to its capability to burn the unavoidable boil-off gas (BOG) directly in the power boiler. However, advances in the design of dual-fuel diesel engines, shipboard BOGre-liquefaction plants and marine gas turbines have provided meaningful alternatives to the traditional steam power plant (Belchior and Marques 2015). Moreover, propulsion systems based on slow speed two-stroke diesel engines driving fixed pitch propellerswith onboard re-liquefaction system have been successfully used in large LNGCs. However, when conventional fuel prices are higher than LNG price, the operational expenditure of propulsion systems that are unable to use BOG as fuel is increased (Mokhatab et al. 2014). Moreover, conventional fuels are not as clean as BOG, once natural gas is considered environmentally friendly (Kumar et al. 2011). An option to overcome these drawbacks is to apply dual-fuel diesel engines, which are compression ignition ones capable to work in two operational modes: diesel mode and gas mode. During diesel mode they work as a conventional diesel engine, burning ordinary liquid fuels such as marine gas oil, marine diesel oil and heavy fuel oil. In gas mode they burn essentially a gaseous fuel and only a little fraction of liquid pilot fuel is required to start the combustion process (Woodyard 2009).

Since the prime mover is usually operated until the end of the ships lifetime, its selection is one of the major steps in merchant shipbuilding projects. Based on interviews with a group of technical experts and managers of selected shipping companies, Bulut et al. (2015) placed power on the top of the selection criteria list. This is because the engine needs to be capable to provide enough power to satisfy the ships operational profile. Since the propulsion power required by the ship depends on the weather conditions, it is advisable to apply an approach that considers the added resistance due to weather to perform the appropriate selection of the prime mover.

A.6 Sixth article

Elsevier Editorial System(tm) for Applied Energy
Manuscript Draft

Manuscript Number: APEN-D-17-05771

Title: Optimising the engine-propeller matching for a liquefied natural gas carrier under rough weather

Article Type: Research Paper

Keywords: optimisation; propulsion; dual-fuel diesel engine; fixed pitch propeller; fuel consumption

Corresponding Author: Mr. Crístofer Hood Marques, Sc.M

Corresponding Author's Institution: FURG

First Author: Crístofer Hood Marques, Sc.M

Order of Authors: Crístofer Hood Marques, Sc.M; Carlos Rodrigues P Belchior, Sc.D; Jean David J Caprace, Ph.D

Abstract: Dual-fuel diesel engines have become the most interesting alternative for liquefied natural gas carriers (LNGCs), since they are able to use boil-off gas (BOG) as fuel. However, there is a lack of studies about the optimisation of propulsion system selection considering weather conditions in an integrated approach. Thus, the present work aims to provide a comprehensive approach to perform the optimisation of engine-propeller matching for an LNGC under rough weather. A weather condition was included in the assessment of total resistance, and thereby affected the propeller's open water efficiency, shaft speed and brake power. Constraints were included to the approach in order to avoid propellers that could present issues concerning strength, cavitation and vibration. A differential evolution optimisation algorithm was applied in which the objective function minimises fuel expenditure for propulsion for a round trip. The case study was designed using an LNGC with a cargo capacity of 175,000 m^3 sailing in laden condition from Lake Charles (USA) to Tokyo Bay (Japan), via Panama Canal, and returning in ballast. All suitable matchings for 5346 propellers were found in 2.8 hours and over 28% of them were constrained. The method has shown a gain of 19% between the worst individual of the initial population and the worst individual of the final population. The required brake power was approximately 20% higher for rough weather than for still water. Therefore, the approach used here has shown a significant gain and highlighted the value of exploring a broad range of propellers and engines in an integrated manner, as well as considering the weather condition.